COMPOSITE RCS SPACE FRAME SYSTEMS:

CONSTRUCTABILITY AND PERFORMANCE

A Thesis

by

JOHN PHILLIP STEELE

Submitted to the Office of Graduate Studies of
Texas A&M University
in partial fulfillment of the requirements for the degree of

MASTER OF SCIENCE

December 2003

Major Subject: Civil Engineering

COMPOSITE RCS SPACE FRAME SYSTEMS:

CONSTRUCTABILITY AND PERFORMANCE

A Thesis

by

JOHN PHILLIP STEELE

Submitted to Texas A&M University
in partial fulfillment of the requirements
for the degree of

MASTER OF SCIENCE

Approved as to style and content by:

Joseph M. Bracci (Chair of Committee)	Terry Kohutek (Member)
Peter B. Keating (Member)	Paul Roschke (Interim Head of Department)

December 2003

Major Subject: Civil Engineering

ABSTRACT

Composite RCS Space Frame Systems: Constructability and Performance.

(December 2003)

John Phillip Steele, B.S., Texas A&M University

Chair of Advisory Committee: Dr. Joseph M. Bracci

The objective of this research program is to further evaluate the performance and constructability of reinforced concrete (RC) column-steel beam-slab systems (RCS) for use in low- to mid-rise space frame buildings located in regions of high wind loads and/or moderate seismicity. To better understand these systems, two full scale RCS cruciform specimens were tested under bidirectional quasi-static reversed cyclic loading. The experimental portion of this research program included the construction and testing of two full-scale cruciform specimens with identical overall dimensions but with different joint detailing. The two joint details evaluated were joint cover plates and face bearing plates with localized transverse ties. The construction process was recorded in detail and related to actual field construction practices. The specimens were tested experimentally in quasi-static reversed cyclic loading in both orthogonal loading directions while a constant axial force was applied to the column, to simulate the wind loads in a subassembly of a prototype building. To compliment the experimental work, nonlinear analyses were performed to evaluate the specimen strength and hysteretic degradation parameters for RCS systems. In addition, current recommendations in the

literature on the design of RCS joints were used to estimate specimen joint strength and were compared with the experimental findings.

ACKNOWLEDGMENTS

I would like to gratefully thank the members of the thesis committee: Dr. Joseph Bracci, Dr. Peter Keating, and Dr. Terry Kohutek, who provided guidance and assistance throughout the research process. Andrew Fawcett, Jeff Perry, and Matt Potter of the Testing, Machining and Repair Facility at Texas A&M University deserve special thanks for helping during the construction and testing of the cruciform specimens. Without their oversight in the lab, the experimental part of this research would not have run as smoothly as it did. I would like to also thank Brent Baldwin, an undergraduate student that aided during the construction of the experimental specimens, and Suraphong Powanusorn (Eck), who provided guidance with the analytical work and assisted during construction and experimental testing of the experimental specimens. Hirschfeld steel and SMI-Texas helped make the experiment possible with donations of the steel components for the test setup and cruciform test specimens. In addition, supplemental funding and collaboration from Walter P. Moore and Associates are greatly appreciated.

The research study described was funded by the National Science Foundation Grant No. CMS-9733959 through S.C. Liu, Walter P. Moore and Associates, and the Department of Civil Engineering at Texas A&M University. This support is gratefully acknowledged. Any opinions, findings, conclusions, and recommendations expressed in this thesis are those of the writer and do not necessarily reflect the views of the sponsors.

TABLE OF CONTENTS

Page

ABSTRACT iii

ACKNOWLEDGMENTS v

TABLE OF CONTENTS vi

LIST OF FIGURES viii

LIST OF TABLES xiii

CHAPTER I INTRODUCTION 1

1.1 HISTORICAL BACKGROUND 1
1.2 RESEARCH OBJECTIVE 2
1.3 SCOPE OF WORK 2

CHAPTER II BACKGROUND AND PRESENT STATE OF KNOWLEDGE 4

2.1 GENERAL 4
2.2 RESEARCH AT THE UNIVERSITY OF TEXAS 4
2.3 RESEARCH AT CORNELL UNIVERSITY 7
2.4 ASCE GUIDELINES 9
2.5 U.S-JAPAN COOPERATIVE RESEARCH PROGRAM 16
2.6 RESEARCH AT THE UNIVERSITY OF MICHIGAN 17
2.7 RESEARCH AT TEXAS A&M UNIVERSITY 23
2.8 JAPANESE RESEARCH AND GENERAL PRACTICES 32

CHAPTER III PROTOTYPE RCS SPACE FRAME SYSTEM 34

3.1 BACKGROUND 34
3.2 STRUCTURAL STRENGTH AND STIFFNESS 35
3.3 CONSTRUCTION PROCESS 43
3.4 JOINT DETAILING AND ISSUES 45

CHAPTER IV EXPERIMENTAL PROGRAM 47

4.1 GENERAL 47
4.2 SPECIMEN DESIGN 47
4.3 JOINT DETAILS 49
4.4 MATERIAL PROPERTIES 52

Page

4.5 EXPERIMENTAL SETUP 53
4.6 LOAD APPLICATION 55
4.7 INSTRUMENTATION AND DATA ACQUISITION 56

CHAPTER V SPECIMEN CONSTRUCTION……63

5.1 SUMMARY 63
5.2 SPECIMEN CONSTRUCTION PROCESS 64
5.3 CONSTRUCTABILITY ISSUES AND SOLUTIONS 79

CHAPTER VI EXPERIMENTAL RESULTS……..84

6.1 GENERAL 84
6.2 OVERALL SUBASSEMBLY PERFORMANCE 84
6.3 JOINT BEHAVIOR 90
6.4 COMPOSITE BEAM BEHAVIOR 97
6.5 SLAB STEEL 104
6.6 CONCRETE STRAIN GAGES IN JOINT 117
6.7 BEAM WEB STRAINS IN JOINT 119
6.8 LARGE DEFORMATION TEST RESULTS 122

CHAPTER VII ANALYTICAL COMPARISON…….……126

7.1 CALCULATION BASED ON ASCE (1994) 126
7.2 UNIVERSITY OF MICHIGAN 128
7.3 ANALYTICAL COMPARISONS 129

CHAPTER VIII CONCLUSIONS…….....……..140

8.1 SUMMARY 140
8.2 CONCLUSIONS 141
8.3 RECOMMENDATIONS FOR FUTURE WORK 143

REFFERENCES 144

APPENDIX A NOTATION 147

VITA 151

LIST OF FIGURES

FIGURE Page

2.1 Joint Failure Mechanisms (ASCE 1994) 5

2.2 Resistance to Joint Panel Shear (ASCE 1994) 6

2.3 Additional Joint Components (Kanno 1993) 8

2.4 ASCE Recommended Joint Shear Resistance Components (ASCE 1994) 12

2.5 Steel Erection Column Horizontal Force Transfer to Outer Concrete Compression Field (ASCE 1994) 13

2.6 Outer Compressive Concrete Strut Width (Parra-Montesinos and Wight 2001) 23

2.7 Specimen #1 Joint Detailing (Bugeja et al. 1999) 26

2.8 Specimen #2 Joint Detailing (Bugeja et al. 1999) 27

2.9 Specimen #3 Joint Detailing (Bugeja et al. 1999) 28

2.10 Specimen #4 Joint Detailing (Bugeja et al. 1999) 29

2.11 Specimen #5 Joint Detailing (Bugeja et al. 1999) 30

2.12 Specimen #6 Joint Detailing (Bugeja et al. 1999) 31

2.13 Typical RCS Joint Details in Japan (AIJ, 1994) 33

3.1 Typical Mid-Rise Space Frame 34

3.2 First Yield Beam Moment Calculation 36

3.3 Loading Directions 38

3.4 Plastic Moment Calculation 39

3.5 Ultimate Interaction Diagrams for Column 42

FIGURE Page

3.6 RCS Construction Sequence (Griffis 1986) 44

3.7 Joint Formwork 45

4.1 Cruciform Cut Out of Space Frame 48

4.2 Overall Specimen Dimensions 48

4.3 Joint Moment Connection Detail 50

4.4 Joint Detailing Closeup 51

4.5 Experimental Setup 54

4.6 Column Gage Mount Anchorage 57

4.7 Clinometer and LVDT Placement 58

4.8 Photograph of Clinometers and LVDTs 59

4.9 Rebar Strain Gage Placement 59

4.10 Concrete Gage Placement 60

4.11 Photographs of Concrete Gages 61

4.12 Rossette Strain Gage Placement 62

5.1 Erection Steel Tree 65

5.2 Joint Moment Connection Detail 66

5.3 Joint Detailing 68

5.4 Shear Stud Placement 70

5.5 Slab Reinforcement Placement 71

5.6 Slab Reinforcement and Shear Stud Photoghraph 71

5.7 Column Reinforcement Elevation 73

FIGURE Page

5.8 Column Reinforcement - Cross Sections 74

5.9 Seat Compressive Concrete Strut 75

5.10 Outer Compressive Concrete Strut 76

5.11 Photographs of Column Forms 78

5.12 Photograph of Confinement Plate Clamp 81

5.13 Voids and Honeycombing in Joint Region 82

5.14 Repaired Joint Region 83

6.1 Specimen Displacement Components 86

6.2 Major Component Response (CP) 88

6.3 Minor Component Response (CP) 88

6.4 Major Component Response (FBP) 89

6.5 Minor Component Response (FBP) 89

6.6 Joint Deformation Components (Bugeja et al. 1999) 91

6.7 Crack in Joint (FBP) 92

6.8 Inner Concrete Core (CP) 93

6.9 Joint Response (CP) 94

6.10 Joint Response (FBP) 95

6.11 Joint Elongation (CP) 96

6.12 Joint Elongation (FBP) 96

6.13 Beam Moment Rotations (CP) 98

6.14 Beam Moment Rotations (FBP) 99

FIGURE Page

6.15 Beam Deformation During Testing (CP) 100

6.16 Beam Deformation During Testing (FBP) 102

6.17 Rebar Strain Gages Global Position and Loading Diagram 106

6.18 Rebar Strains, Major Direction (CP) Actuator A100 Max. Negative Displacement 107

6.19 Rebar Strains, Major Direction (FBP) Actuator A100 Max. Negative Displacement 108

6.20 Rebar Strains, Major Direction (CP) Actuator A100 Max. Positive Displacement 109

6.21 Rebar Strains, Major Direction (FBP) Actuator A100 Max. Positive Displacement 110

6.22 Rebar Strains, Minor Direction (CP) Actuator A50 Max. Negative Displacement 111

6.23 Rebar Strains, Minor Direction (FBP) Actuator A50 Max. Negative Displacement 112

6.24 Rebar Strains, Minor Direction (CP) Actuator A50 Max. Positive Displacement 113

6.25 Rebar Strains, Minor Direction (FBP) Actuator A50 Max. Positive Displacement 114

6.26 Slab Behavior of Composite Beam-Slab (CP) 115

6.27 Slab Behavior of Composite Beam-Slab (FBP) 116

6.28 Concrete Gages (CP) 118

6.29 Concrete Gages (FBP) 118

6.30 Joint Web Principle Strains (CP) 120

6.31 Joint Web Principle Strains (FBP) 121

FIGURE Page

6.32 Large Deformation Beam Moment Rotations (CP) 123

6.33 Large Deformation Beam Moment Rotations (FBP) 124

6.34 Joint Panel Shear Failure (FBP) 125

7.1 Tri-Linear Backbone Curve (Kunnath 2002) 131

7.2 Hysteretic Parameters (Kunnath 2002) 132

7.3 Equivalent Imposed Drift Angles 133

7.4 Predicted Total Response (CP) 136

7.5 Predicted Total Response (FBP) 137

7.6 Correlated Total Response (CP) 138

7.7 Correlated Total Response (FBP) 139

LIST OF TABLES

TABLE Page

2.1 k Values for Design Equations (Parra-Montesinos et al. 2003) 21

2.2 k Values for Model Equations (Parra-Montesinos and Wight 2001) 21

4.1 Concrete Compressive Strengths 52

7.1 Average Actuator Force to Induce Component Failure 129

7.2 Composite Beam Properties 130

7.3 Hysteretic Parameters 131

CHAPTER I

INTRODUCTION

1.1 HISTORICAL BACKGROUND

Composite reinforced concrete (RC) column-steel beam (RCS) frame systems have been used in high-rise building construction in zones of low to moderate seismic risk in the United States (Griffis 1986). The systems typically have a perimeter lateral load resisting system (two-dimensional framing) which consists of RC columns with a small embedded steel I-shape to carry construction loads and structural steel beams which are continuous through the columns. The structural steel skeleton expedites the construction process by creating a vertical spread of construction activities of structural steel framing, metal deck floor work, concrete floor placement, column forming, and concrete column placement. The steel beams can also be attached with shear studs to the RC slab to form a full or partially composite steel beam-concrete slab cross section. These moment frame systems have comparatively higher stiffness and lower material costs than structural steel framing alone, which increases the efficiency of the system to resist lateral loads and decreases the overall costs. However, potential failure mechanisms of composite moment frames may occur in the beam-column joint connections when resisting lateral loading. In order to better understand these joint failure mechanisms, significant research has been conducted over the past 15 years on two-dimensional composite RCS subassemblies with various joint details. In addition,

previous research at Texas A&M University was performed to evaluate the performance of three-dimensional space frame RCS systems.

1.2 RESEARCH OBJECTIVE

Extensive research has been devoted to testing and analyzing two-dimensional frames utilizing RCS structural components for application in perimeter moment frame structures. There has been limited research on three-dimensional space frame systems. The proposed research is an extension to the three-dimensional testing of RCS systems. The key uncertainty with such three-dimensional systems is the performance of the beam-column joint regions. Therefore, the emphasis of this research is to further identify RCS joint details that are constructable and have performance advantages over traditional construction materials. Joint strength models are compared with experimental data and the overall system performance is simulated with an inelastic analytical model.

1.3 SCOPE OF WORK

This chapter provides an overview and the research objectives for the thesis. Chapter II provides a literature review for both two-dimensional and three-dimensional RCS frame systems that investigates composite joint behavior and failure mechanisms. The particulars of implementing the RCS joint systems in three-dimensional space frames are discussed in Chapter III. Chapter IV outlines a plan for addressing critical issues concerning RCS construction and behavior by experimentally testing two cruciform specimens with different joint details. The construction of the composite

cruciform specimens is described in Chapter V and the resolution of constructability issues that arose during construction is addressed with relation to real world applications of the joint details that are tested. In Chapter VI, the experimental results from the acquired data are presented to describe the specimen components and joint behaviors. Chapter VII compares the results of the experimental results with that of the analytical inelastic predictions. Conclusions made from both the experimental and analytical research and recommendations for future research and design of RCS moment frames are given in Chapter VIII.

CHAPTER II

BACKGROUND AND PRESENT STATE OF KNOWLEDGE

2.1 GENERAL

Previous research in the United States and abroad on RCS frame systems is discussed in this chapter. The various joint details tested and major findings of the previous programs are overviewed.

2.2 RESEARCH AT THE UNIVERSITY OF TEXAS

Fifteen two-thirds scale cruciform-shaped specimens were tested experimentally at The University of Texas at Austin (Sheikh 1987; Deierlein 1988; Deierlein et al. 1989) on two-dimensional reinforced concrete (RC) column-steel beam assemblies. The research was instrumental in identifying two beam-column joint failure mechanisms. One of the failure mechanisms was joint panel shear (Fig. 2.1a), which is a pure shear mechanism. The components of the joint shear resistance were identified as from the steel beam web, inner concrete compressive strut, and outer concrete compressive strut (Fig. 2.2). Web panel resistance was increased when web doubler plates were added by welding a plate within the joint region to the steel beam web. Face bearing plates or web stiffeners across the full depth of the beams were welded to the beam web and flanges at the column faces to activate the inner concrete compressive strut that is located within the structural steel beam flanges. Confining ties

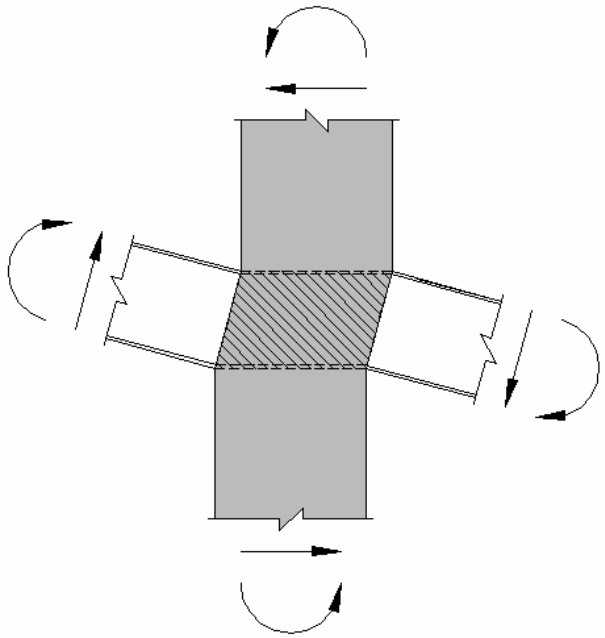

(a) Panel Shear

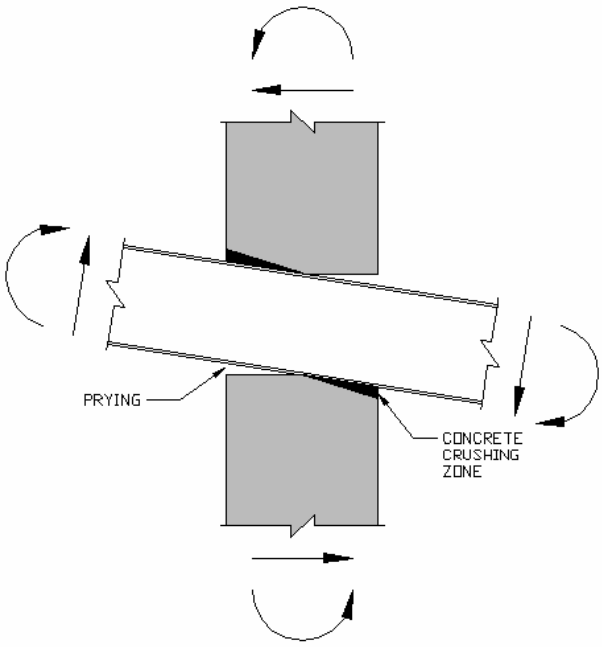

(b) Vertical Bearing

FIG. 2.1 JOINT FAILURE MECHANISMS (ASCE 1994)

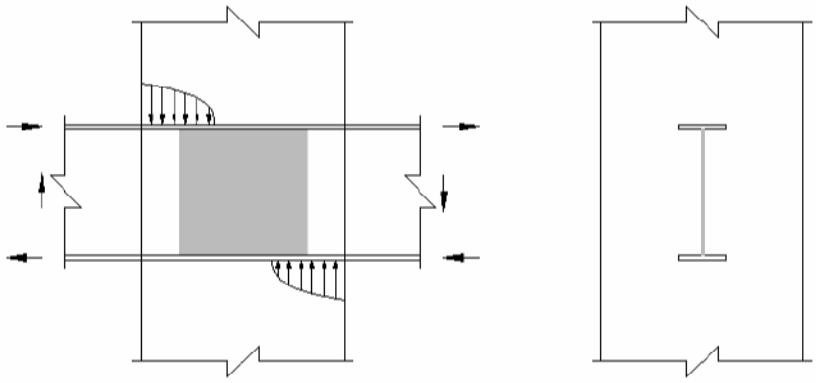

(a) Structural Steel Web

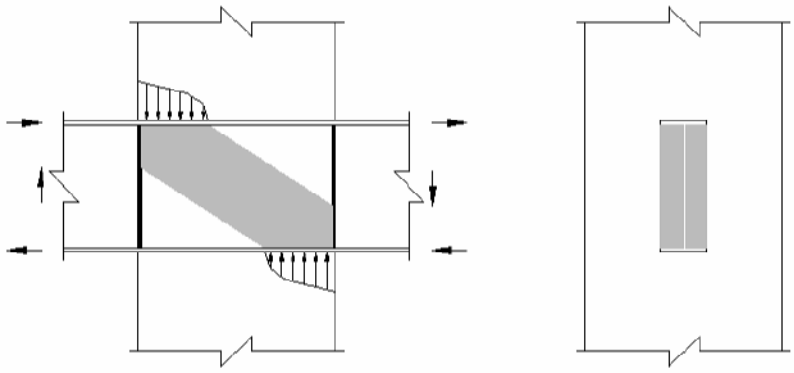

(b) Inner Concrete Compression Strut

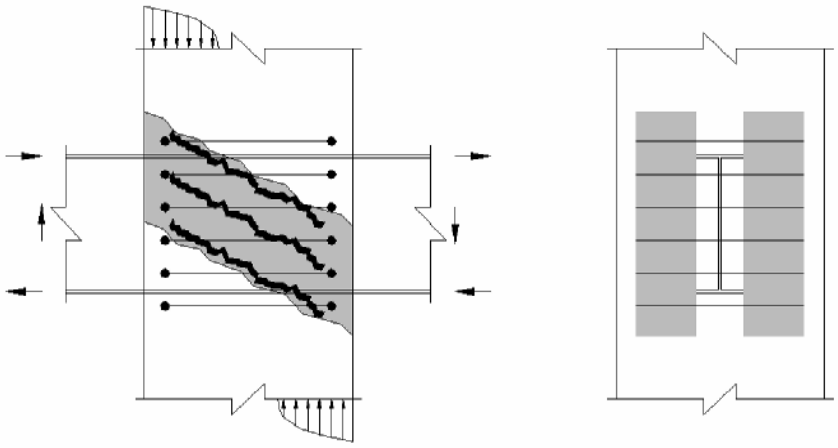

(c) Outer Concrete Compressive Strut

FIG. 2.2 RESISTANCE TO JOINT PANEL SHEAR (ASCE 1994)

located within and adjacent to the joint were used to activate the outer concrete strut, which formed outside the flanges of the structural steel beam extending from below the joint to above the joint. The other joint failure mechanism, vertical bearing failure (Fig. 2.1b), was caused by concrete crushing directly above and below the structural steel beam as it rotated as a rigid body through the joint. Reinforcing steel bars welded vertically to the flanges of the beams and extended face bearing plates were used to prevent vertical bearing failure. Extended face bearing plates (E-FBP) to improve the outer strut shear mechanism are vertical plates that are welded to the flanges above and below the structural steel beam which bears against the concrete column. E-FBPs are typically stiffened with a plate that is welded orthogonally to the E-FBP and to the center line of the beam flanges.

2.3 RESEARCH AT CORNELL UNIVERSITY

As an extension to the research done at The University of Texas, research was conducted at Cornell University (Kanno 1993) on 19 RCS two-dimensional interior beam-column specimens under quasi-static reversed cyclic loading. In addition to the details used at The University of Texas, band plates, joint plates, and transverse beams were evaluated for joint performance (Fig. 2.3). Band plates encompassed the RC column above and below the beam and were intended to confine the concrete in these areas as well as protect the joint against vertical bearing. The band plates also enhanced the shear resistance of the outer concrete compression strut. Joint plates completely encased the joint and were lined with shear studs to increase bonding to the RC column.

The joint plates increased the shear capacity of the joint by adding confinement and enhancing the width of the inner concrete strut. The transverse beams and axial column load were also found to enhance the shear strength of the joint.

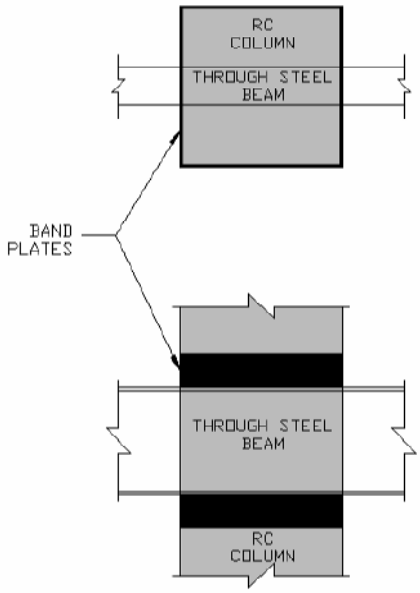

(a) Band Plates

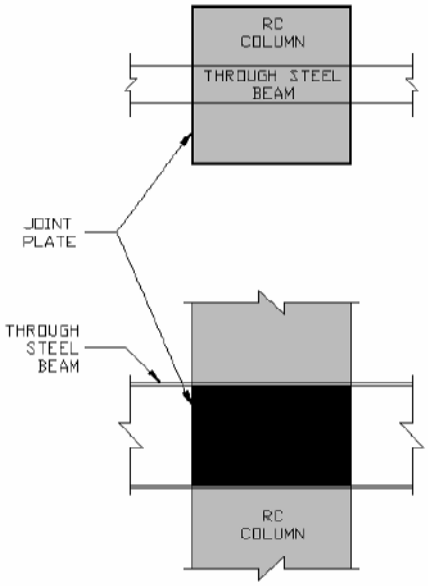

(b) Joint Plates

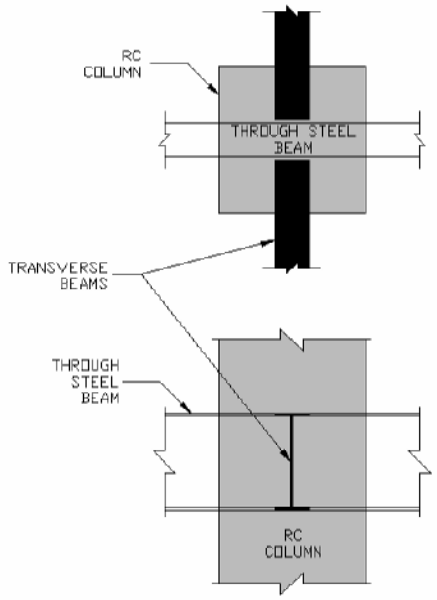

(c) Transverse Beam

FIG. 2.3 ADDITIONAL JOINT COMPONENTS (Kanno 1993)

2.4 ASCE GUIDELINES

Based primarily on the research conducted at The University of Texas and Cornell University, recommendations for joint vertical bearing and panel shear strengths and detailing requirements were developed (ASCE 1994). The vertical bearing strength calculations are summarized in Eqs. (2.1) – (2.10).

$$\Sigma M_c + 0.35 h_c \Delta V_b \le \phi \left[0.7 h_c C_{cn} + h_{vr} \left(T_{vrn} + C_{vrn} \right) \right] \tag{2.1}$$

$$\Sigma M_c = \left(M_{c1} + M_{c2} \right) \tag{2.2}$$

$$\Delta V_b = V_{b2} - V_{b1} \tag{2.3}$$

$$C_{cn} = 0.6 f_c' b_j h_c \tag{2.4}$$

$$\left(T_{vrn} + C_{vrn} \right) \le 0.3 f_c' b_j h_c \text{ - vertical reinforcement limitation} \tag{2.5}$$

where

M_{c1}, M_{c2} = moment demand on RC columns adjacent to joint at ends 1 and 2
V_{b1}, V_{b2} = shear demand in steel beams adjacent to joint at ends 1 and 2
h_c = depth of RC column measured parallel to the structural steel beam
ϕ = strength reduction factor for bearing failure (0.7)
h_{vr} = distance between vertical joint reinforcement
C_{cn} = nominal concrete bearing strength
T_{vrn} = nominal strength of vertical joint reinforcement in tension
C_{vrn} = nominal strength of vertical joint reinforcement in compression
f_c' = ultimate compressive concrete stress
b_j = effective width of joint panel

The procedure necessary to determine the effective width of the joint panel is outlined in Eqs. (2.6) – (2.10).

$$b_j = b_i + b_o \tag{2.6}$$

$$b_o = C\left(b_m - b_i\right) < 2d_o \tag{2.7}$$

$$b_m = \frac{\left(b_f + b\right)}{2} < b_f + h_c < 1.75b_f \tag{2.8}$$

$$C = \left(\frac{x}{h_c}\right)\left(\frac{y}{b_f}\right) \tag{2.9}$$

$$d_o = 0.25d \text{ if steel column is present} \tag{2.10}$$

where

b_i = inner panel width, which is the larger of the FBP width and beam flange width
b_o = outer panel width
b_m = maximum effective width of the joint region
b = RC column width measured perpendicular to steel beam
C = coefficient that is based on joint demensions
x = location of steel column
y = width of steel column
b_f = width of steel beam flange
d_o = depth of outer compression field extension
d = depth of steel beam

Joint panel shear strength calculations are shown in Eqs. (2.11) – (2.29).

$$\Sigma M_c - V_b\left(jh\right) \le \phi\left[V_{sn}d_f + 0.75V_{csn}d_w + V_{cfn}\left(d + d_o\right)\right] \tag{2.11}$$

$$(jh) = \frac{\Sigma M_c}{\phi\left(T_{vrn} + C_{vrn} + C_c\right) - \Delta V_b / 2} \geq 0.7 h_c \tag{2.12}$$

$$C_c = 2 f_c' b_j a_c \tag{2.13}$$

$$a_c = \frac{h_c}{2} - \sqrt{\frac{h_c^2}{4} - K} \leq 0.3 h_c \tag{2.14}$$

$$K = \frac{1}{\phi 2 f_c' b_j}\left[\Sigma M_c + \Delta V_b h_c / 2 - \phi\left(T_{vrn} + C_{vrn}\right) h_{vr}\right] \tag{2.15}$$

where

V_b = shear demand on structural steel beam adjacent to joint
(jh) = horizontal distance between bearing force resultant
ϕ = strength reduction factor for shear (0.7)
V_{sn} = nominal shear resistance of steel web panel
d_f = center-to-center distance between the steel beam flanges
V_{csn} = nominal shear resistance of inner concrete compression strut
d_w = depth of steel beam web
V_{cfn} = nominal shear resistance of outer concrete compression strut
C_c = vertical bearing force
a_c = length of concrete bearing zone
K = coefficient

The three components (steel web panel, inner compressive strut, and outer compressive strut) that resist joint panel shear are shown in Fig. 2.4. The resistance provided by the structural steel beam web panel is shown in Eq. (2.16).

$$V_{sn} = 0.6 F_{ysp} t_{sp} (jh) \tag{2.16}$$

where

F_{ysp} = yield strength of steel web panel

t_{sp} = thickness of steel web panel

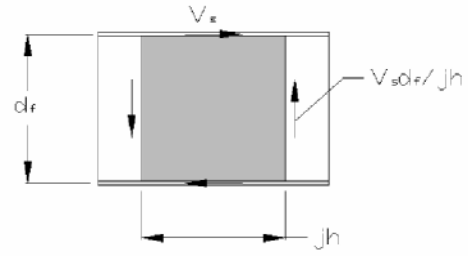

(a) Steel Panel

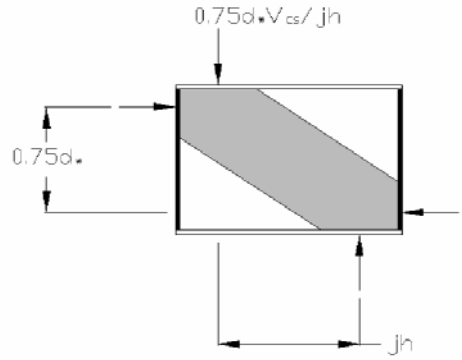

(b) Inner Compressive Concrete Strut

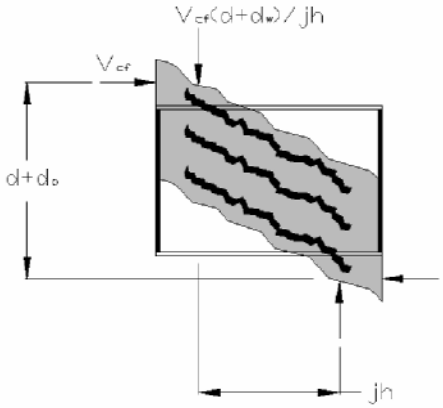

(c) Outer Compressive Concrete Strut

FIG. 2.4 ASCE RECOMMENDED JOINT SHEAR RESISTANCE COMPONENTS (ASCE 1994)

The resistance provided by the inner concrete strut is shown in Eqs. (2.17) and (2.18).

$$V_{csn} = 1.7\sqrt{f_c'}b_p \le 0.5 f_c' b_p d_w \tag{2.17}$$

$$b_p \le b_f + 5t_p \le 1.5 b_f \tag{2.18}$$

where

b_p = effective face bearing plate width
t_p = thickness of face bearing plate

The resistance provided by the outer concrete strut is shown in Eqs. (2.19) – (2.22) assuming the minimum joint reinforcement configurations comply with Eqs. (2.23) and (2.24). The horizontal force transfer of the outer concrete compression strut for both the face bearing plate and steel erection column details are shown in Fig. 2.5.

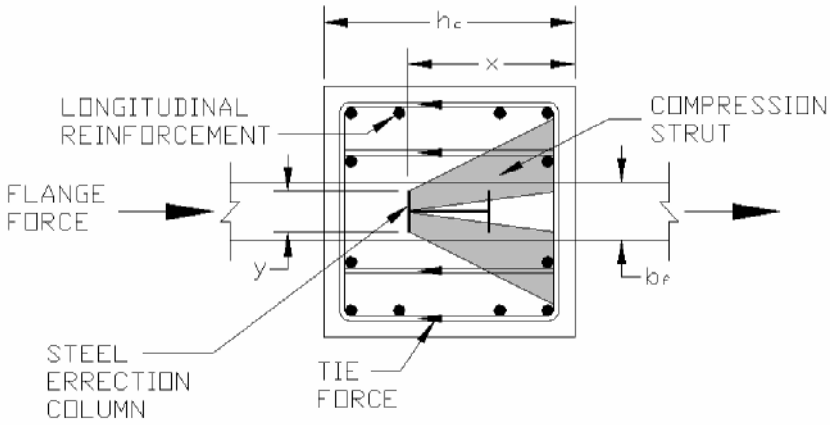

FIG. 2.5 STEEL ERECTION COLUMN HORIZONTAL FORCE TRANSFER TO OUTER CONCRETE COMPRESSION FIELD (ASCE 1994)

$$V_{cfn} = V_c' + V_s' \le 1.7\sqrt{f_c'}b_o h_c \quad \text{where } f_c' \text{ is in MPa} \tag{2.19}$$

$$V_c' = 0.4\sqrt{f_c'}b_o h_c = 0 \text{ if the column is in tension } \left(\text{where } f_c' \text{ is in MPa}\right) \tag{2.20}$$

$$V_s' = \frac{a_{sh} F_{ysh} 0.9 h_c}{s_h} \tag{2.21}$$

$$a_{sh} \ge 0.004 b s_h \tag{2.22}$$

where

V_c' = nominal concrete strength in outer concrete compressive field
V_s' = nominal transverse reinforcement strength in outer concrete compressive field
a_{sh} = cross-sectional area of reinforcing bars in each layer of ties
F_{ysh} = yield strength of transverse reinforcing steel
s_h = spacing between transverse reinforcing steel

As a minimum for all joints, three layers of ties should be provided above and below the beam, and the bars in each layer should be at least equivalent to the following:

$$\begin{aligned} &b \le 500 \text{ mm} \quad \rightarrow \quad 4-10 \text{ mm bars} \\ &500 \text{ mm} \le b \le 750 \text{ mm} \quad \rightarrow \quad 4-12 \text{ mm bars} \\ &b \ge 750 \text{ mm} \quad \rightarrow \quad 4-16 \text{ mm bars} \end{aligned} \tag{2.23}$$

Where the outer compression field is used to resist shear, the minimum tie requirement above and below the beam may be governed by Eq. (2.24).

$$A_{tie} \ge \frac{V_{cf}}{F_{ysh}} \tag{2.24}$$

where

A_{tie} = total cross-sectional transverse reinforcement area
F_{ysh} = yield strength of the transverse reinforcement

The transverse reinforcement should be closed rectangular ties that can resist tension parallel and perpendicular to the beam. The three layers should be located within a distance of $0.4d$ above and below the beam.

The required thickness of the FPB is a function of geometry, support conditions, yield strength, and distribution of concrete bearing forces. Face bearing plates should be detailed to meet the conditions outlined in Eqs. (2.25) – (2.29) to allow proper force transfer.

$$t_p \geq \frac{\sqrt{3}}{b_f F_{up}}\left(V_{cs} - b_f t_w F_{yw}\right) \tag{2.25}$$

$$t_p \geq \frac{\sqrt{3}V_{cs}}{2b_f F_{up}} \tag{2.26}$$

$$t_p \geq 0.20\sqrt{\frac{V_{cs} b_p}{F_{yp} d_w}} \tag{2.27}$$

$$t_p \geq \frac{b_p}{22} \tag{2.28}$$

$$t_p \geq \frac{\left(b_p - b_f\right)}{5} \tag{2.29}$$

where

t_p = thickness of face bearing plate
V_{cs} = inner concrete compressive field force $\left(\leq V_{csn}\right)$
F_{up} = specified tensile strength of the face bearing plate
t_w = thickness of steel beam web
F_{yp} = yield strength of the face bearing plate
b_p = width of face bearing plate

Welds connecting the face bearing plate to the structural steel beam should be sized to resist V_{csn} in both shear and flexure.

2.5 U.S-JAPAN COOPERATIVE RESEARCH PROGRAM

In 1979, the National Science Foundation of the United States and the Architectural Institute of Japan began the U.S.-Japan Cooperative Research Program. The objective of this program was to improve seismic safety practices in both countries (U.S.-Japan Planning Groups 1992). Using both reduced and full scale model testing and analytical modeling, the program was divided into five phases: reinforced concrete, structural steel, masonry, precast/prestressed concrete and composite steel/reinforced concrete structures.

Composite RC columns and steel (S) beams, when used in unison to create a RCS moment frame, potentially serves as an alternative to traditional concrete or steel moment frames used in high seismic zones. Research performed in both countries was

conducted to formulate design criteria and gain an understanding of system behavior in seismic regions. The coordinated U.S.-Japan research has improved seismic design models and criteria by: testing and analyzing RCS beam-column connection subassemblies; testing and analyzing RCS moment frames; simulating RCS building systems; and developing design guidelines. Even though RCS construction utilizes traditional construction of both RC and steel, the behavior of the beam-column connections was not completely understood during seismic loading; thus the connection region was the focus of the research. Many different connection configurations were tested to gain a better understanding of the force-transfer mechanisms that resist horizontal loads. It was shown in these research programs that proper joint detailing can provide reliable strength and ductility for seismic design.

2.6 RESEARCH AT THE UNIVERSITY OF MICHIGAN

As part of the U.S.-Japan cooperative research program, research conducted at the University of Michigan (Parra-Montesinos and Wight 2000) consisted nine three-quarter scale exterior through-beam RCS connections subjected to cyclic lateral loading. Joint detailing consisted of various configurations of confinement plates, face bearing plates, band plates, bearing bars and stirrups within the joint. Steel fiber concrete and an Engineered Cementitious Composite (ECC) were compared to conventional high strength concrete to evaluate comparative advantages of using more sophisticated building materials in the joint regions for resisting lateral loading. Minimum hoop volume of 0.9% and spacing requirements based on the beam depth and column width

were obtained to provide adequate confinement and joint shear strength based on experimental testing. It was also determined that 80% of the steel beam web embedded within the joint participated in resisting shear deformations of the joint. Longitudinal reinforcing bars in the columns were found to slip under cyclic loading before reaching their yield strength. Rigid body rotations of the steel beam caused by bearing deformations contributed up to half of the total story drift measured in the test specimens.

Design and modeling equations for RCS joints by Parra-Montesinos and Wight, 2001 and Parra-Montesinos and Wight, 2003 were proposed to predict joint panel shear as follows:

$$\left(V_j\right)_{\max} \le \phi V_{njh} \tag{2.30}$$

where

$\left(V_j\right)_{\max}$ = maximum applied joint shear force demand under factored loading
ϕ = strength reduction factor for shear failure (strength - 0.85, joint damage and drift - 0.7)
V_{njh} = combined joint shear resistance

The maximum shear force transferred into the connection is defined in Eq. (2.31).

$$\left(V_j\right)_{\max} = \frac{\Sigma\left(M_u\right)_{\text{beam}}}{d - t_f} - \left(V_u\right)_{\text{col}} \tag{2.31}$$

where

$\Sigma(M_u)_{\text{beam}}$ = sum of the nominal moment capacities of composite beam-slab sections at both sides of the joint

d = depth of the steel beam

t_f = flange thickness of the steel beam

$(V_u)_{col}$ = maximum column shear force demand under factored loading

The resistance to shear is provided by the sum of three mechanisms: structural steel beam web, inner concrete strut, and outer concrete strut which is shown in Eq. (2.32).

$$V_{njh} = V_{wh} + V_{ih} + V_{oh} \tag{2.32}$$

The resistance provided by the structural steel web is shown in Eq. (2.33).

$$V_{wh} = k_w \frac{f_y}{\sqrt{3}} t_w h_c \tag{2.33}$$

where

V_{wh} = shear strength of steel beam web

k_w = stength factor of steel beam web

(0.9 interior joint or 0.8 exterior joint)

f_y = yield strength of steel beam

t_w = web thickness of steel beam

h_c = depth of the RC column measured parallel to the steel beam

The shear strength of the inner concrete strut can be predicted from the Eqs. (2.34) and (2.35).

$$\begin{aligned} V_{ih} &= k_i f_c' \left(1.13 - 0.0048 f_c'\right) h_c \left(b_f - t_w\right) \quad \text{where } f_c' \text{ is in MPa} \\ &= k_i f_c' \left(1.13 - 0.03307 f_c'\right) h_c \left(b_f - t_w\right) \quad \text{where } f_c' \text{ is in ksi} \end{aligned} \tag{2.34}$$

$$\begin{aligned} V_{nih} &= 0.3 \nu_{ibase} f_c' \left(1.13 - 0.0048 f_c'\right) k_1 k_2 h_c \left(b_f - t_w\right) \quad \text{where } f_c' \text{ is in MPa} \\ &= 0.3 \nu_{ibase} f_c' \left(1.13 - 0.03307 f_c'\right) k_1 k_2 h_c \left(b_f - t_w\right) \quad \text{where } f_c' \text{ is in ksi} \end{aligned} \tag{2.35}$$

where

V_{ih} = design shear strength of inner concrete strut mechanism
V_{nih} = nominal shear strength of inner concrete strut mechanism
ν_{ibase} = non-demensional strength factor for the inner strut (1.07 interior joint or 0.70 exterior joint)
k_i = strength factor for inner strut (Table 2.1)
k_1 = joint loading due to location (Table 2.2)
k_2 = accounts for confinement conditions for the inner concrete strut (Table 2.2)

The shear strength of the outer concrete strut can be predicted from the Eqs. (2.36) and (2.37).

$$\begin{aligned} V_{oh} &= k_o f_c' \left(1.13 - 0.0048 f_c'\right) h_c b_o \quad \text{where } f_c' \text{ is in MPa} \\ &= k_o f_c' \left(1.13 - 0.03307 f_c'\right) h_c b_o \quad \text{where } f_c' \text{ is in ksi} \end{aligned} \tag{2.36}$$

$$\begin{aligned} V_{noh} &= 0.30 \nu_{obase} f_c' \left(1.13 - 0.0048 f_c'\right) k_1 k_2 k_3 h_c b_o \quad \text{where } f_c' \text{ is in MPa} \\ &= 0.30 \nu_{obase} f_c' \left(1.13 - 0.03307 f_c'\right) k_1 k_2 k_3 h_c b_o \quad \text{where } f_c' \text{ is in ksi} \end{aligned} \tag{2.37}$$

where

V_{oh} = design shear strength of outer concrete strut mechanism

V_{noh} = nominal shear strength of outer concrete strut mechanism

k_o = strength factor for outer compressive strut (Table 2.1)

ν_{obase} = non-demensional strength factor for the outer strut $(0.53$ interior joint or 0.34 exterior joint$)$

k_3 = effect of confinement on concrete $(\text{Table } 2.2)$

TABLE 2.1 k VALUES FOR DESIGN EQUATIONS (Parra-Montesinos et al. 2003)

			Standard Joint Detail	
Target Shear Deformation	Performance Level	k Factor	Interior	Exterior
0.50%	Immediate Occupancy	k_i	0.25	0.17
		k_o	0.14	0.10
1.20%	Collapse Prevention	k_i	0.32	0.21
		k_o	0.17	0.11

TABLE 2.2 k VALUES FOR MODEL EQUATIONS (Parra-Montesinos and Wright 2001)

Factor	Exterior Joint	Interior Joint	Joint Details
k_1	1.0	1.0	Standard joint with hoops
k_1	1.2	1.1	Steel band plates without hoops, dowel bars, or fiber reinforced concrete
k_1	1.4	1.2	Steel band plates with hoops or steel confinement plate
k_2	1.0	1.0	No transverse beams
k_2	1.15	1.15	Transverse beams
k_3	1.1	1.1	Standard joint with hoops
k_3	1.3	1.3	Steel band plates without hoops
k_3	1.5	1.5	Steel band plates with hoops
k_3	2.0	2.0	Steel confinement plates

The width of the outer strut which is engaged by a structural steel column is shown in Fig. 2.6 and is defined as Eq. (2.38).

$$b_o = \frac{\left(h_c + d_{scol}\right)}{3} + b_{scol} - b_f \le b_{core} - b_f \tag{2.38}$$

where

V_{oh} = shear strength of outer concrete strut mechanism
k_o = strength factor for outer compressive strut (Table 2.1)
ν_{obase} = non-demensional strength factor for the outer strut $\left(0.53 \text{ interior joint or } 0.34 \text{ exterior joint}\right)$
k_3 = effect of confinement on concrete $\left(\text{Table } 2.1\right)$
b_o = width of outer concrete strut
d_{scol} = depth of structural steel column
b_{scol} = flange width of structural steel column

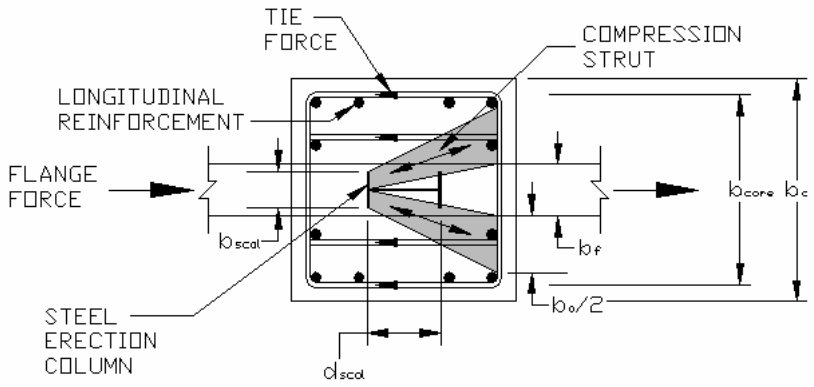

(a) Steel Column Orientation Used in Design and Model Equations

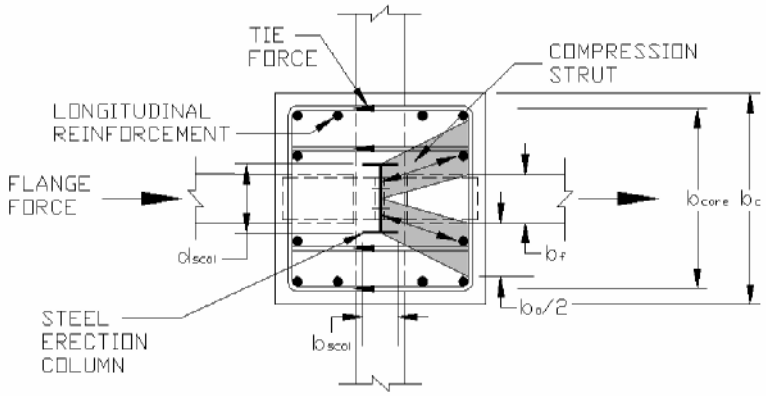

(b) Steel Column Orientation used in Experiment

FIG. 2.6 OUTER COMPRESSIVE CONCRETE STRUT WIDTH (Parra-Montesinos and Wight 2001)

2.7 RESEARCH AT TEXAS A&M UNIVERSITY

At Texas A&M University, an experimental and analytical program was conducted to evaluate the seismic performance and required detailing for space frame RCS assemblies (Bracci et al. 1999). Six cruciform specimens were tested, varying only in their joint detailing and shown in Fig. 2.7 – Fig. 2.12 (Bugeja et al. 1999 and 2000).

The first two (labeled #1 and #2) utilized face bearing plates and transverse reinforcement in the joint. Both specimens were intentionally designed to fail in the joint by either joint panel shear or vertical bearing mechanisms, respectively. Specimen #1 had vertical bars welded to the flanges of the continuous through-beams to enhance vertical bearing strength, and specimen #2 had web doubler plates plug welded to the continuous through-beam to increase the joint panel shear strength. All specimens incorporated joint details that include steel band plates around the joint directly above and below the steel beam to prevent vertical bearing failure and enhance shear strength except for specimens #1 and #2. The third specimen (#3) had bent joint (confinement) plates that were welded to face bearing plates to increase the joint strength. The fourth (#4) and fifth (#5) specimens utilized a hexagon-shaped joint to relocate the beam hinge further from the composite column. Both joints utilized bent plates that were welded to face bearing plates to form a hexagon shaped joint that encompassed the square RCS column, the only difference was that one system used extended bent face bearing plates to simplify the construction process by reducing the field welding complications. Compared to the first five specimens that modeled interior column configurations, the final specimen (#6) represented an exterior column connection that utilized extended bent face bearing plates to form a hexagon shaped joint.

The success of the joint details tested in this program was determined on the weak beam/strong joint and column criterion during a seismic event. This criterion was met for specimens #1 - #3 in the direction of the continuous through-beam and for

specimens #4 - #6 where a desirable beam failure mechanism developed. However, specimens #1 and #2 had undesirable joint failure mechanisms as predicted. Specimen #3 had an unexpected failure due to vertical bearing and fractures that occurred in the joint (confinement) plates. The joint (confinement) plates that encompassed the joint fractured at the 90° bend most likely due to torsion transmitted from the beams in flexure.

Constructability issues related to RCS construction were also addressed in this research program. While previous research focused on implications of RCS systems during seismic excitations, it was noted that RCS construction has been typically used in areas of low seismic risk where the design of high rise systems were controlled by wind loads. The most prevalent constructability issue was related to beam-column joint strength and confinement. A typical detail used in construction was the overlapping cross-ties that were passed through holes drilled in the webs of the structural steel beams that frame into the joint. This detailing was utilized in specimens #1 and #2 and has proven in the past to be difficult to construct.

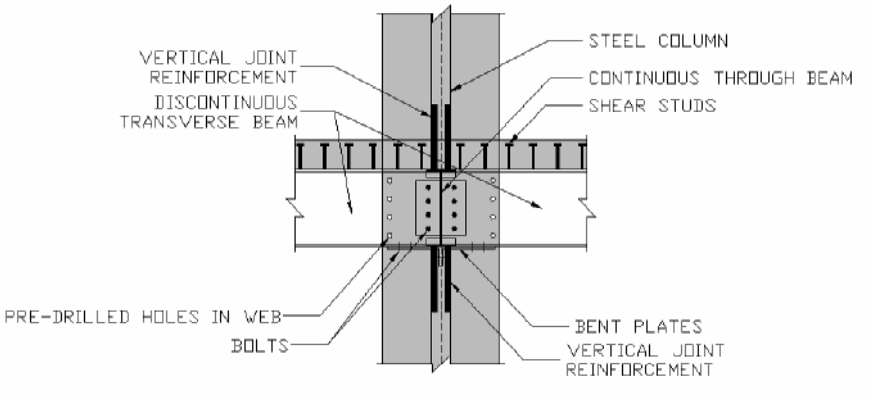

(a) Interior Joint Detailing

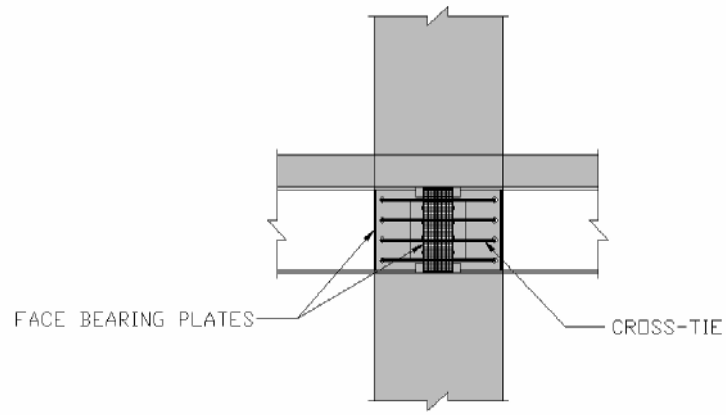

(b) Exterior Joint Detailing

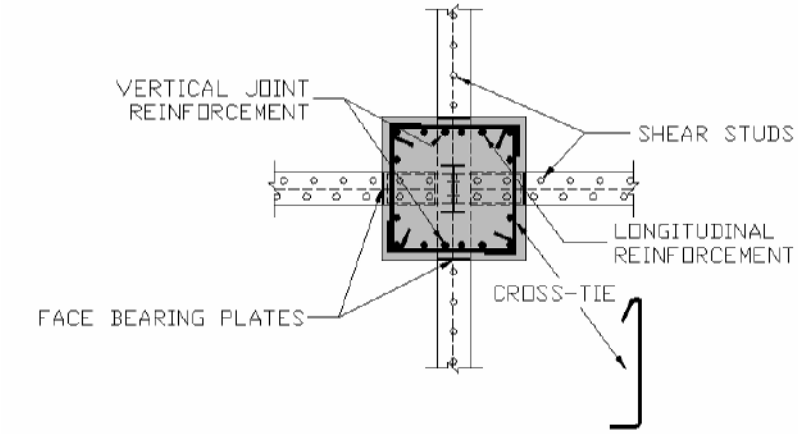

(c) Joint Cross Section

FIG. 2.7 SPECIMEN #1 JOINT DETAILING (Bugeja et al. 1999)

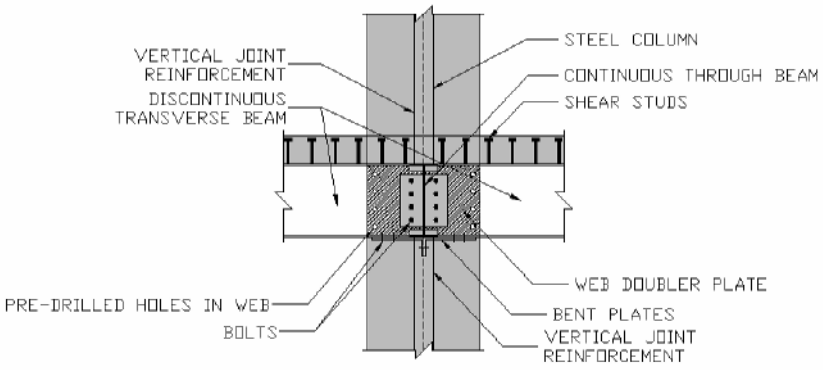

(a) Interior Joint Detailing

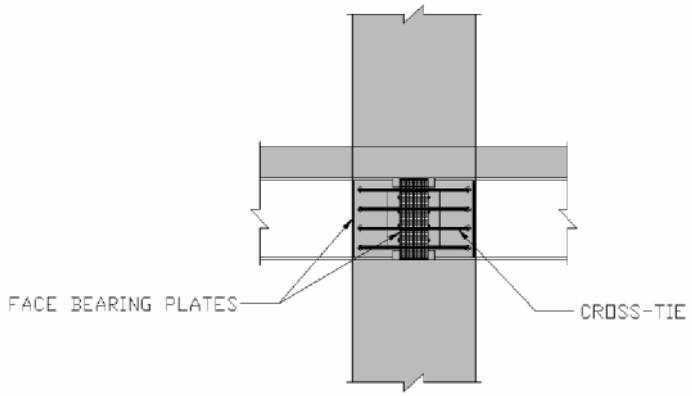

(b) Exterior Joint Detailing

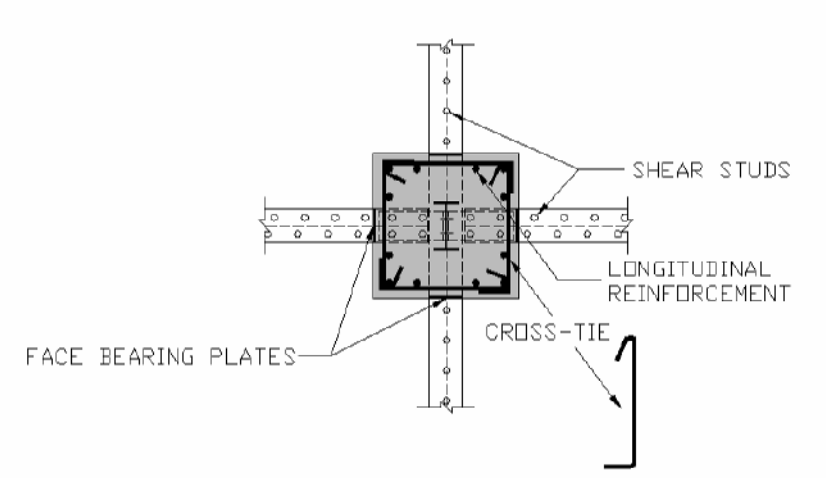

(c) Joint Cross Section

FIG. 2.8 SPECIMEN #2 JOINT DETAILING (Bugeja et al. 1999)

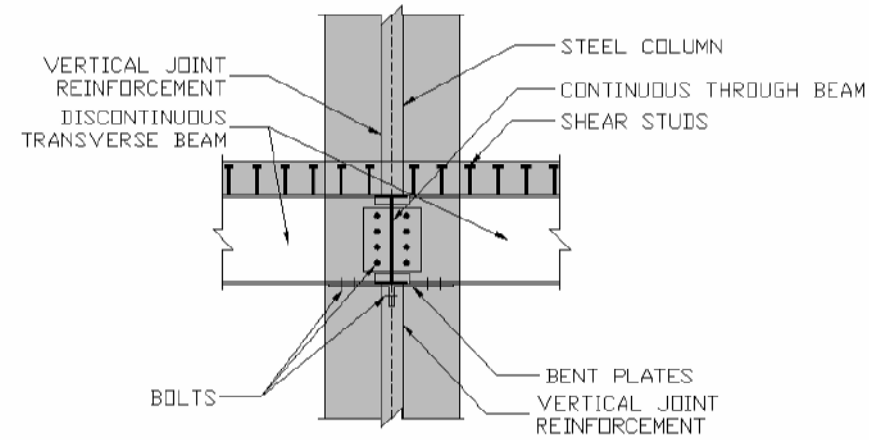

(a) Interior Joint Detailing

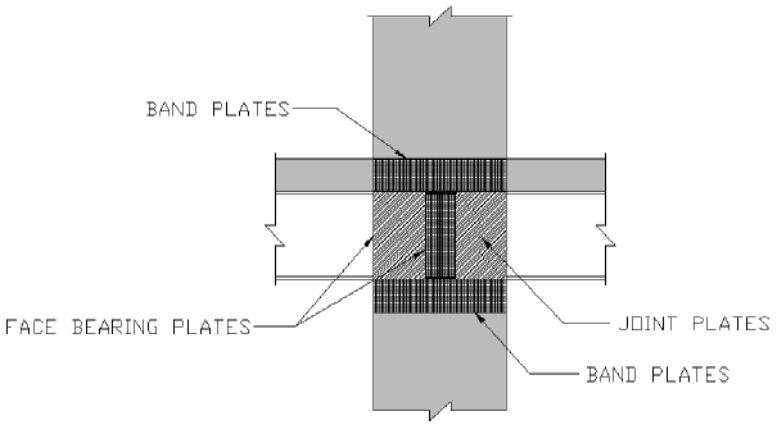

(b) Exterior Joint Detailing

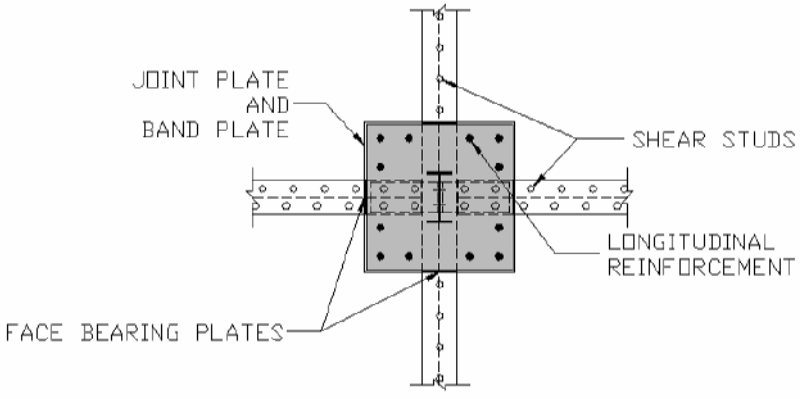

(c) Joint Cross Section

FIG. 2.9 SPECIMEN #3 JOINT DETAILING (Bugeja et al. 1999)

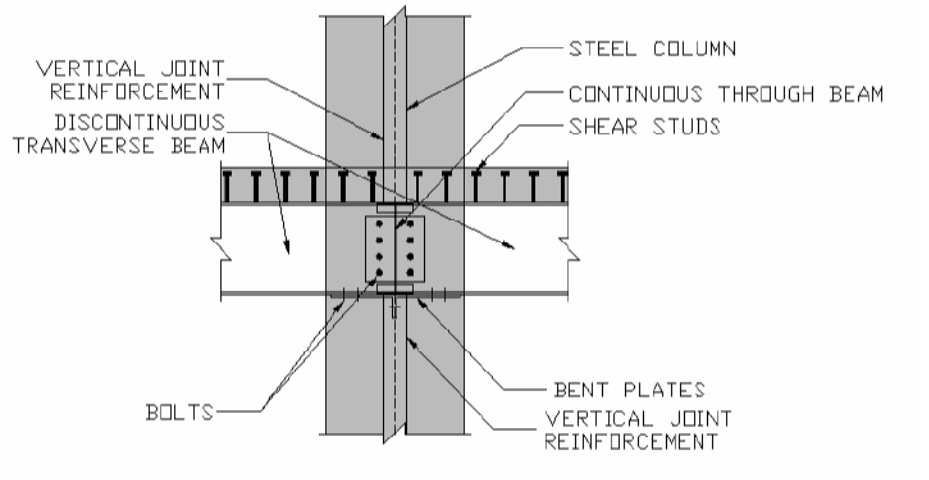

(a) Interior Joint Detailing

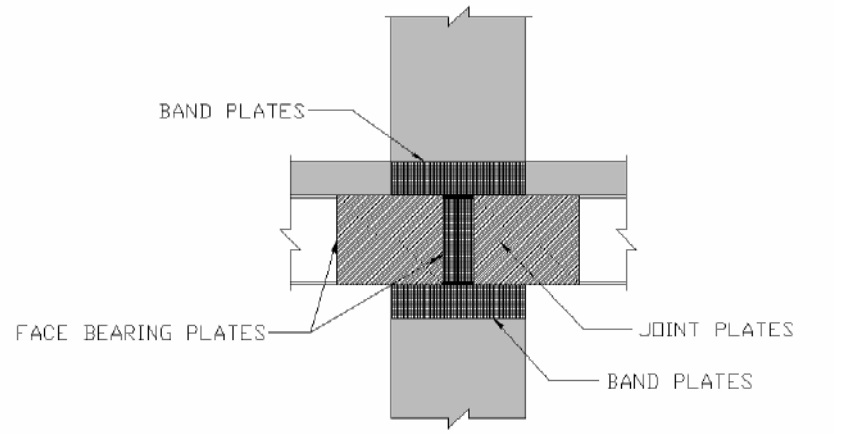

(b) Exterior Joint Detailing

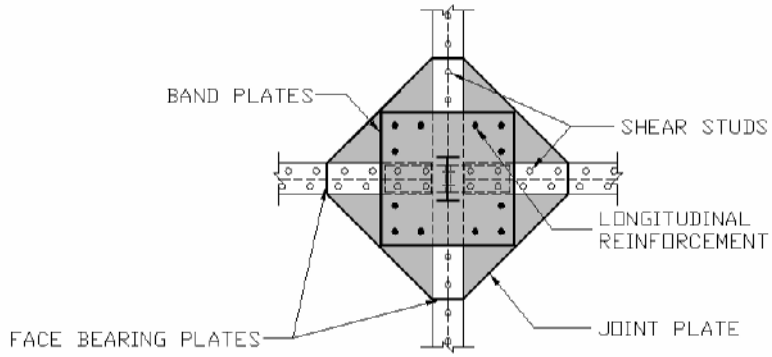

(c) Joint Cross Section

FIG. 2.10 SPECIMEN #4 JOINT DETAILING (Bugeja et al. 1999)

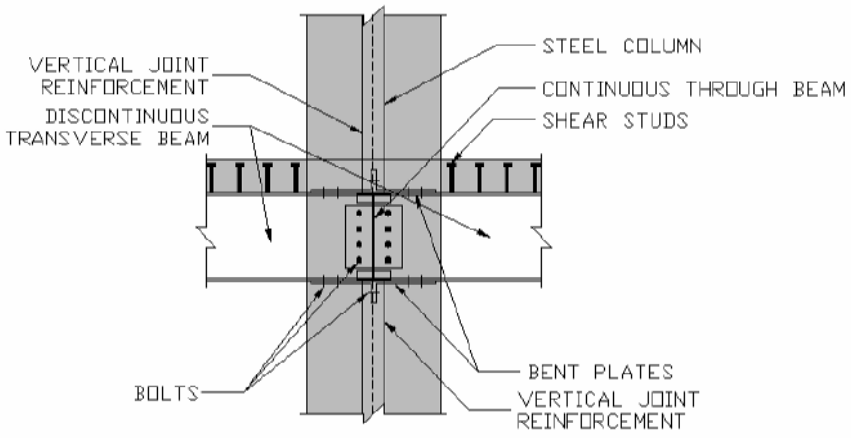

(a) Interior Joint Detailing

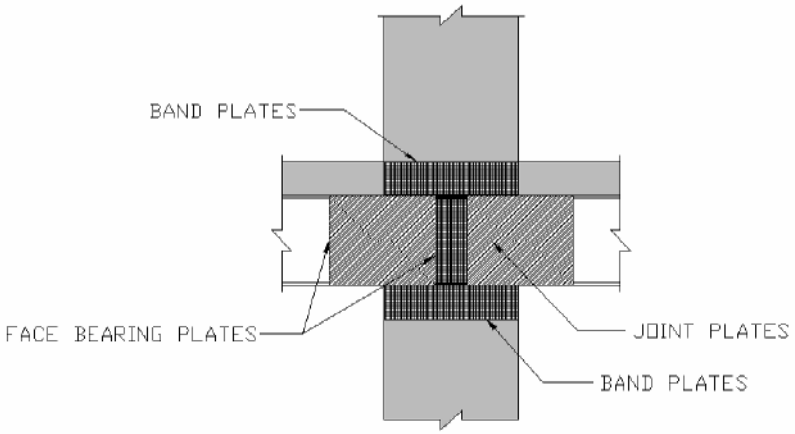

(b) Exterior Joint Detailing

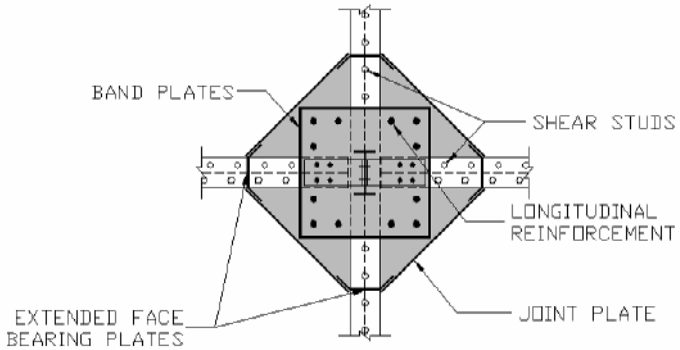

(c) Joint Cross Section

FIG. 2.11 SPECIMEN #5 JOINT DETAILING (Bugeja et al. 1999)

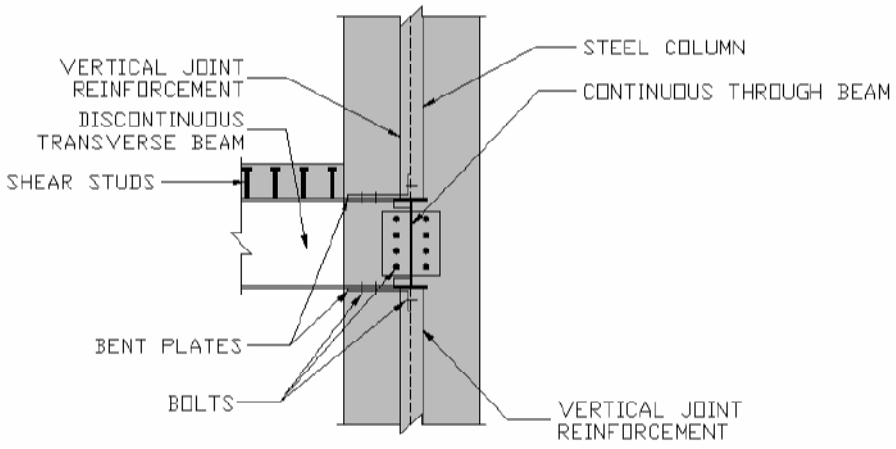

(a) Interior Joint Detailing

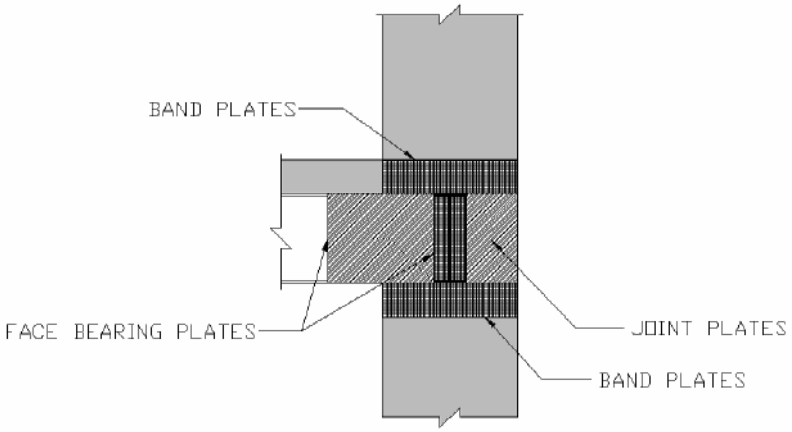

(b) Exterior Joint Detailing longitudinal

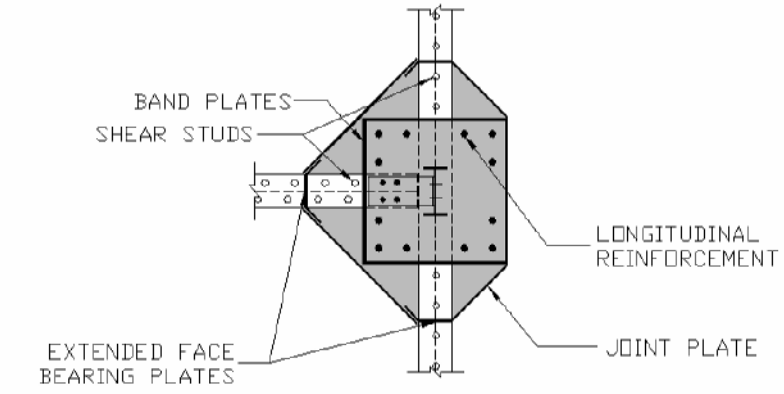

(c) Joint Cross Section

FIG. 2.12 SPECIMEN #6 JOINT DETAILING (Bugeja et al. 1999)

2.8 JAPANESE RESEARCH AND GENERAL PRACTICES

In addition to U.S. practice, Japanese practice of RCS construction typically utilize heavy steel columns that are continuous through the joint and later encased in concrete, and beams that connect to the steel columns, defined as SRC construction (Wakabayash et al. 1983). SRC frame systems are typically implemented in low- to mid-rise space frame systems.

Over 400 specimens were proof tested during the 1980's and early 1990's but did not address the internal joint force transfer mechanisms. With the foundation of the U.S.-Japan Cooperative Research Program, 56 specimens were tested to identify the force-transfer mechanisms for certain connection detailing. This research identified the same joint panel shear and vertical bearing mechanisms found in U.S. research (Nishimura et al. 1986). Simple design equations were produced by the AIJ (Architectural Institute of Japan) to predict the joint shear strength and following research intended to develop joint detailing that increased joint strength and simplify construction (Sakaguchi et al. 1988). The guidelines for joint panel shear generally agree with that of the ASCE guidelines (1994) and Kanno's (1993) joint bearing strength model was adopted to predict joint bearing resistance mechanism. Typical RCS joint details that evolved out of this program are shown in Fig. 2.13, which incorporate both RCS joint categories: through-column and through-beam. Bi-directional loading was also proven to reduce the connection strength of the joint and a large selection of joint detail configurations were specified by design standards that were created from this

research, many of which utilize joint plates. Three-dimensional nonlinear finite element models were used by Noguchi and Kim (1997 and 1998) to examine the internal force transfer mechanisms of the RCS joint. Research varying axial load found that higher axial loads up to 70% of the column crushing strength increased the joint strength, yet decreased the ductility of the composite joint. Research has shown that when the RCS joints are properly detailed, forcing failure in the beam rather than the joint region, that it is possible for the system to provide sufficient strength and ductility to resist earthquakes.

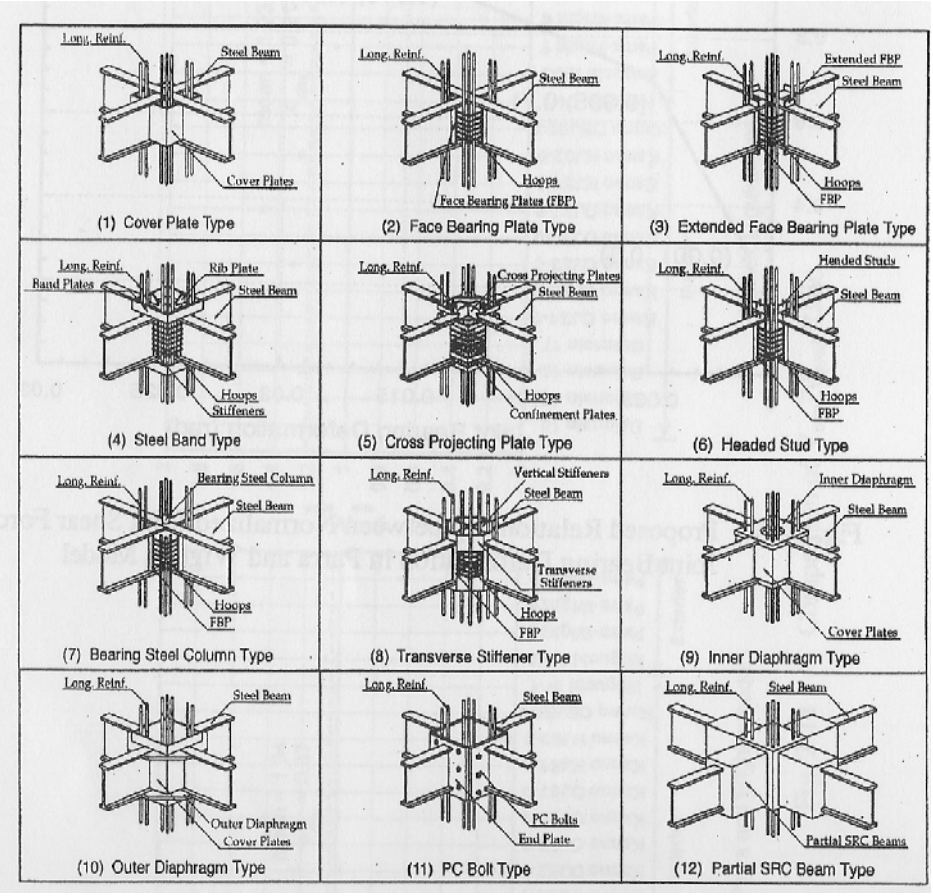

FIG. 2.13 TYPICAL RCS JOINT DETAILS IN JAPAN (AIJ, 1994)

CHAPTER III
PROTOTYPE RCS SPACE FRAME SYSTEM

3.1 BACKGROUND

The research in this thesis is an extension of previous research conducted at Texas A&M University on the behavior of RCS three-dimensional space frame systems under bidirectional lateral loading. The focus of this research is to evaluate various joint details for performance and constructability that may be relevant for low-to mid-rise buildings located in regions of moderate seismicity or prone to high wind loads. Fig. 3.1 shows a typical low-to mid-rise space frame which relies on moment connections throughout the building to resist lateral loads.

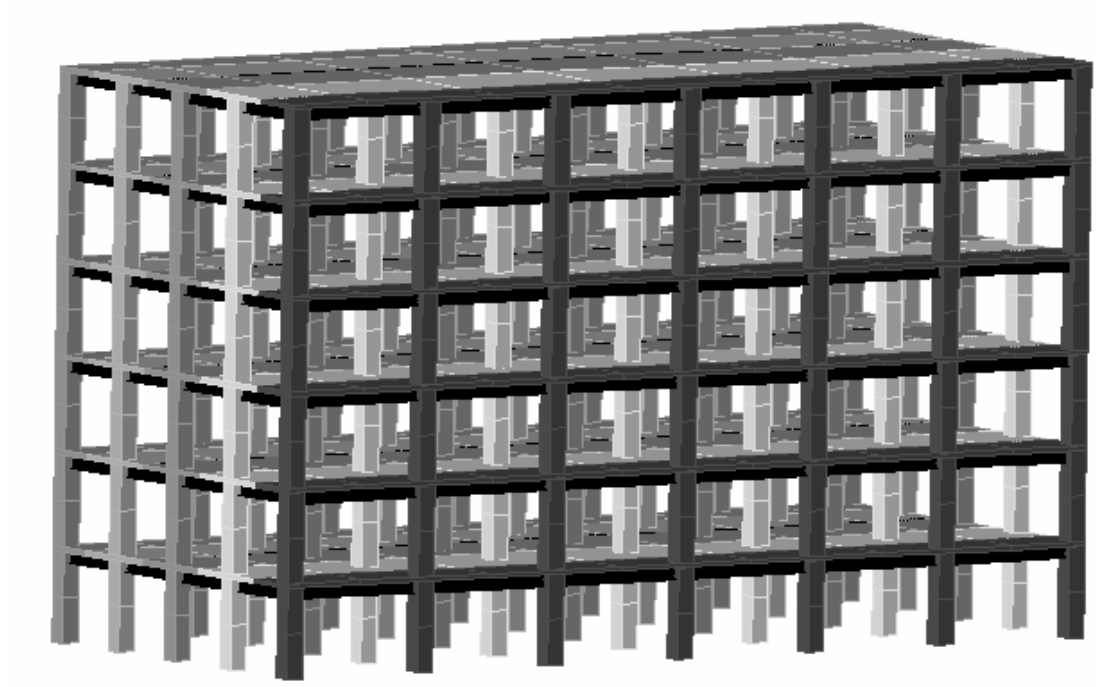

FIG. 3.1 TYPICAL MID-RISE SPACE FRAME

3.2 STRUCTURAL STRENGTH AND STIFFNESS

Composite reinforced concrete column-steel beam (RCS) frame systems combine the desirable material properties and constructability advantages of both structural steel and reinforced concrete (RC). Structural steel provides ductility and strength to the system, and can be erected quickly. RC construction enhances the structural stiffness of the system and creates significant material cost savings.

The general RCS frame system has composite columns and beams that are connected to form moment resisting connections. The composite columns are basically a RC column with a small structural steel shape in the center, which is surrounded longitudinal and transverse reinforcing steel. The composite beams are typically composed of structural steel wide-flange shapes that are mechanically connected to the RC slab with shear studs. The columns and beams are connected with a variety of joint details that are designed to utilize the ductility of the steel and the stiffness provided by the confined concrete.

3.2.1 First Yield Moment

The first yield calculations for the composite beam-slab cross section were made by assuming a linear strain distribution across the composite beam-slab cross section and the neutral axis was located by satisfying force equilibrium (Fig. 3.2). The Hogenstad equations (Eqs. (3.7) - (3.10)) were implemented to account for low stress levels in the concrete because it directly relates concrete strain to the imposed stress. The stress of

the steel components was calculated by multiplying the strain by the modulus of elasticity of steel. The concrete was assumed to have no tensile strength and was neglected at the location of the corrugated metal decking. The stress was converted into force components that were summed about the neutral axis of the cross section. The positive first yield moment $\left(M^{\pm}_{yield}\right)$ was assumed to be when the bottom of the lower structural steel beam flange yielded and negative yield moment was assumed to be when the slab steel yielded.

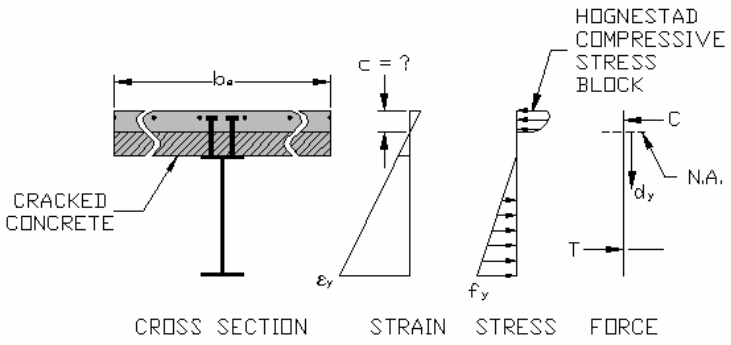

(a) Positive

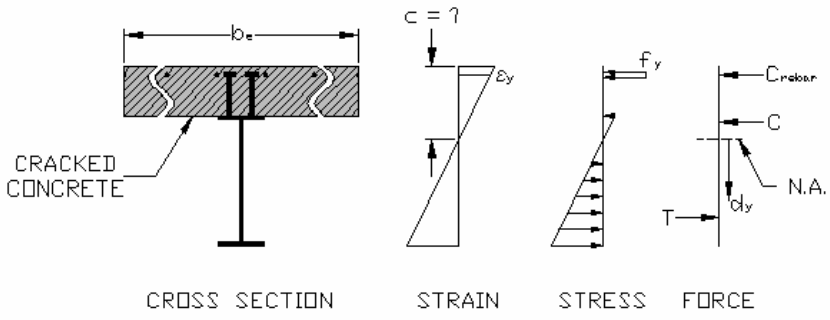

(b) Negative

FIG. 3.2 FIRST YIELD BEAM MOMENT CALCULATION

$$\varepsilon_o = \frac{2f_c'}{E_c} \tag{3.7}$$

$$\text{If } \varepsilon \geq 0 \text{ Then } f = 0 \tag{3.8}$$

$$\text{If } \varepsilon \geq \varepsilon_o \text{ Then } f = -f_c'\left(2\frac{\varepsilon}{\varepsilon_o} - \left(\frac{\varepsilon}{\varepsilon_o}\right)^2\right) \tag{3.9}$$

$$\text{If } \varepsilon \leq \varepsilon_o \text{ Then } f = -f_c'\left(1 - 0.15\left(\frac{\varepsilon - \varepsilon_o}{-0.0038 - \varepsilon_o}\right)\right) \tag{3.10}$$

where

ε_o = strain which yields maximum compressive concrete stress
ε = abitrary strain (negative is defined as compressive)
f = abitrary concrete stress (negative is defined as compressive)
f_c' = ultimate compressive concrete stress

3.2.2 Plastic Moment

Both positive and negative plastic moment capacities are predicted to ensure that the forces provided by the actuators would cause failure of the specimen in the major loading direction. The major loading direction (Fig. 3.3) is defined for this experimental testING as the direction parallel to the transverse beams which resisted loading from the larger 489 kN (110 K) actuators.

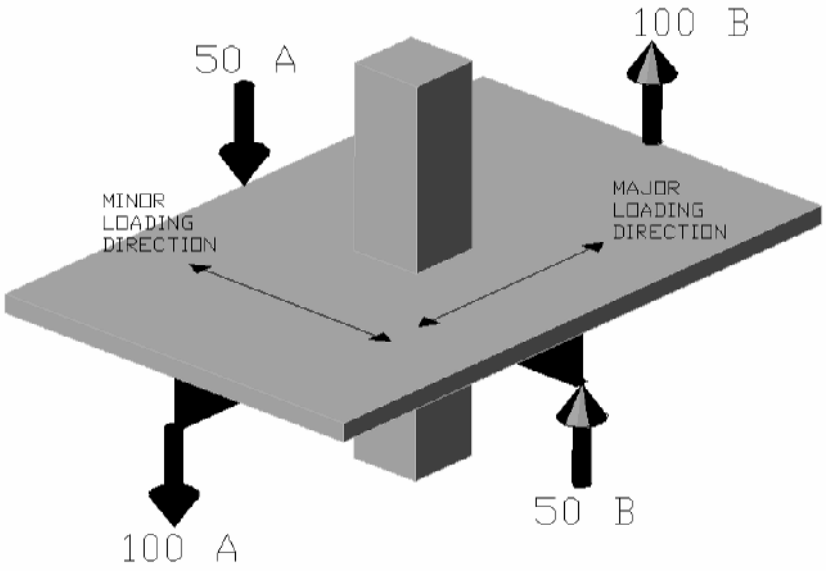

FIG. 3.3 LOADING DIRECTIONS

The plastic moment capacities of the member sections can be determined by using basic structural mechanics for both the composite beam-slab (Fig. 3.4) and the composite column. Some of the basic assumptions are that plane sections remain plane across the entire cross section, the entire section is fully composite (no slip between the concrete slab and structural steel beam), and the concrete does not participate in tension.

Calculation of the positive plastic moment is shown in Eqs. (3.1) – (3.4). A linear strain distribution is assumed across the composite beam-slab cross section were the strain at the top of the RC slab is assumed to be 0.003. The smaller magnitude force is chosen between full yielding of the structural steel beam and the crushing of the RC slab excluding the region with corrugated metal decking. Determine the depth of the compressive strain field by ensuring force equilibrium. Sum the components of the

compressive and tensile stresses about a common point to determine the positive plastic moment.

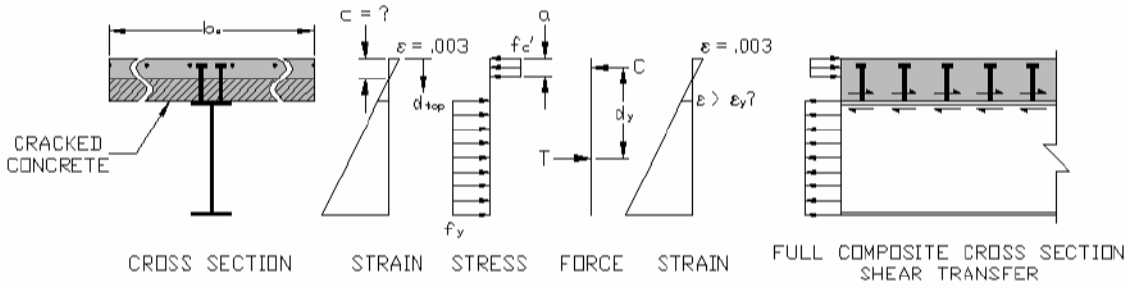

(a) Positive

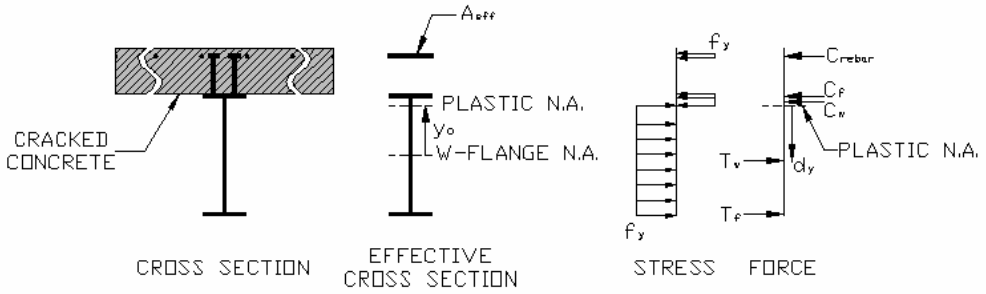

(b) Negative

FIG. 3.4 PLASTIC MOMENT CALCULATION

Calculation of the negative plastic moment is shown in Eqs. (3.5) – (3.6). Plastic neutral axis is determined for the structural steel beam and the effective area of the slab reinforcement. The effective area of the slab reinforcement is an area of steel with the same yield stress of the structural steel beam that will provide the same amount of force as the actual reinforcing steel area and yield stress. The force components of the yielded steel components are then summed about the plastic neutral axis to determine the negative plastic moment.

$$T = A_b\left(F_y\right)_b = 9.12(50) = 456\ K = 2028\ kN \tag{3.1}$$

$$a = \frac{T}{.85 f_c' b_e} = \frac{456}{.85(4)(90)} = 1.49\ in = 38\ mm \tag{3.2}$$

$$\begin{aligned} \varepsilon_{top\,b} &= \frac{\varepsilon_{ult}}{c}\left(d_{top} - c\right) = \frac{0.003}{1.5}(6 - 1.5) = 0.009 \\ \varepsilon_{top\,b} &\geq \left(\varepsilon_y\right)_b = \frac{\left(F_y\right)_b}{E_s} = \frac{50}{29000} = 0.0017 \end{aligned} \tag{3.3}$$

$$M^+_{plastic} = Td_y = 456\left(\frac{15.88}{2} + 6 - \frac{1.49}{2}\right) = 6016.9\ K - in = 679.8\ kN - m \tag{3.4}$$

$$y_o = \frac{A_r \big/ 2}{t_w}\left(\frac{\left(F_y\right)_r}{\left(F_y\right)_b}\right) = \frac{3 \big/ 2}{0.275}\left(\frac{60}{50}\right) = 6.6\ in = 168\ mm \tag{3.5}$$

$$\begin{aligned} M^-_{plastic} &= \Sigma F_y A_o d_y \\ &= 3(60)\left(\frac{15.88}{2} + 6 - 1 - 6.6\right) + 5.525(0.44)(50)\left(\frac{15.88}{2} - \frac{0.44}{2} - 6.6\right) \\ &\quad + 0.275(0.95)(50)\left(\frac{0.95}{2}\right) + 0.275(14.05)(50)\left(\frac{14.05}{2}\right) \\ &\quad + 5.525(0.44)(50)\left(\frac{15.88}{2} - \frac{0.44}{2} + 6.55\right) \\ &= 4391\ K - in = 496.1\ kN - m \end{aligned} \tag{3.6}$$

where

T = tensile force
A_b = area of structural steel beam
$\left(F_y\right)_b$ = yield stress of the steel beam
a = depth of Whitney stress block
f_c' = ultimate compressive stress of concrete
b_e = effective flange width of RC slab

$\varepsilon_{top\,b}$ = strain at the top of the structural steel beam

ε_{ult} = ultimate compressive strain of concrete (0.003)

c = depth of compressive stress field

d_{top} = arbitrary depth measured from the top of the composite beam-slab cross section

$\left(\varepsilon_y\right)_b$ = yield strain of the structural steel beam

E_s = modulus of elasticity for steel $\left(200000\text{ MPa}\left(29000\text{ ksi}\right)\right)$

M_p^+ = positive plastic moment capacity

d_y = depth from common location from which moments are summed

y_o = distance from neutral axis of structural steel beam to plastic neutral axis of composite beam-slab

A_r = area of rebar

t_w = web thickness of structural steel beam

$\left(F_y\right)_r$ = yield stress of steel reinforcement

M_p^- = negative plastic moment capacity

F_y = arbitrary yield stress

A_o = arbitrary unit of area

3.2.3 Column Interaction Diagram

An interaction diagram was constructed for the composite column taking in to account the effects of the axial load and ensured that the column remained in the elastic region throughout the duration of the test (Fig. 3.5). Linear strain distributions were assumed across the RC column cross section from pure compression to pure tension. Concrete was assumed not to participate in tension. The stress distribution was related to the strain distribution by the Whitney Stress Block. Summation of the force components determined the axial load of the column and summation of the force

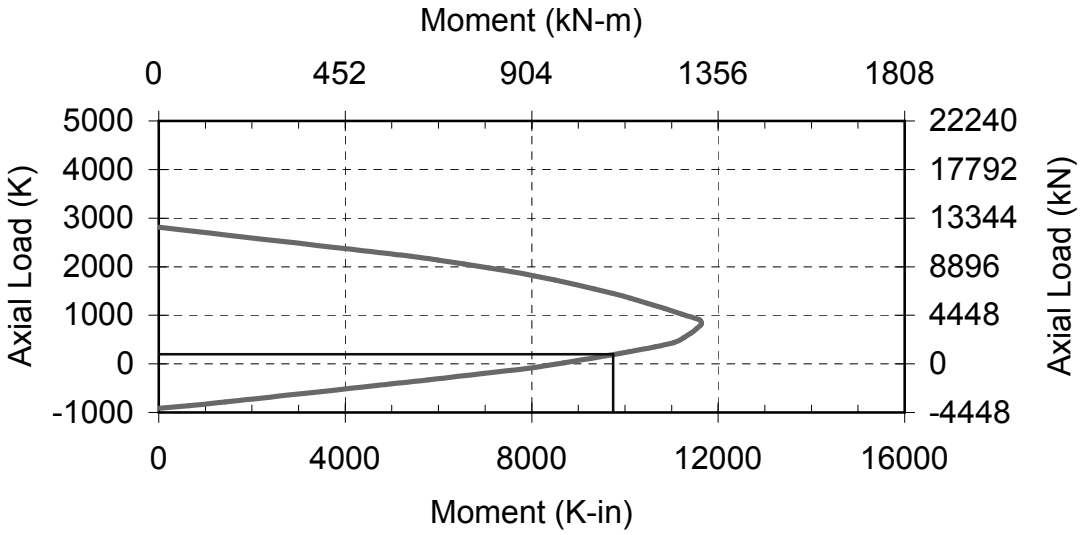

(b) f_c' = 27.6 Mpa (4 ksi)

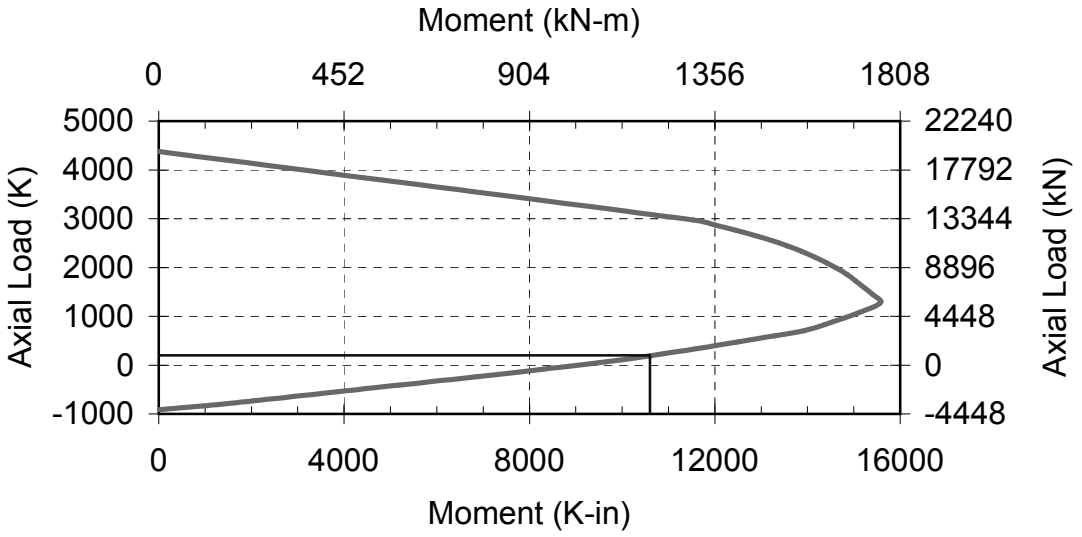

(b) f_c' = 50.3 Mpa (7.3 ksi)

FIG. 3.5 ULTIMATE INTERACTION DIAGRAM FOR COLUMN

components about the neutral axis determined the ultimate moment capacity of the RC column.

3.3 CONSTRUCTION PROCESS

In an effort to reduce construction costs of RCS buildings, joints must designed for sufficient strength and ductility, and must have details that can be erected quickly. Improved joint detailing was considered because it is the most complicated region in the moment frame and can be a detriment to the speed of construction. The joint region is potentially the most difficult and time consuming aspect of moment frame construction due to complexity and congestion both of which can be improved with better joint details. Improved joint configurations allow the structural steel erection to progress more rapidly, thus allows for a vertical spread of construction activities. Some joint configurations, such as joint plates, eliminate the need for column formwork in the joint region and expedite the remaining column formwork placement.

A vertical spread of construction processes, which can be achieved by using a RCS structural system, greatly increases the construction rate a building. An example of this construction process is given in Griffis (1986) (Fig. 3.6) as follows at an instance of time: levels 11-12 involve structural steel erection, levels 9-10 have connections bolted and welded, simultaneously with the placement of corrugated metal decking, levels 7-8 have shear studs welded and slab reinforcement placed, levels 5-6 have the RC slabs being poured, levels 3-4 have column reinforcement being placed, and levels 1-2 have column forms being placed and columns being poured.

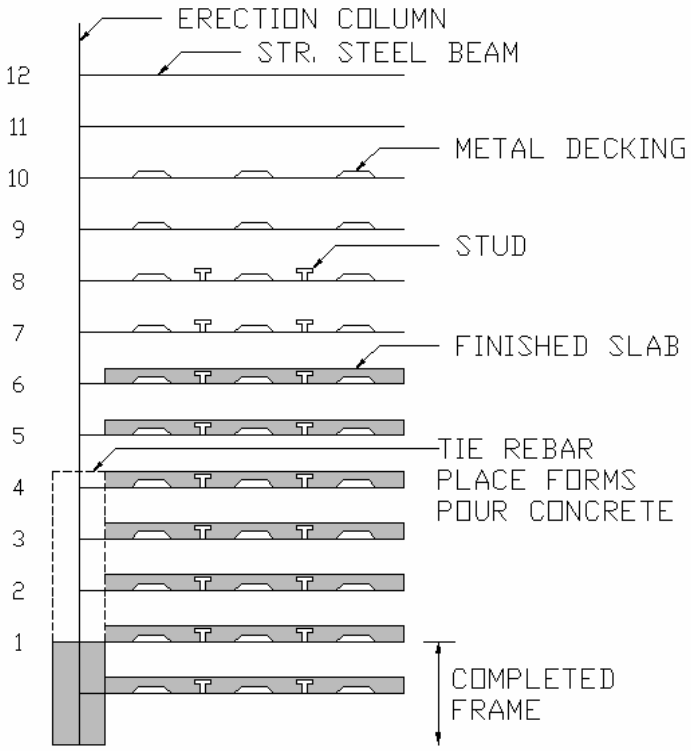

FIG. 3.6 RCS CONSTRUCTION SEQUENCE (Griffis 1986)

Joints that incorporate prefabricated joint detailing can significantly simply formwork placement. Prefabricated joints allow standardized column forms to be used and reused throughout the construction process. An example of a prefabricated joint as later described in the experimental program is shown in Fig. 3.7a. This photograph demonstrates that simple uniform forms could easily be placed and reused. There were voids above the confinement plate where the fluke of the metal decking was located. These areas where plugged with a small piece of plywood and sealed with silicon caulk. Bracing the forms in the joint region so that the forms do not deform under the hydrostatic pressures applied by uncured concrete is difficult. These problems are shown in Fig. 3.7b which is a traditional face bearing plate detail. The forms in the joint

region are all unique to ensure a proper seal along the metal decking. The steel bands that hold the face bearing plates in place and prevent deformation during the concrete pour are welded to the face bearing plates. The placement and removal of these steel bands was difficult and time consuming process.

(a) Prefabricated Joint Detail **(b) Traditional Joint Detail**

FIG. 3.7 JOINT FORMWORK

3.4 JOINT DETAILING AND ISSUES

The joint region of a RCS space frame is complicated because of the number of different components that are located in a small space and the behavior of which under lateral loading is difficult to predict. In RCS construction, joints consist of a continuous steel beam through the joint in one direction (defined as the minor [Fig. 3.3] loading direction in the experimental work), two transverse beams that orthogonally frame into the continuous beam (defined as the major [Fig. 3.3] loading direction in the experimental work), and a discontinuous steel erection columns both above and below the joint. Full moment connections allow the transverse beams to provide similar

resistance as that of the continuous through-beam. The mechanics of this connection is discussed in detail in Section 5.2. Proper confinement must be provided in the joint region to mobilize an internal concrete strut which allows the joint to utilize the full potential of the concrete stiffness. Confinement can be provided with transverse steel reinforcement, face bearing plates, confinement plates, band plates or a combination of similar structural components. These components create other constructability problems, for instance placing transverse reinforcement through the webs of the structural steel beams is difficult and time consuming, and components such as confinement plates bring additional costs due to copious amounts of field welds required for installation. Predicting the behavior of these joints is complicated by the effects of bidirectional loading on the joint in space frame systems. All of these joint detailing problems are addressed in this research program.

CHAPTER IV

EXPERIMENTAL PROGRAM

4.1 GENERAL

To resolve issues addressed in Chapter III, an experimental program of three-dimensional subassemblies was carried out in the Testing, Machining and Repair Facility at Texas A&M University. Specific test details for two cruciform specimens are described in this chapter.

4.2 SPECIMEN DESIGN

The two cruciform specimen dimensions are based on a prototype building that was designed for wind loading located in Houston, Texas. The cruciform specimen, shown in Fig. 4.1, was created by cutting an interior connection out of the prototype RCS space frame system at the beam mid-spans in both orthogonal directions and at the column mid-height. The steel skeleton was composed of W16x31 structural steel beams and W8x10 structural steel columns. The W16x31 beams were reduced slightly from the actual size of the designed prototype to accommodate the maximum loading of the test setup. A 152 mm (6 in.) RC slab that was 3.4 m (11 ft) wide by 5.2 m (17 ft) long was mechanically attached to the structural steel beams. The steel erection columns were encased in a 610 mm (24 in.) square RC column that was 3.3 m (10.8 ft) high between pin connections. The two RCS cruciform specimens were constructed with

identical overall dimensions and member cross sections but had different joint detailing. Fig. 4.2 shows the major dimensions of the test specimens.

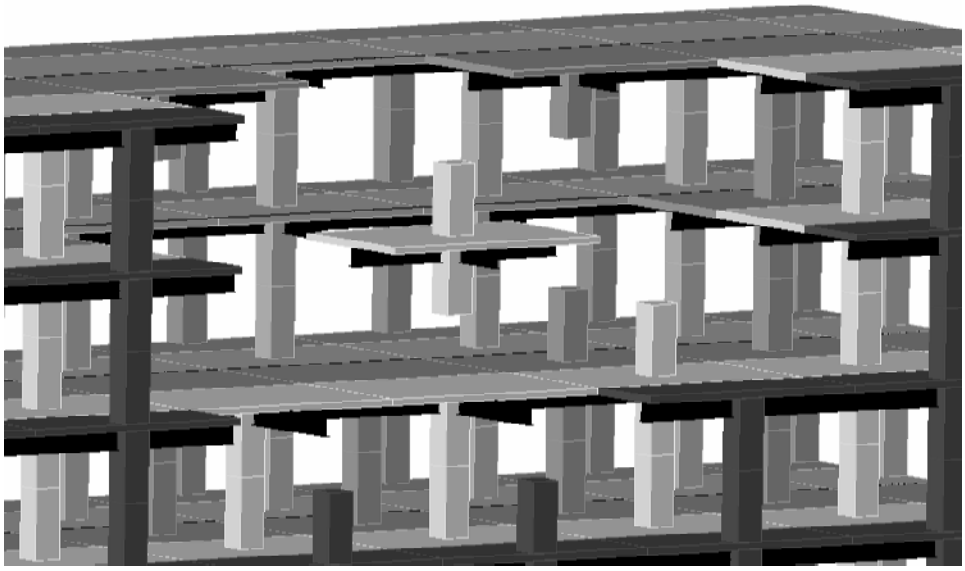

FIG. 4.1 CRUCIFORM CUT OUT OF SPACE FRAME

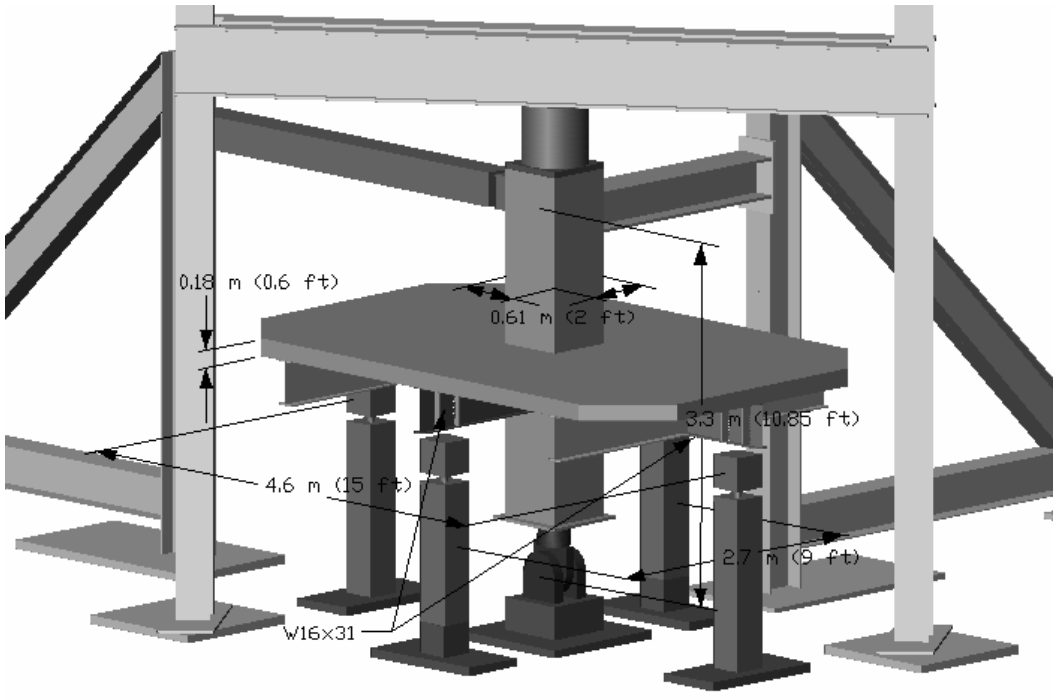

FIG. 4.2 OVERALL SPECIMEN DIMENSIONS

The composite steel beam-RC slab sections were designed based on provisions in AISC (2001). The composite beams have a positive plastic moment capacity of 679.8 kN-m (6017 k-in) and a negative plastic moment capacity of 496.1 kN-m (4391 k-in) as shown in Section 3.2. The plastic moment capacity of the composite beam was determined by summing the force components about the neutral axis of the cross section. It was assumed that the cross section was fully composite due to the shear studs connecting the steel flange to the RC slab. In addition, a full moment connection was provided by the top and bottom seat angles and the column transverse reinforcement. The moment capacity of the composite column was determined to be 1181.2 kN-m (10455 k-in) with a compressive axial force of 889.6 N (200 k) which is approximately $0.2A_g f_c'$ where A_g is the gross area of the RC column and f_c' is the 28 day compressive strength of the concrete.

4.3 JOINT DETAILS

The joint strengths of the cruciform specimens calculated according to ASCE guidelines for vertical bearing failure mechanisms and modeling recommendations from the University of Michigan concerning joint panel shear, which were outlined in Sections 2.4 and 2.6. The joint was designed to test the design recommendation limits compared with the joint forces generated by the calculated composite beam-slab section plastic moment. A very important joint detail for these specimens was the top and seat angles that connect the beam flanges of the transverse beams in the specimen. These

bend plates were welded to the top and bottom flanges of the transverse beams, respectively, and were bolted to the web of the columns (Fig. 4.3). The steel moment frame resistance relied on the rigidity provided by the seat and top angle to transfer the forces in the structural steel beam flanges into the joint region and rectangular transverse reinforcement. The two details that were tested in this experimental program were face bearing plates alone and joint confinement plates. The face bearing plates are a typical detail used in past composite RCS construction and serves as a baseline to gage the performance of the joint confinement plate (Fig. 4.4). The joint confinement plates were intended to provide confinement in the joint region and engage more of the outer compression strut, which the joint provides more lateral stiffness and strength to the system.

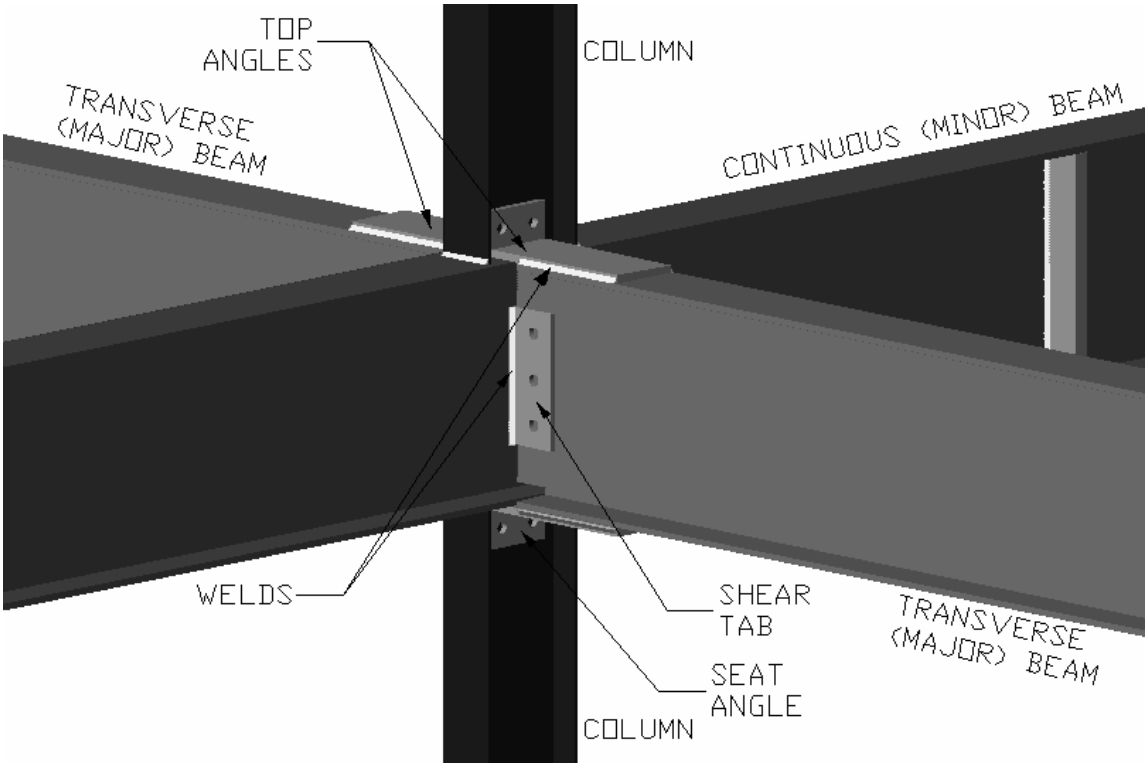

FIG. 4.3 JOINT MOMENT CONNECTION DETAIL

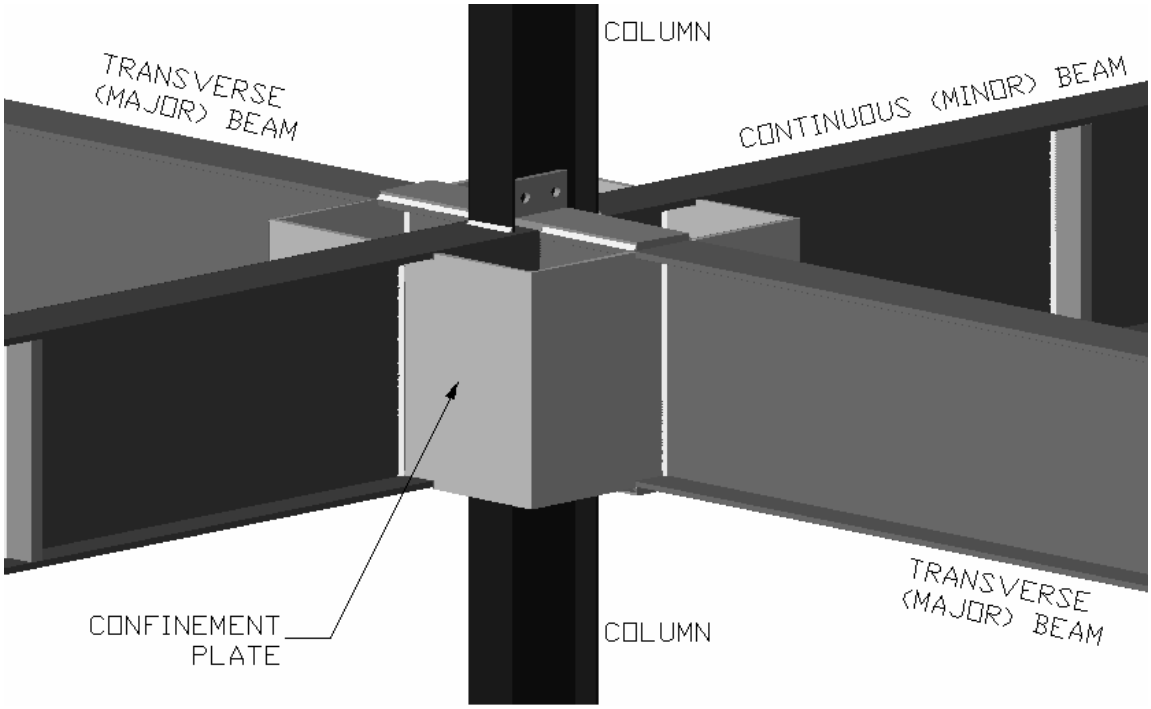

(a) Confinement Plate

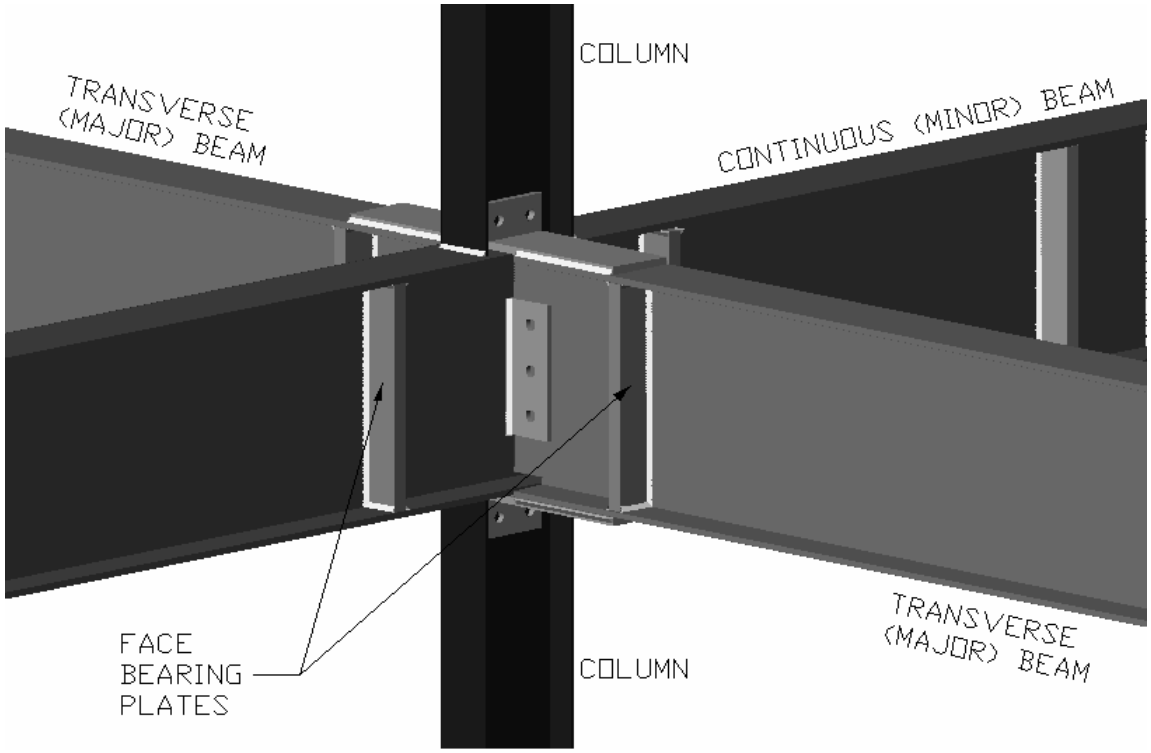

(b) Face Bearing Plate

FIG. 4.4 JOINT DETAILING CLOSEUP

4.4 MATERIAL PROPERTIES

A variety of steel and concrete components were used in the composite specimen construction. A 20.7 MPa (3 ksi) 28-day strength concrete mix was requested for the slab pour and a 27.6 MPa (4 ksi) 28-day strength mix was used for the column pour. Emaco S77 CI, which was used to repair voids in the joint region that are described in detail in Section 5, was designed to have a 7-day strength of 55.2 MPa (8 ksi) and 28-day strength of 82.8 MPa (12 ksi). The results from 28-day and test day compressive concrete strength 152 x 304 mm (6 x 12 in) test cylinders are shown in Table 4.1 and were determined according to provisions outlined by ASTM (1998) and ASTM (2001). The Emaco S77 CI that was tested at 7-days had a compressive strength of 35.76 MPa (5.18 ksi). The test day data reported is the average of the two tests which were 21 days apart. The difference in strength increase was found to be insignificant. ASTM A615 Grade 60 steel was used for slab reinforcement, longitudinal column reinforcement and transverse column reinforcement. The structural steel beams and columns were composed of ASTM A572 steel with a minimum yield strength of 345 MPa (50 ksi) and a minimum ultimate strength of 449 MPa (65 ksi) and the plate and bent plate components of the specimen were composed of ASTM A36 steel with a minimum yield strength of 248 MPa (36 ksi) and an minimum ultimate strength of 400 MPa (58 ksi).

TABLE 4.1 CONCRETE COMPRESSIVE STRENGTHS

	f'c (28 days)		fc (test day)	
	ksi	MPa	ksi	MPa
Slab	5.20	35.87	6.89	47.56
Column	6.25	43.15	7.30	50.36

4.5 EXPERIMENTAL SETUP

To test the composite cruciform, an experimental setup (Fig. 4.5) was constructed to hold the specimen in place and apply loads. The bottom column was attached to a swivel assembly from a 979 kN (220 K) actuator which was bolted to a pedestal that was bolted to the strong floor. The swivel was a ball and socket connection which allowed rotation in both directions and was capable of resisting shear and axial forces. The top connection consists of a beam that was bolted into the top of the column in the direction of the minor loading direction or parallel with the continuous through-beam which frames into a reaction frame that was capable of resisting horizontal shear forces generated by the column. In the major loading direction, a 979 kN (220 K) actuator that was set in displacement control to maintain zero displacement transmits the shear forces from the column to the reaction frame. The two reaction frames and base swivel were capable of rigidly holding the specimen in position for testing. The axial load, which was applied by a pneumatic piston to the top of the column, pushed against a steel girder that ran diagonally over the specimen. The steel girder was bolted to columns that were bolted at the base to large steel plates, which in turn were attached to the lab strong floor. Rigid pedestals and large plates anchored the actuators to the lab strong floor at a height where the full stroke of the actuator could be utilized during testing. These actuators were used to load the specimen by applying vertical compressive and tensile loads at the ends of the composite beams of the cruciform.

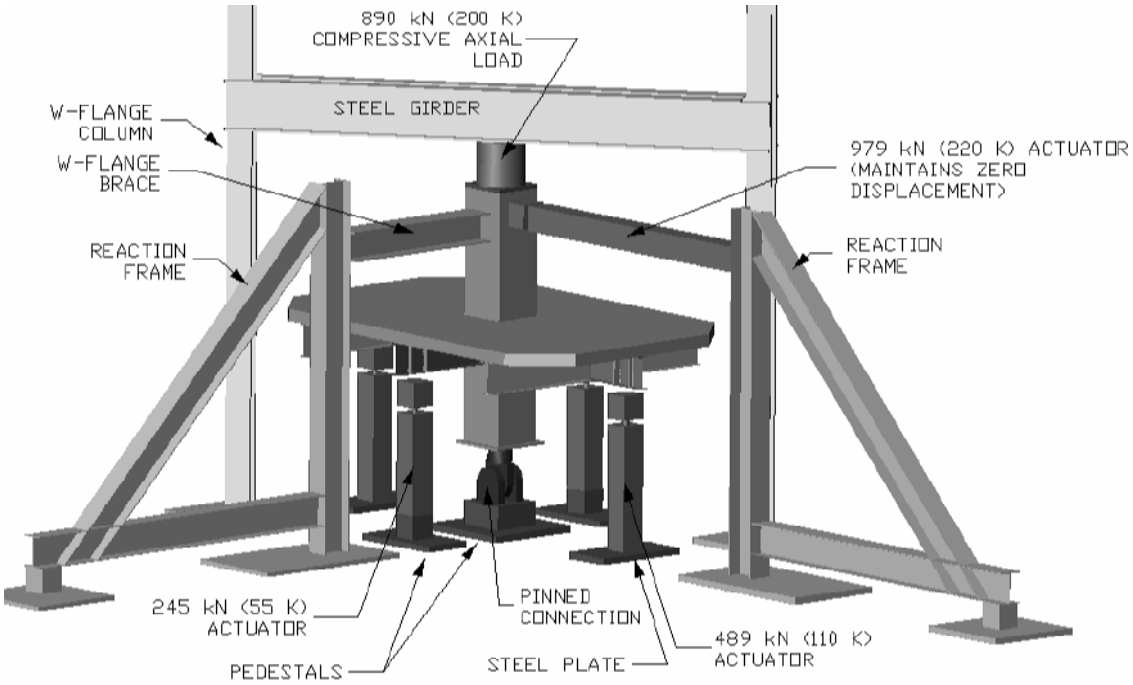

(a) Diagram

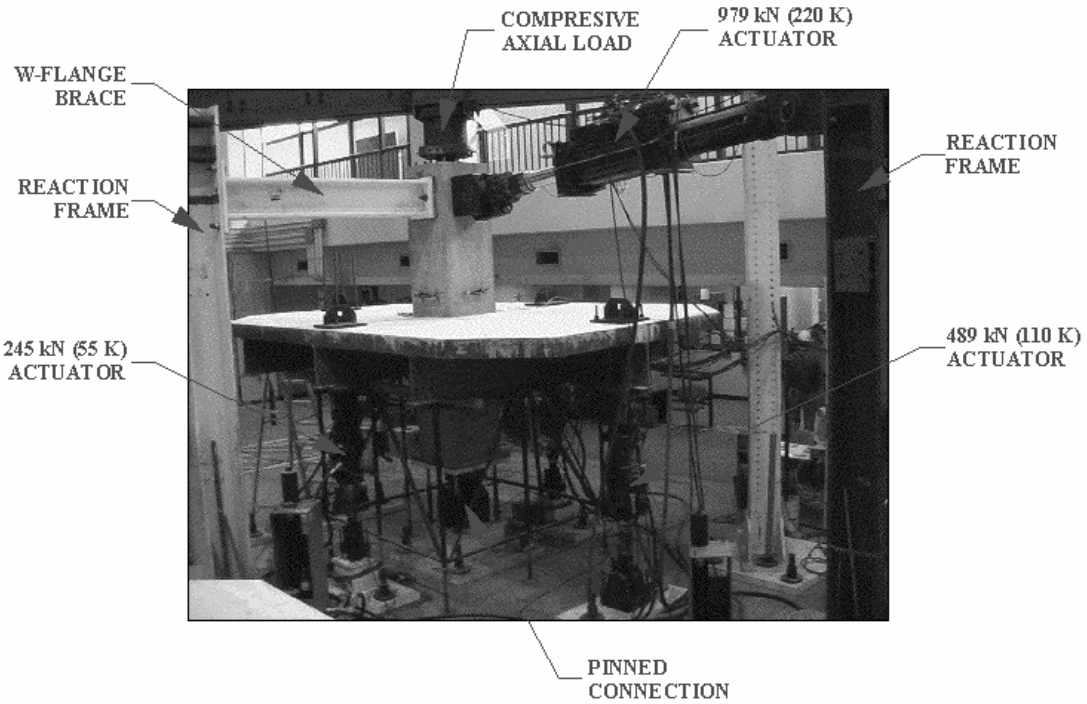

(b) Photograph

FIG. 4.5 EXPERIMENTAL SETUP

4.6 LOAD APPLICATION

Simulated gravity and cyclic lateral loading was applied to the specimens through the use of hydraulic actuators and a pneumatic piston. Lateral loads were applied to the cruciform by four servo-controlled actuators that applied vertical forces to the outer ends of the composite beams. The actuators were programmed to apply quasi-static reversed cyclic loading under incremental displacement amplitudes to the specimens. Bidirectional loading was applied to the specimens by loading the actuators in both the minor and major loading directions simultaneously (Fig. 3.3). In the major loading direction of the specimen, 489 kN (110 K) actuators were placed at the ends of the transverse beams that frame orthogonally into the continuous beams and 245 kN (55 K) actuators were placed at the ends of the continuous through-beam, which applied loads in the minor loading direction. The specimens were loaded by two full cycles at each progressing incremental displacement level. The 489 kN (110 K) actuators cycled between ±76 mm (±3 in.) at 6.35 mm (¼ in.) increments from a displacement of 6.35 mm (¼ in.) to 38.1 mm (1 ½ in.) and 12.7 mm (½ in.) increments from a displacement of 38.1 mm (1 ½ in.) to 76.2 mm (3 in.) in displacement control. Simultaneously, the 245 kN (55 K) actuators were cycled in load control and applied a load proportional to the existing displacement of the 489 kN (110 K) actuators compared to that of full stroke. For the second phase of testing, the 489 kN (110 K) actuators were repositioned to allow the specimen to be cycled from a displacement of 0.0 mm (0.0 in.) to 152.4 mm (6 in.) at increments of 25.4 mm (1 in.). During these tests, the 245 kN (55 K) actuators

were disengaged so that the specimen was tested only in the major loading direction. The pneumatic piston placed on the top of the RCS column applied a constant column axial compressive force of 890 kN (200 K) through out the entire testing process.

4.7 INSTRUMENTATION AND DATA ACQUISITION

Force and displacement readings were taken from sensors embedded within the actuators. The column axial force was determined from pressure measurements within the pneumatic piston. Clinometers were placed on the column face, webs of the W16x31 beams, and confinement plates or face bearing plates to measure joint and member rotations. The clinometers were attached to the steel surfaces of the test specimens with 6.35 mm (¼ in.) all-thread tack welded to the steel components with care not to alter the structural integrity of the components. The clinometers were mounted in the center of rigid plates that spanned 203.2 mm (8 in.) between the all-thread on which the plastic strips were bolted. Linear Variable Displacement Transducers (LVDT) were attached to a steel bracket that surrounded the column and was placed under the beams to record vertical movement of the beams due to joint bearing mechanism. Clinometers measuring column rotations and LVDTs were mounted on steel bracket that were attached to the concrete columns using the anchorage detailing shown in Fig. 4.6. Together the clinometers and LVDTs detected the specimen deformation contributions and joint failure components (Figs. 4.7 and 4.8). Strain gauges were also placed on select slab reinforcement and positioned to take readings in both axes of the specimen and on either side of the joint (Fig. 4.9 reference figure on pg. 71 for global location).

Concrete strain gages were placed within the concrete in the joint orientated approximately 45° from vertical in locations (Figs. 4.10 and 4.11) such that they would detect concrete strains from the inner and outer struts that formed in the major loading direction of the joint. Four rossette strain gages were placed on the web of the structural steel beams at mid-height and equally spaced from the joint center and the face of the column (Fig. 4.12) which measured web contributions to joint shear mechanism.

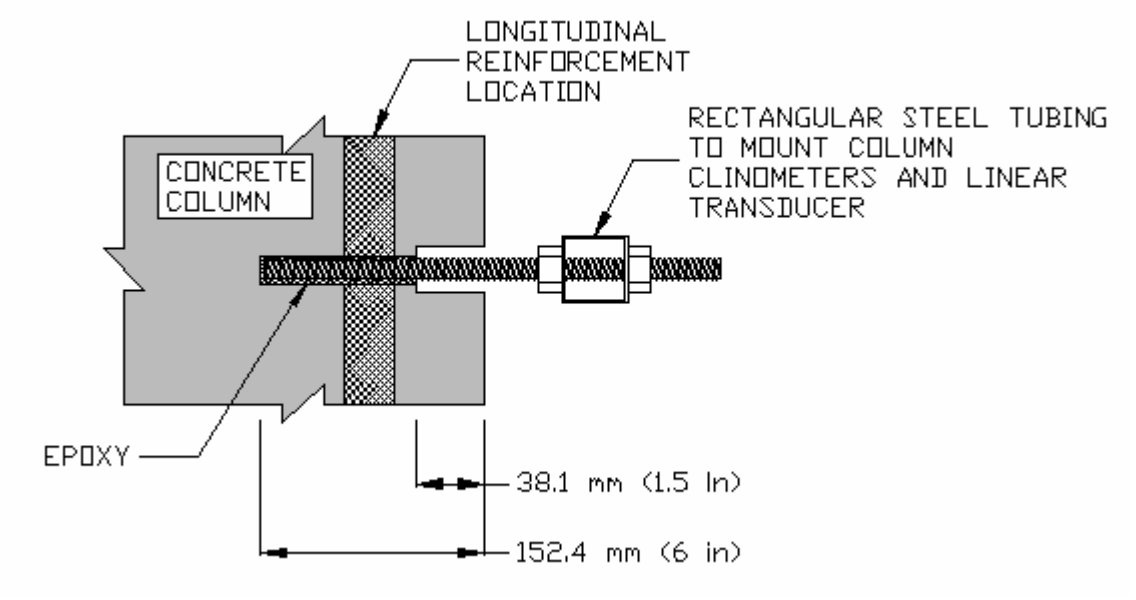

FIG. 4.6 COLUMN GAGE MOUNT ANCHORAGE

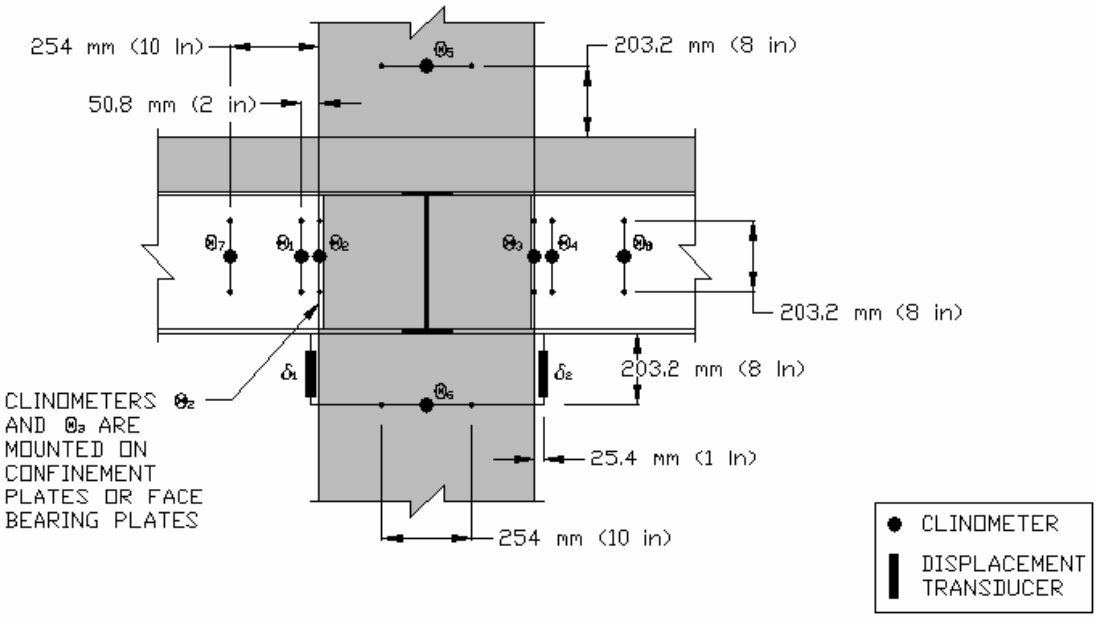

(a) Major Loading Direction

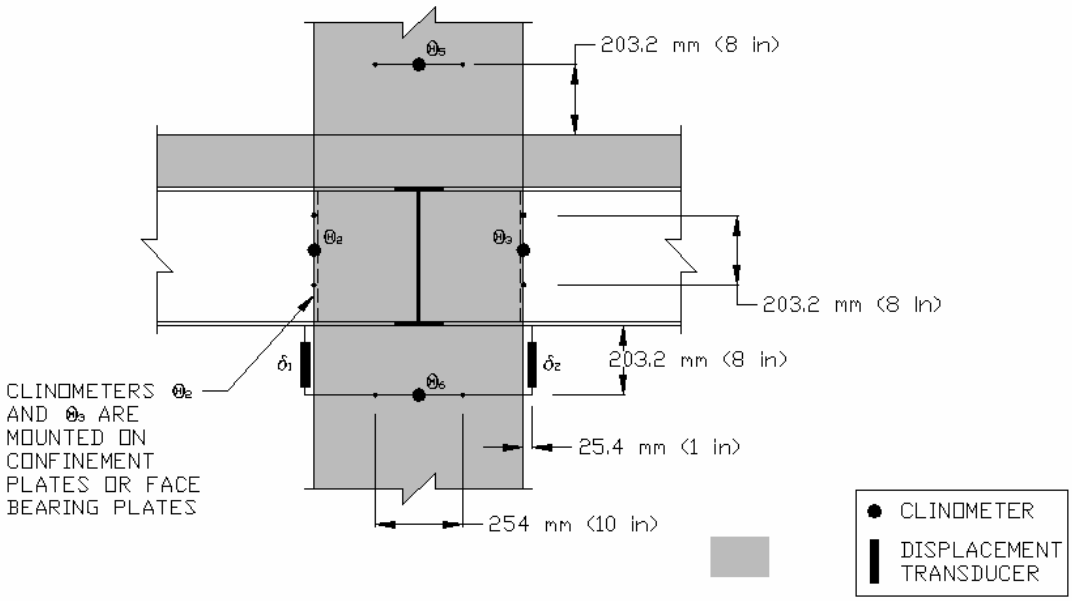

(b) Minor Loading Direction

FIG. 4.7 CLINOMETER AND LVDT PLACEMENT

FIG. 4.8 PHOTOGRAPH OF CLINOMETERS AND LVDTs

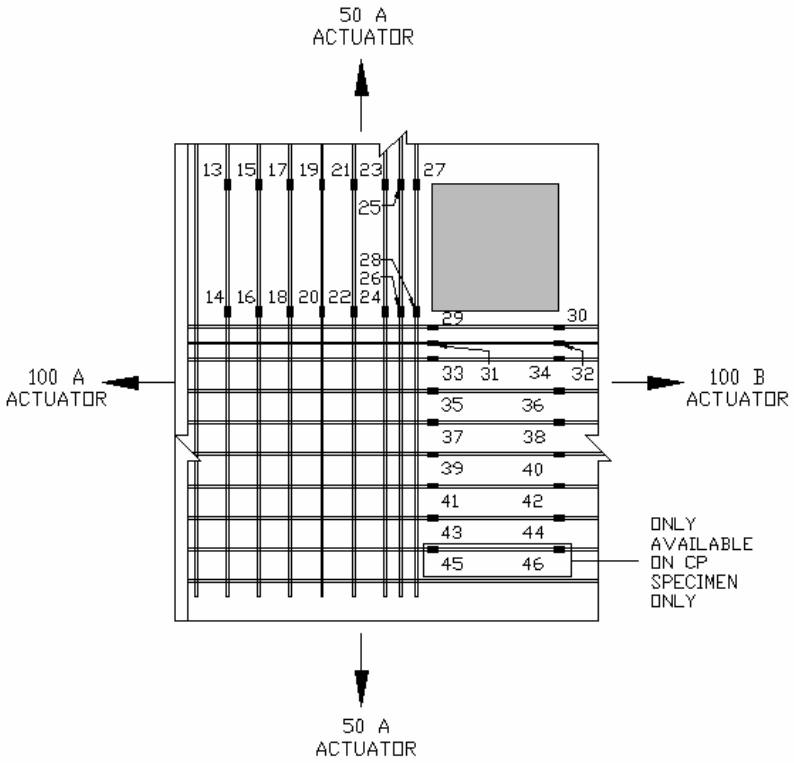

FIG. 4.9 REBAR STRAIN GAGE PLACEMENT
(GLOBAL LOCATION FIG 5.5)

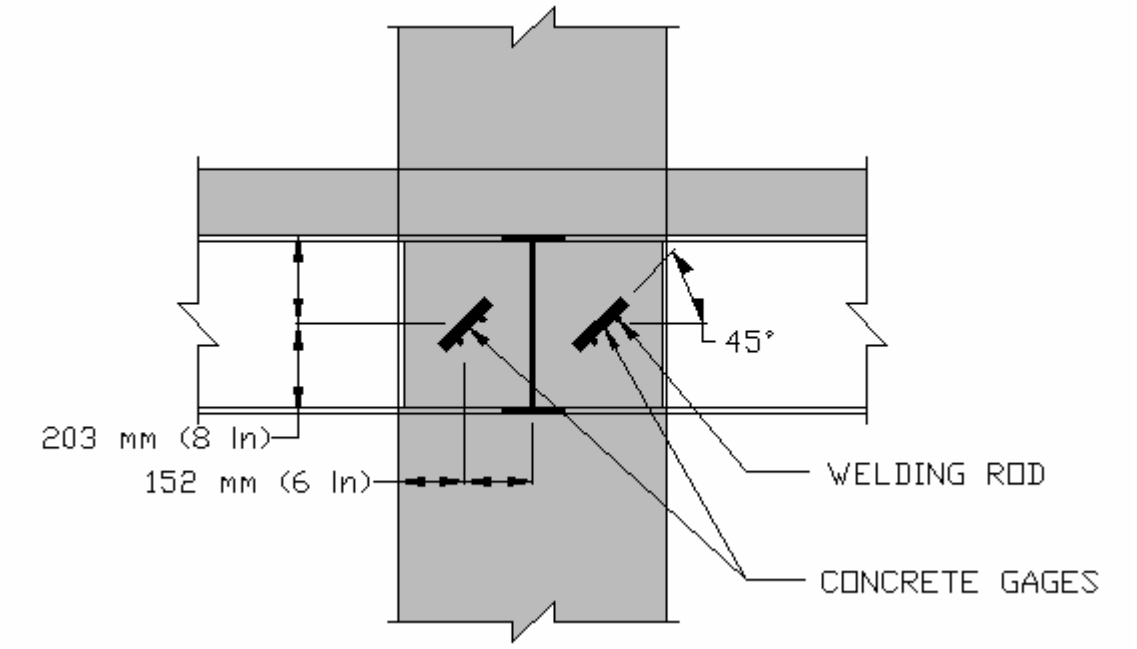

(a) Side View, Major Loading Direction

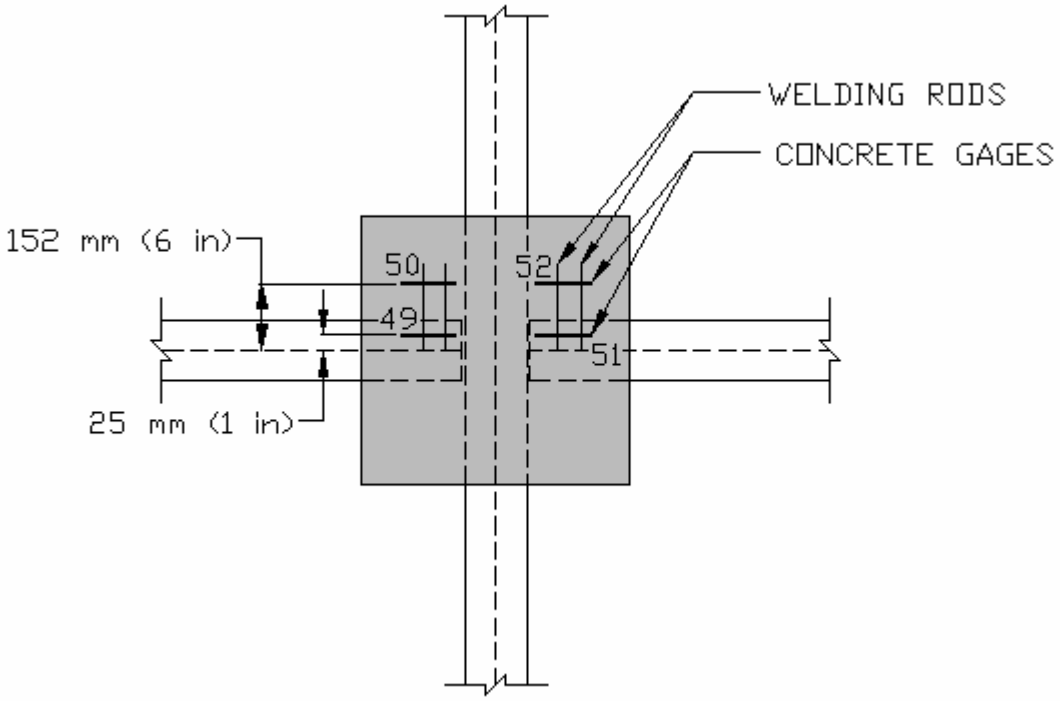

(b) Cross Section

FIG. 4.10 CONCRETE GAGE PLACEMENT

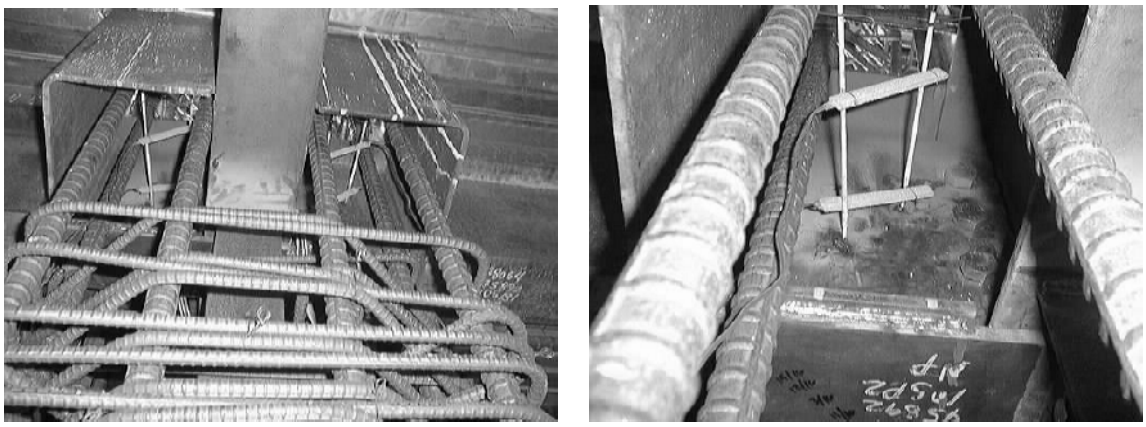

(a) Confinement Plate Joint Detail

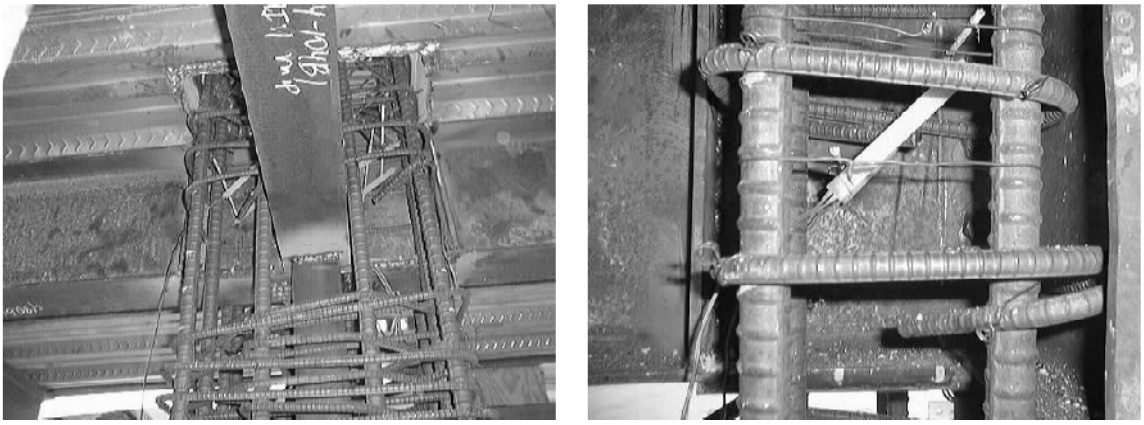

(b) Face Bearing Plate Joint Detail

FIG. 4.11 PHOTOGRAPHS OF CONCRETE GAGES

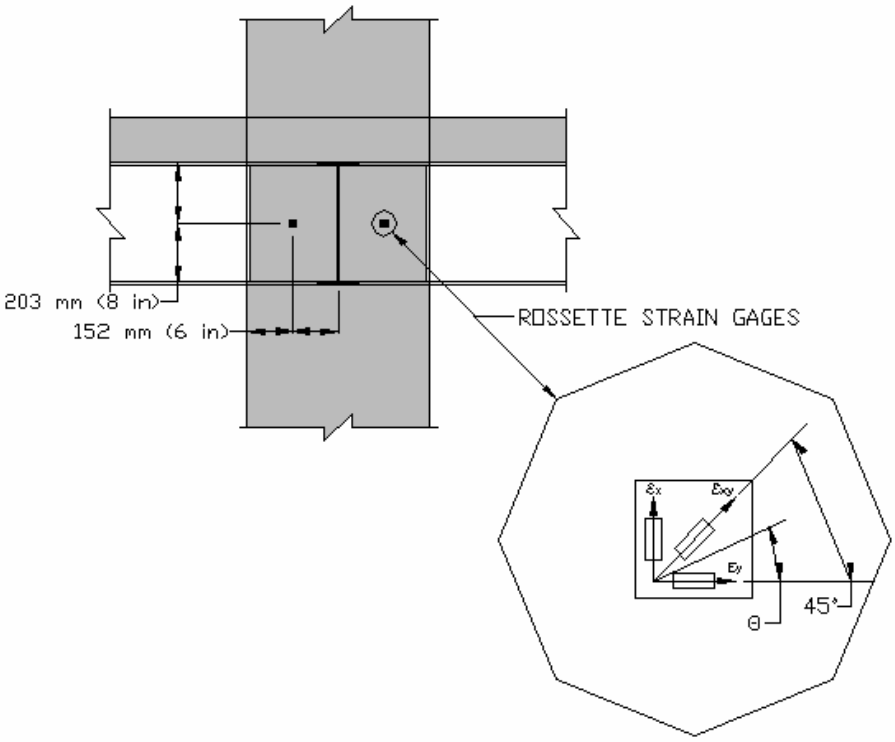

FIG. 4.12 ROSSETTE STRAIN GAGE PLACEMENT (TYPICAL IN BOTH DIRECTIONS)

CHAPTER V

SPECIMEN CONSTRUCTION

5.1 SUMMARY

The detailing of the joint region is essential for adequate performance of the RCS frame system. However, constructability and cost concerns may restrict the structural effectiveness of this system. The proposed joint designs in the experimental program are intended to reduce the costs and construction time by utilizing prefabricated and simplified joint components. In the field as presented by Griffis (1986), steel members are shipped to the construction site as subassemblies, and are hoisted into location in the steel frame. The steel skeleton is designed to resist the construction loads and dead weight of the uncured concrete. As the steel frame continues skyward, corrugated metal decking is placed and shear studs welded through the decking to the top flange of the structural steel beams. Reinforced steel is tied in both the slab and column. The concrete slab is placed without the aid of shoring or additional forms, which greatly increases the rate at which the concrete is placed. Following behind, the columns are encased with forms and the concrete column is poured. Most of the lab tests thus far have not addressed issues that could arise during construction of RCS systems. A typical lab practice is to pour the RC column while lying on its side which allows easy access to the joint region but is not feasible in the field. The construction process that is used in the lab is intended to mimic situations that are found in the field to assess the constructability of these structural systems.

5.2 SPECIMEN CONSTRUCTION PROCESS

The specific details of the construction process for the RCS subassemblies in the experimental program are outlined below in order of construction activity.

5.2.1 Structural Steel Erection

The bottom column was fabricated with a 25 mm (1 in.) thick base plate, 762 mm (30 in.) square, which was welded to the base or lower end of the column. The purpose of this plate was two fold, to contain the curing concrete and to provide rigidity between the specimen and pin connection which attached to the lab floor. The top end of the bottom column was tack welded in the laboratory to the center of the bottom flange of the continuous beam. The column major axis of bending was orientated in the same direction as the major axis of bending of the continuous through-beam, the minor loading direction. The continuous beam was 3.35m (11 ft.) in length and composed the smaller specimen dimension in plan. The top column was then tack welded, in the same orientation as the bottom column, to the center of the top flange of the continuous beam. At this point in actual construction, a similar assembly would be hoisted into its permanent location within the building and attached.

When the subassembly was in place, the transverse beams were attached to create the steel skeleton of the structural steel frame (Fig. 5.1). The major beams were then bolted in the major loading direction to the prefabricated shear tabs welded to the web of

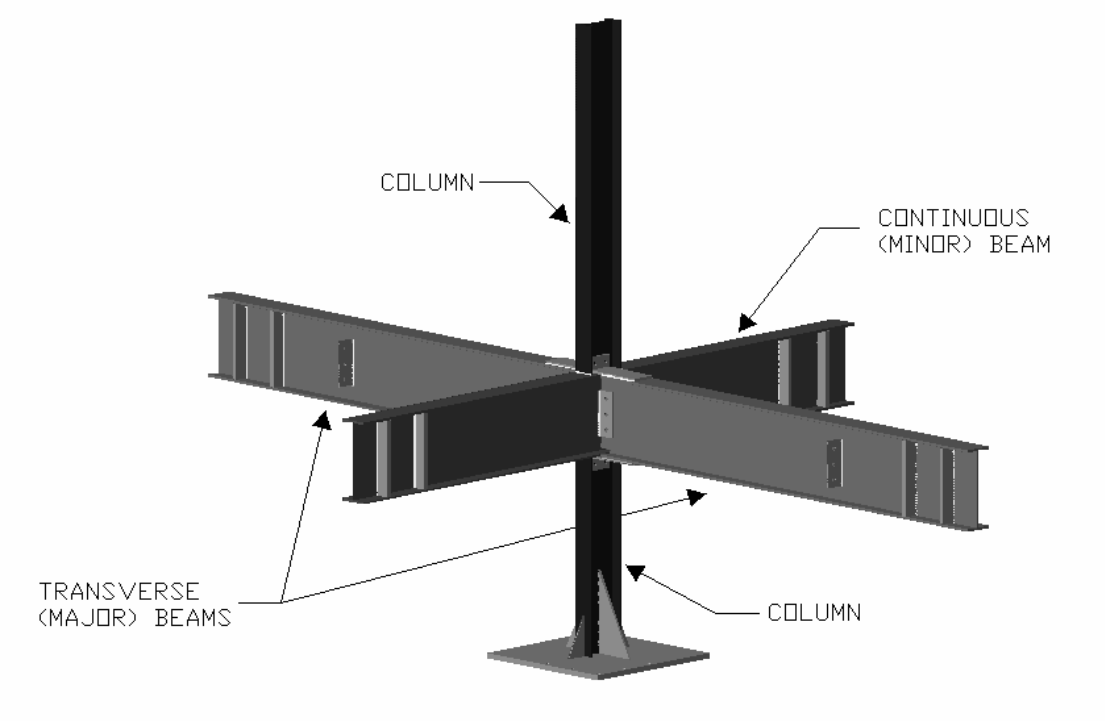

(a) Steel Skeleton

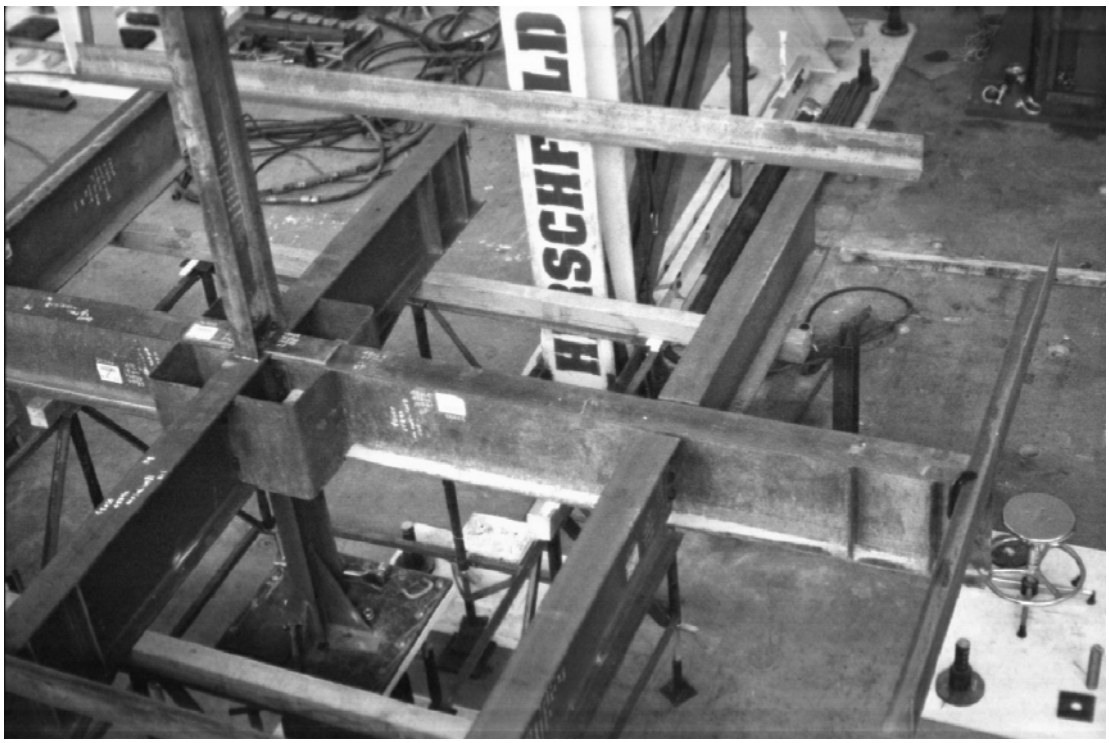

(b) Photograph of Tree with Confinement Plate Joint Detail

FIG. 5.1 ERECTION STEEL TREE

the continuous beam. The major beams had mechanical connections that were capable of resisting the full plastic moment of the composite beam-slab section with the assistance of the RC column. There were two major beams approximately 2.6 m (8.5 ft.) that framed into either side of the continuous beam to form the larger specimen dimension of 5.2 m (17 ft.). The transverse beams were prefabricated to decrease the amount of field welds with the 6.35 mm (¼ in.) thick confinement plates or face bearing plates in a location that corresponds with the face of the concrete column. Top and bottom seats were welded, respectively, to the top and bottom flanges of the transverse (major) beams and were bolted through the webs of the steel columns (Fig. 5.2).

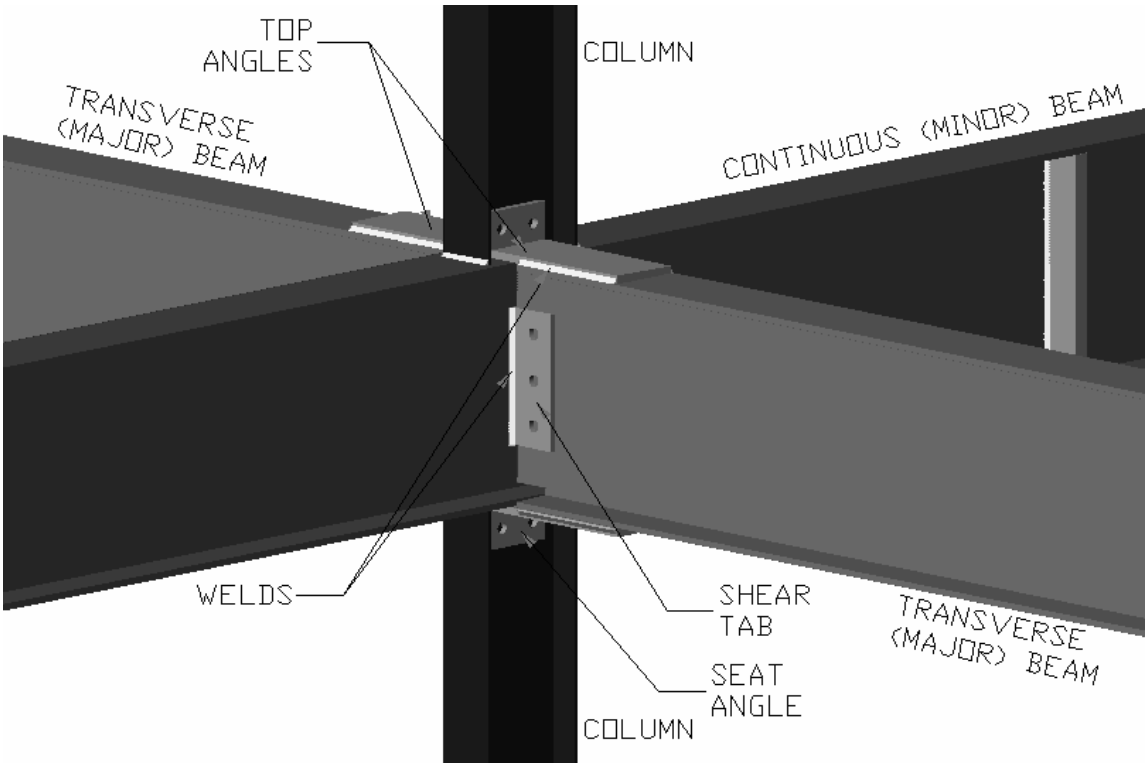

FIG. 5.2 JOINT MOMENT CONNECTION DETAIL

To support the dead load of the concrete slab, support beams were then attached to the transverse (major) beams and ran to the outer edge of the slab in the minor loading direction. The support beams were attached 1.07 m (3.5 ft.) from the outside end of the transverse beams by a bolted shear tab connection and were 1.68 m (5.5 ft) in length.

5.2.2 Joint

Fig. 5.3 highlights the two joint detailing variables that were experimentally tested: (1) confinement plates; and (2) face bearing plates in conjunction with column transverse reinforcement ties within the joint. The confinement plates were 6.35 mm (¼ in.) thick steel bent plates that were welded to only the webs of the W16x31 beams that framed into the joint. The confinement plates were not welded to the flanges so that the high strains in the beam flanges due to bending would not be transmitted in the form of torsion and potentially cause the plates to fail. No horizontal reinforcement was used in the joint of this setup. The other setup consisted of face bearing plates that were welded to both the flanges and web of the W16x31 beams. This system utilized small transverse reinforcing ties that would bind the column longitudinal reinforcement that passed through each joint quadrant to eliminate longitudinal reinforcement buckling.

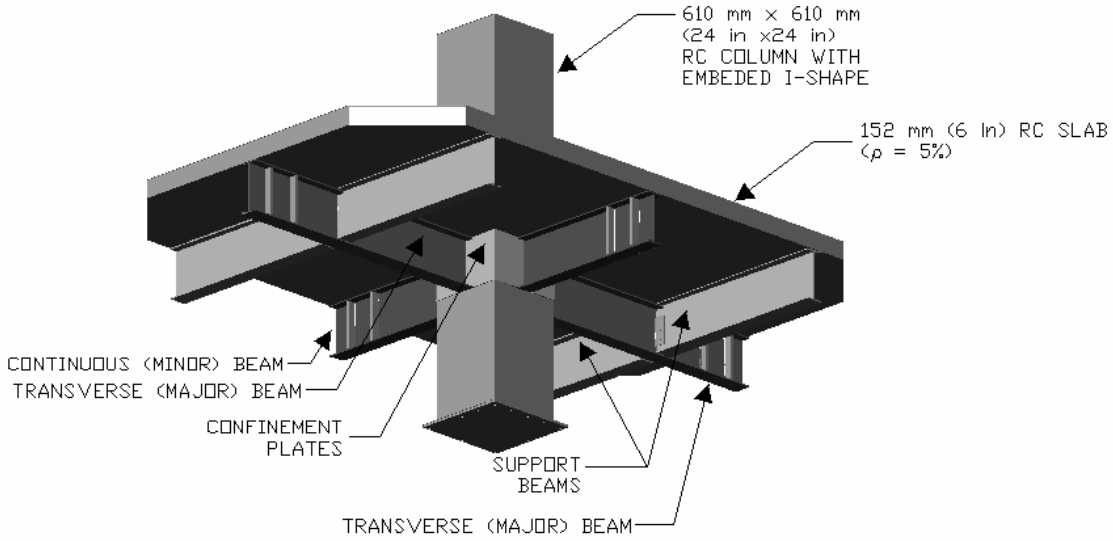

(a) Confinement Plate

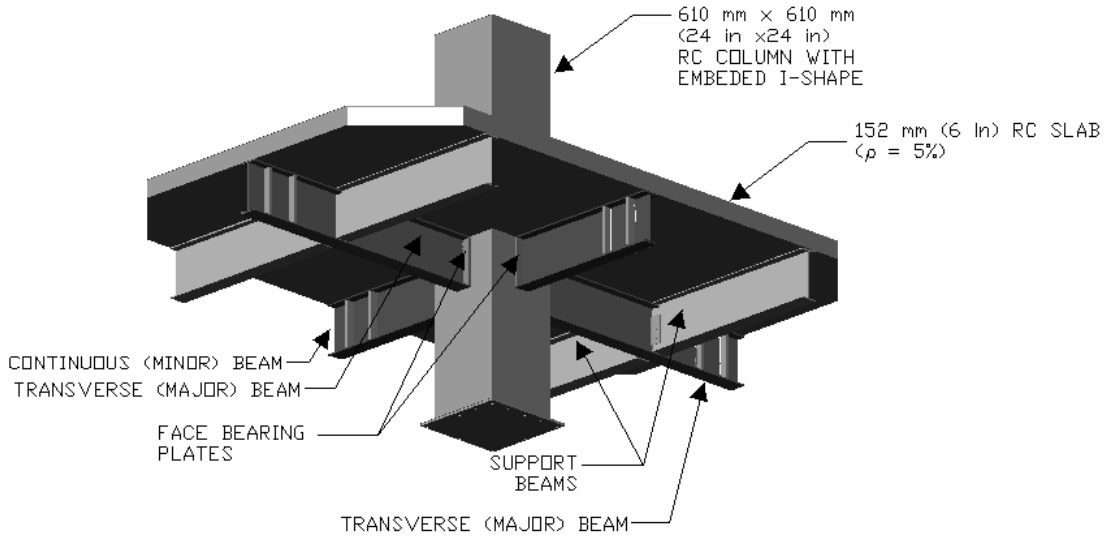

(b) Face Bearing Plates

FIG. 5.3 JOINT DETAILING

5.2.3 Slab

In preparation for pouring the concrete deck, L6x4x¼ steel angle was welded to the outer edges of the beams which formed a rim that would contain the uncured concrete and provide a guide to create a constant 152 mm (6 in.) thick concrete slab. Then, Vulcraft 2 VLI gauge 20 corrugated metal decking was placed on top of the steel beams. The flukes of the metal decking were orientated so that they ran parallel to the major loading direction and allowed for the proper placement of shear studs to create a full composite beam-slab cross section. The 19 mm (0.75 in.) diameter shear studs were placed with a typical welding gun by a licensed welder (Fig. 5.4). Double shear studs were placed on the transverse (major) beams every 152 mm (6 in.) and on the continuous (minor) beam staggered double shear studs were placed in every fluke at a spacing of 12 in. to ensure full composite action. Single shear studs were placed in every fluke of the support beams which added rigidity to the cruciform and helped hold the decking in place. Shear studs were not placed on the beam near the RC column face to prevent brittle fracture in the potential hinge zones.

With all structural steel and metal decking in place, the slab steel was placed. The slab steel was composed of 12.7 mm (#4) reinforcing bars that were placed 19 mm (¾ in.) from the top surface of the concrete slab with plastic chairs. The slab steel ran in both directions with a center to center spacing of 152 mm (6 in.) except for a 1067 mm (42 in.) width along the minor and major beams were the center to center spacing of the reinforcing steel was 76.2 mm (3 in.) which a the reinforcement ratio of about 0.556%

(Fig. 5.5). The slab steel did not pass through the column, which is a typical detail that reduces joint congestion. The steel angle, metal decking, slab steel and shear studs are all shown in Fig. 5.6.

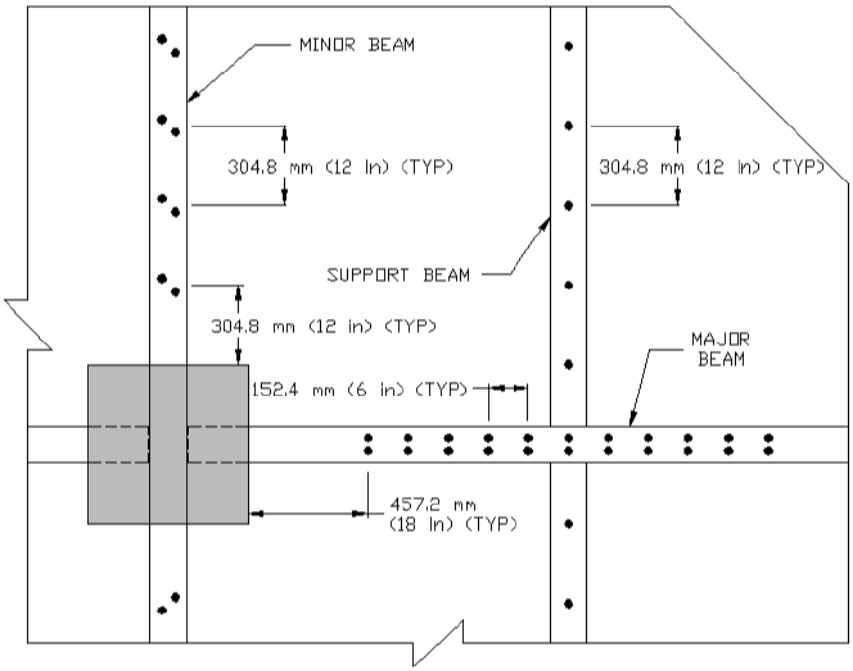

FIG. 5.4 SHEAR STUD PLACEMENT

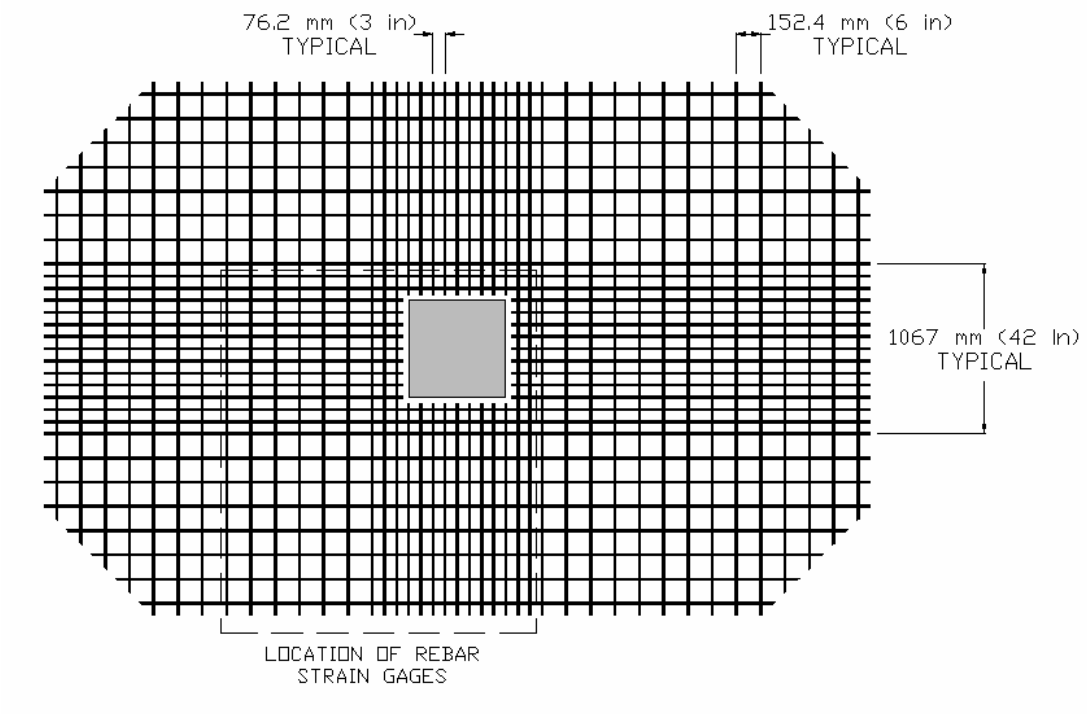

FIG. 5.5 SLAB REINFORCEMENT PLACEMENT

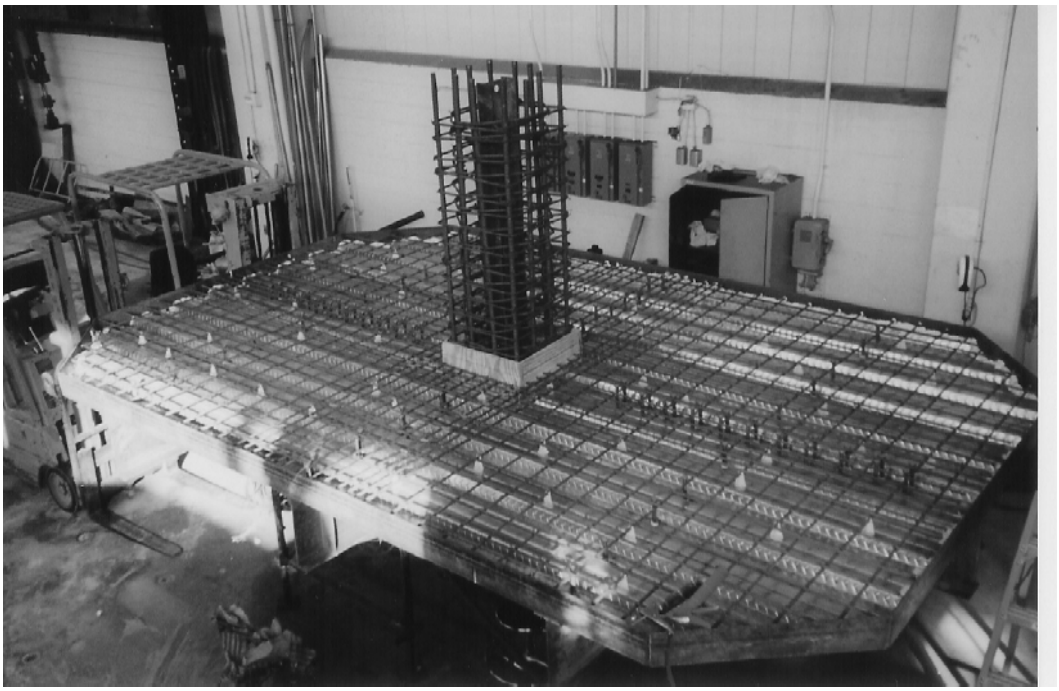

FIG. 5.6 SLAB REINFORCEMENT AND SHEAR STUD PHOTOGHRAPH

5.2.4 RC Column Placement

Column reinforcing steel was then placed around the steel erection column to construct a 610 mm (24 in.) square RC column which followed the ACI-318 (2002) seismic detailing provisions. The longitudinal reinforcement consisted of twelve 28.7 mm (#9) ASTM A615 Grade 60 reinforcing bars with three bars in each of the four quadrants of the column (Figs. 5.7 and 5.8). These bars ran the entire height of the column through the joint and were welded to the base plate following the AWS provisions for welding reinforcing steel. Although welded longitudinal reinforcement transferred the bending and shear forces into the base pin connection, the overall behavior of the subassembly being tested would be preserved. Transverse column reinforcement consisted of both square and octagonal ties made from 12.7 mm (#4) ASTM A615 Grade 60 rebar and were placed at a spacing of 152 mm (6 in.) to conform with ACI-318 (2002) seismic detailing (Fig. 5.8). At 229 (9 in.) above and below the structural steel beams, the spacing was reduced to 76.2 mm (3 in.) and rectangular hoops were added to ensure a fully plastic moment connection. The rectangular hoops were also made from 12.7 mm (#4) rebar and orientated so that the longer dimension of the hoop runs the same direction as the major loading direction. It bound the four interior longitudinal bars that were located closest to the transverse beams. This reinforcement was designed to resist the compressive concrete strut that formed from the seat angles (Fig. 5.9) and the outer compressive concrete strut (Fig. 5.10) during bending of the composite beam-slab section. The seat angles that are welded to the flanges of structural

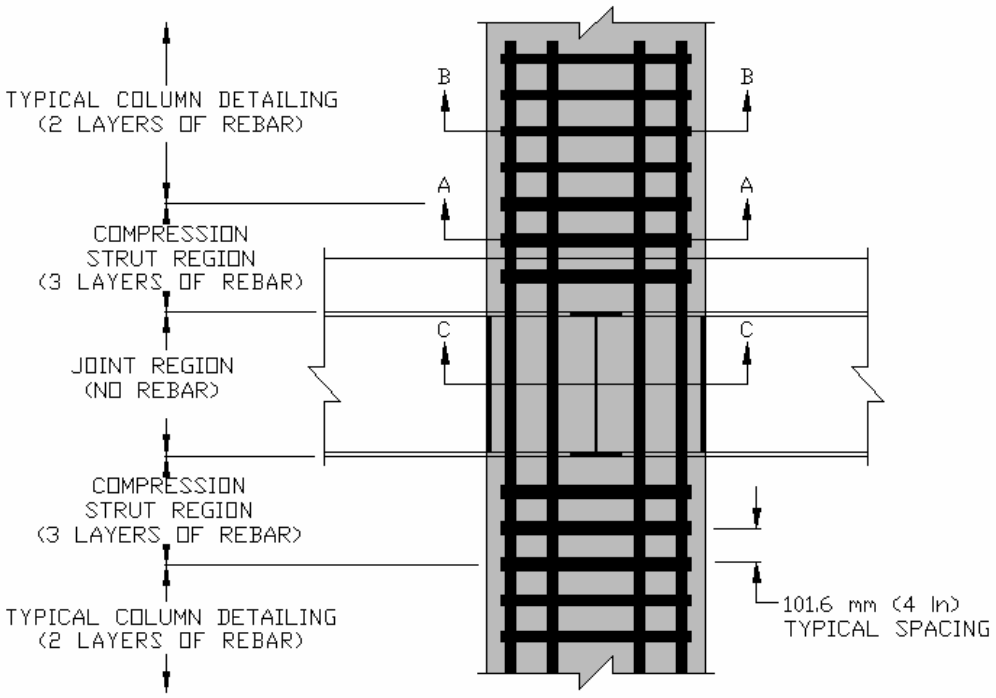

(a) Confinement Plate Detail

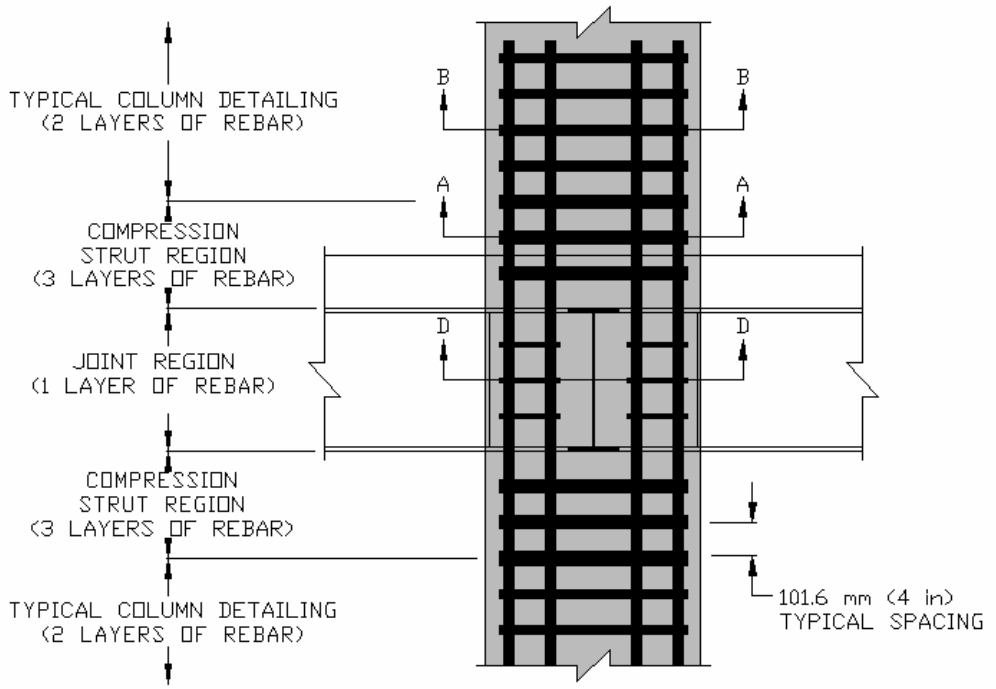

(b) Face Bearing Plate Detail

FIG. 5.7 COLUMN REINFORCEMENT ELEVATION

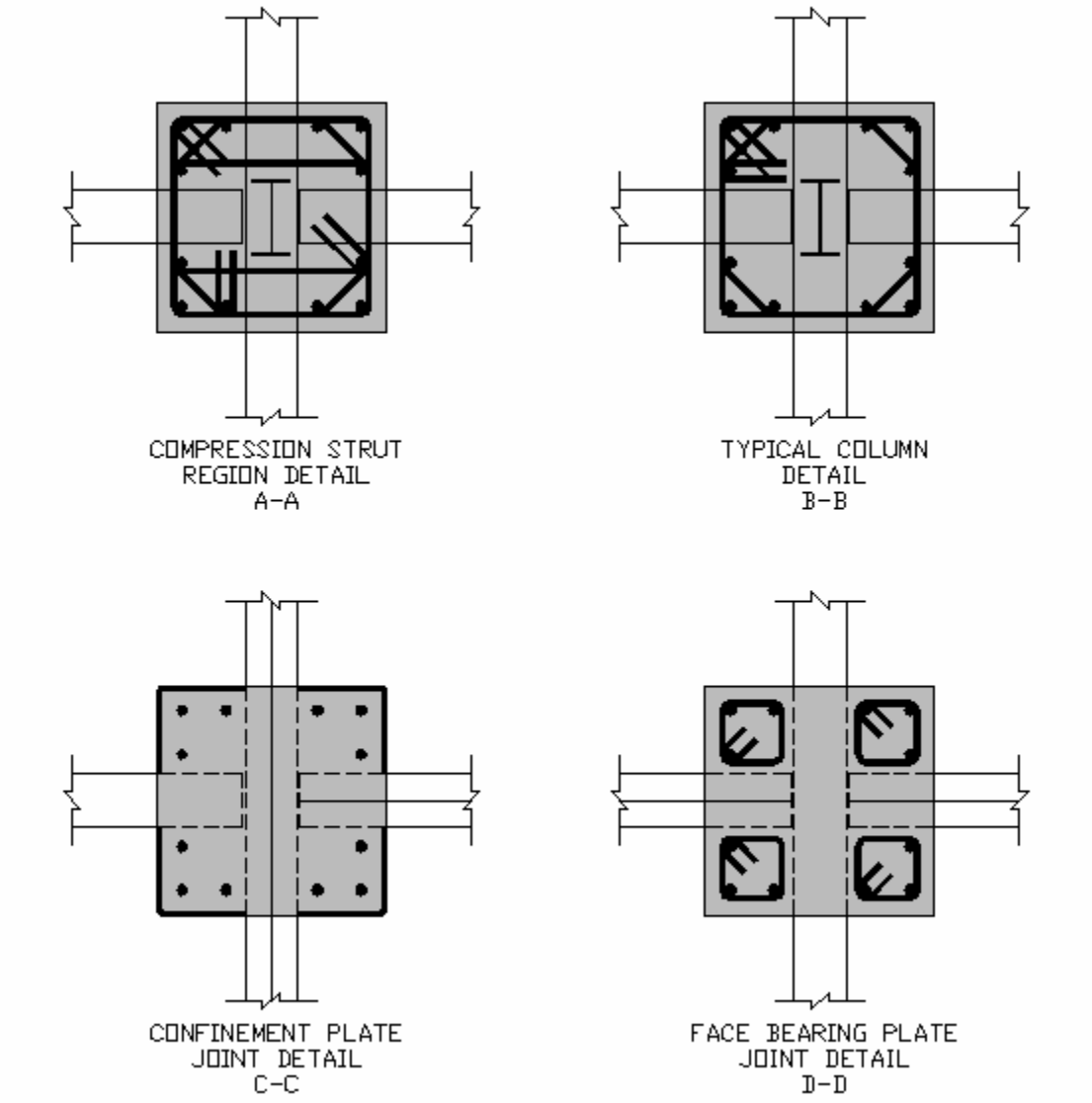

FIG. 5.8 COLUMN REINFORCEMENT - CROSS SECTIONS

steel beam and bolted to the web of the steel column create a moment connection. The angles resist tensile forces from the beam flanges by the bolts and by bearing against the concrete in the immediate vicinity.

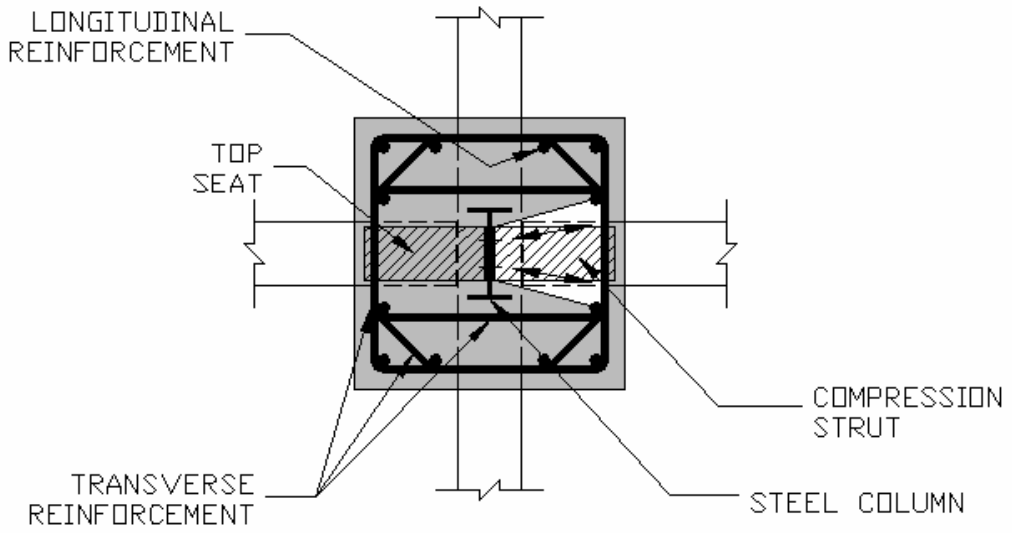

(a) Joint Cross Section (A-A)

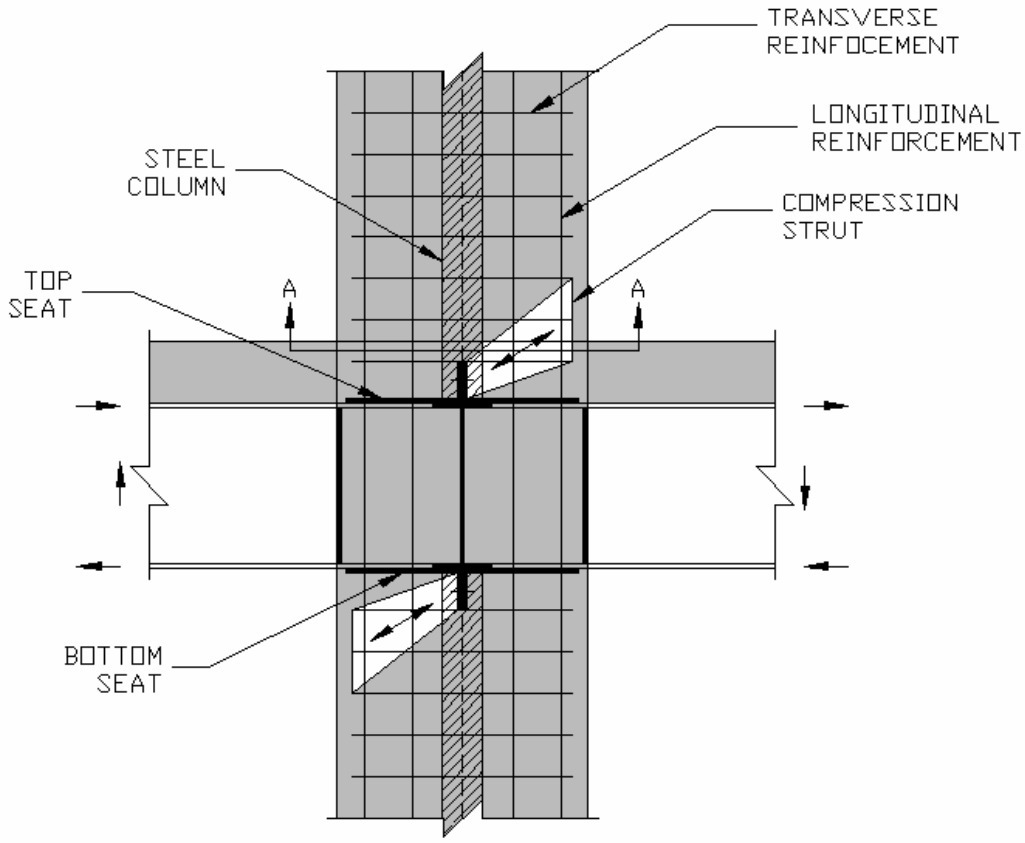

(b) Elevation

FIG. 5.9 SEAT COMPRESSIVE CONCRETE STRUT

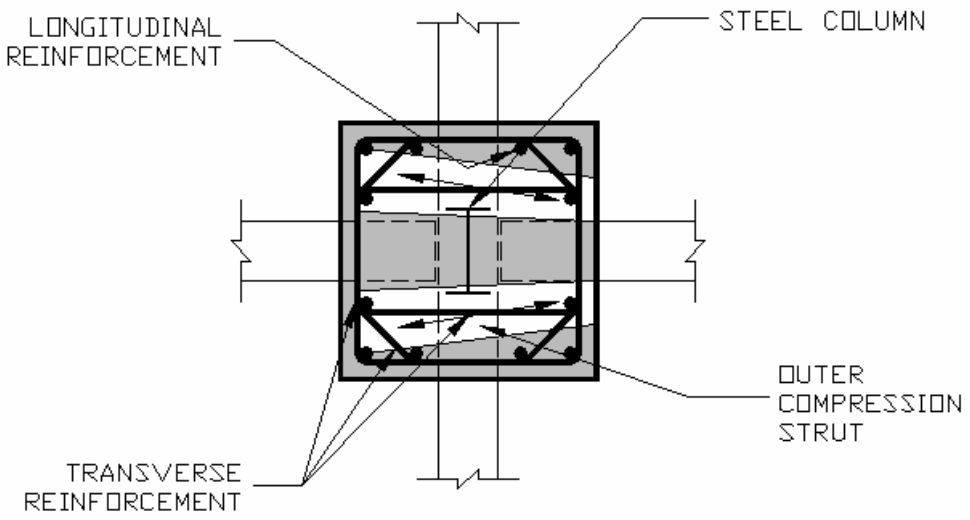

(a) Joint Cross Section (A-A)

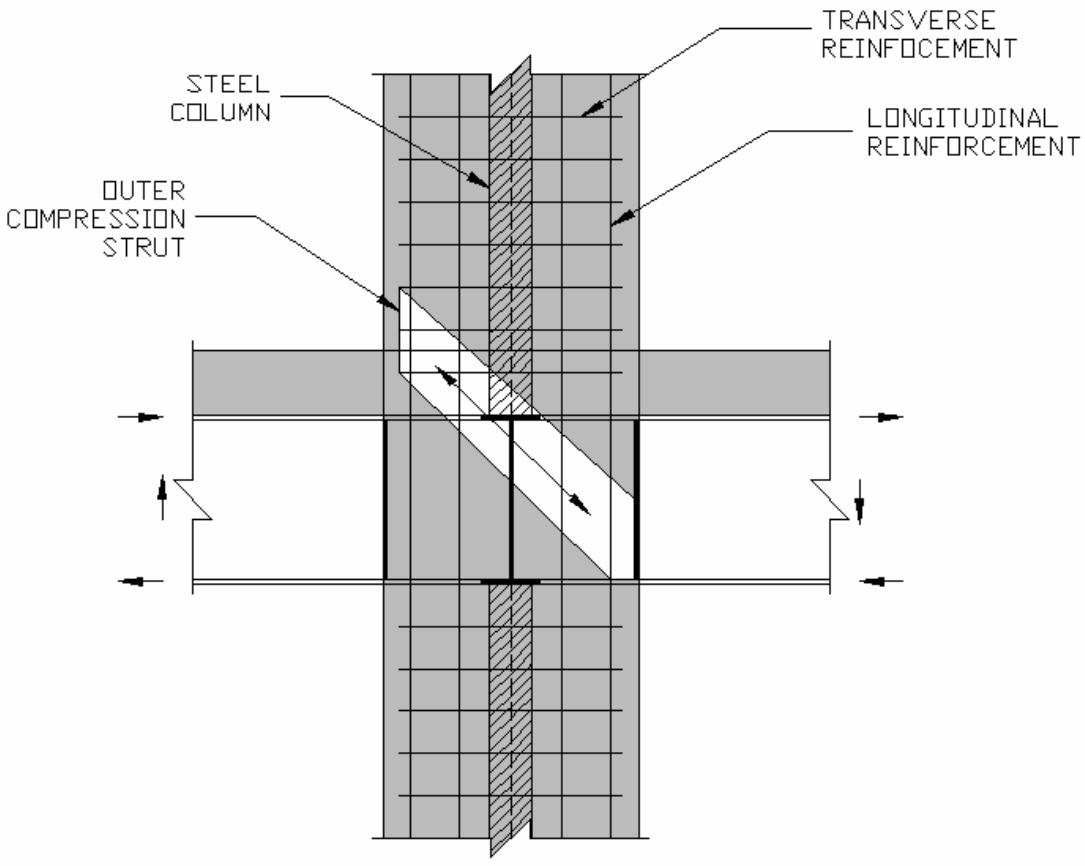

(b) Elevation

FIG. 5.10 OUTER COMPRESSIVE CONCRETE STRUT

The only difference between the column reinforcement of the two specimens was in the joint region. The specimen with the confinement plates around the joint had no transverse reinforcement in the joint region and the specimen with face bearing plates had three square ties in each of the four quadrants that were made from 12.7 mm (#4) rebar. The square ties were spaced at 101.6 mm (4 in.) and bound the three longitudinal bars corresponding to a particular joint quadrant.

5.2.5 Concrete Placement

The concrete was placed in two separate pours; first the slab and then the column. The slab was poured with a 20.7 MPa (3 ksi) mix with a 152 mm (6 in.) slump. The concrete was placed with a large bucket that was maneuvered with an overhead crane, vibrated with a hand-held vibrator, leveled with a 3.7 m (12 ft.) long 2x12 lumber, and then finished. The concrete was allowed to cure under a plastic sheet and continually sprayed with water for the first week to create a moist environment.

Plywood and 2x4 lumber (Fig. 5.11) were used to construct forms for the columns. Steel banding and all-thread were used to hold forms together and prevent the forms from bowing under the hydrostatic pressure of wet concrete. A 27.6 MPa (4 ksi) mix with a 127 (5 in.) slump was chosen for the column pour. The concrete was placed in the bottom half of the column with a ramp which funneled the concrete through a removable access panel that was located in the top form just above the concrete slab. This method of concrete placement was chosen to reduce the risk of damaging or

displacing concrete gages placed in the joint and to reduce the chances of voids forming in the joint region. A small hole in the bottom form allowed the hand held vibrator access to bottom half of the column, which was later plugged when the wet concrete was filled to this level. When the joint filled to the top of the slab, the access panel was replaced and the top column portion of the column was poured from the opening in the top of the form. This was just a precautionary measure taken in the lab so that the concrete gages would not be damaged during the pour and this would not be done during actual construction.

(a) Bottom Form

(b) Confinement Plate Form

(c) Face Bearing Plate Form

(d) Top Form

FIG. 5.11 PHOTOGRAPHS OF COLUMN FORMS

5.3 CONSTRUCTABILITY ISSUES AND SOLUTIONS

During the construction of the cruciform specimens, some constructability issues arose due to steel fabrication tolerances and voids in the joint region when pouring the columns.

Two problems identified with the steel joint detailing: (1) alignment issues with the bent plates; and (2) alignment of the confinement plates. The alignment of the bent plates was a problem because of skewed shear tabs which prevented the beam flanges to align with one another and with the column web. To solve this problem, the holes of the column web were slotted and the bolts were undersized. The bearing strength of the concrete against the bent angle allowed the bolts to be undersize. There was too large a gap between the web of the continuous beam and the confinement plate for the field welding. The gap was due to a combination of errors that accumulate during the fabrication and placement of the confinement plates. The confinement plates were pried and clamped into position then tack welded in position then field wielded at a later time (Fig. 5.12).

Voids and honeycombing were present in both specimens (Fig. 5.13), the cause of which can probably be attributed to several factors. Voids of various sizes formed in several locations: under the bottom flange of the steel beams, under the top flange of the structural beams, beside the web of the steel beams and in the joint region outside the core of the column. The honeycombing was predominant in the concrete cover and

located mostly in the corners. One potential solution is requiring the concrete slump to be higher than 127 (5 in.). Great care was taken not to damage or displace the concrete gages in the joint region during the concrete pour, so the joint region was not sufficiently vibrated. The location of the joint was in the center of the pour which would not be the case with an actual pour where the joint region could be located at the top of the pour, making the joint more accessible with a vibrator. Another contributing factor may have been that the column longitudinal reinforcing steel was welded to the plate attached to the bottom column, and thus would possibly dampen the transfer of vibrations through the column cage. For constructability purposes, it would have better to not weld the column cage to the base plate.

To fix the damaged areas of the joint, first the areas without sufficient binder between the aggregate were removed with a handheld jackhammer. New forms were made with Plexiglas to monitor the placement of the Emaco S77 that was pumped through holes that were plugged as the voids were filled. Holes at the top of the form allowed air to escape and pumping ceased when these holes yielded concrete. Emaco S77 is a ChemRex product that is specifically design for vertical and overhead concrete repair and was chosen because it exhibits desirable qualities such as excellent bond strength, small aggregate size, and high viscosity during placement. The Emaco S77 was placed in levels to minimize bending of the Plexiglas forms and prevent the silicone seals from rupturing. Approximately .0566 cu. m (2.0 cu. ft.) of Emaco S77 per a

specimen was used to repair voids in both the joint and lower column. Pictures of the repaired specimens are shown in Fig. 5.14.

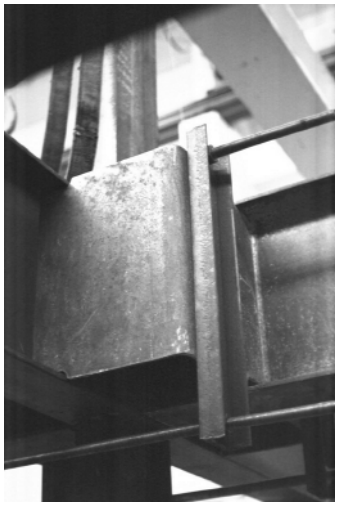

FIG. 5.12 PHOTOGRAPH OF CONFINEMENT PLATE CLAMP

(a) Void Under Beam In Specimen With Confinement Plates

(b) Void And Honeycombing In Joint Region Of Specimen With Face Bearing Plates

FIG. 5.13 VOIDS AND HONEYCOMBING IN JOINT REGION

(a) Repaired Confinement Plate Joint

(b) Repaired Face Bearing Plate Joint

FIG. 5.14 REPAIRED JOINT REGION

CHAPTER VI

EXPERIMENTAL RESULTS

6.1 GENERAL

This chapter presents the results from the two composite test specimens with different joint details: confinement plates (CP) and face bearing plates (FBP). The raw data that was recorded from the strain gages, clinometers, load cells, and LVDTs during the bi-directional quasi-static reversed cyclic loading are presented in the form of graphs to best describe and compare the behavior of the specimens. Actuator force vs. specimen drift angle data is presented to describe the deformation response of the individual components of the composite subassembly. The moment vs. rotation of the beam is compared with the predicted ultimate moment capacity of the composite beam-slab sections based on AISC (2001). Strain gages placed on the slab steel reinforcement are used to measure the magnitude of slab participation at the maximum displacement levels at different locations throughout the slab width. By analyzing the measured response from all of these aspects of the composite subassembly, an accurate evaluation of the specimen performance can be assessed.

6.2 OVERALL SUBASSEMBLY PERFORMANCE

The overall deformations and forces that were applied to each cruciform specimen were recorded by sensors on the actuators. To acquire the force reported in all graphs, an average of the forces applied by the actuators on similar axes were used (Eq.

6.1). The recorded actuator deflections were converted to a percentage drift angle by dividing by the beam length of the resisting beam (Eq. 6.2).

$$\text{Force} = \frac{F_{\text{Left}} - F_{\text{Right}}}{2} \tag{6.1}$$

$$\text{Drift Angle}\,(\%) = \frac{100\delta}{\text{L}} \tag{6.2}$$

where

F_{Left}, F_{Right} = left and right actuator force, respectively
$\delta = \delta_{\text{Support}} + \delta_{\text{Column}}, \delta_{\text{Joint}}, \delta_{\text{Beam}}$ *or* δ_{Total}
L = distance from point of load to center of joint

The total imposed drift angle was broken up into three components: column and support, joint, and beam. These three components are demonstrated in Fig. 6.1. The column and support components account for flexibility in the supporting frame system and the bending deformations of the column. The joint deformations recorded the overall joint deformation attributed to panel shear, vertical bearing, and elongation, as described in Section 6.3. The remaining deformation was allocated to bending in the composite beam-slab sections. The calculations used to derive these components are shown in Eqs. 6.3 – 6.5, respectively.

$$\delta_{\text{Column}} + \delta_{\text{Support}} = \frac{\theta_5 + \theta_6}{2}\text{L} \tag{6.3}$$

$$\delta_{\text{Joint}} = \frac{\left(\theta_2 + \theta_3\right) - \left(\theta_5 + \theta_6\right)}{2} \mathrm{L_o} \tag{6.4}$$

$$\delta_{\text{Beam}} = \delta_{\text{Total}} - \delta_{\text{Joint}} - \left(\delta_{\text{Column}} + \delta_{\text{Support}}\right) \tag{6.5}$$

where

$\theta_1, \theta_2, \theta_3, \theta_4, \theta_5, \textit{and } \theta_6$ = measured rotations (rad) defined in Fig. 4.7
δ_{Total} = total deformation of composite specimen
$\delta_{\text{Column}} + \delta_{\text{Support}}$ = deformation of RC column and supporting frame
δ_{Joint} = deformation of joint region
δ_{Beam} = deformation of composite beam
$\mathrm{L_o}$ = length of the composite beam from the face of the reinforced concrete column to the location of load application

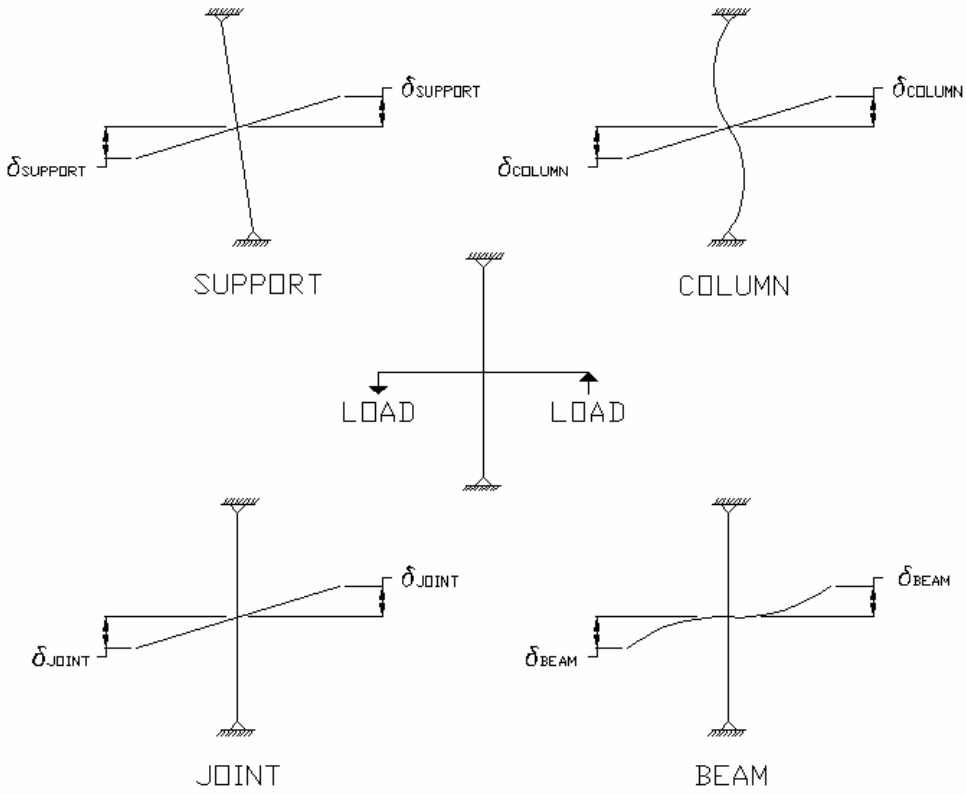

FIG. 6.1 SPECIMEN DISPLACEMENT COMPONENTS

The component response of the confinement plate specimen in the major loading direction is shown in Fig. 6.2 and the minor loading direction is shown in Fig. 6.3. The component response of the face bearing plate specimen in the major loading direction is shown in Fig. 6.4 and the minor loading direction is shown in Fig. 6.5. The total deformation and the deformation found in the column and support was comparatively similar for the two specimens in the major loading direction directions. The column and support component was nearly linear, which was expected, and the offset in the data was attributed to slip in the pin connections located at the ends of the column which was noted during the testing. The joint region of the confinement plate specimen was stiffer than that of the face bearing plate specimen, which enforced more beam deformations in the confinement plate specimen. Pinching found in the joint data was attributed to crushing of the concrete in the joint region. The data in the minor loading direction was relatively similar and remained relatively linear compared to the data for the major loading direction.

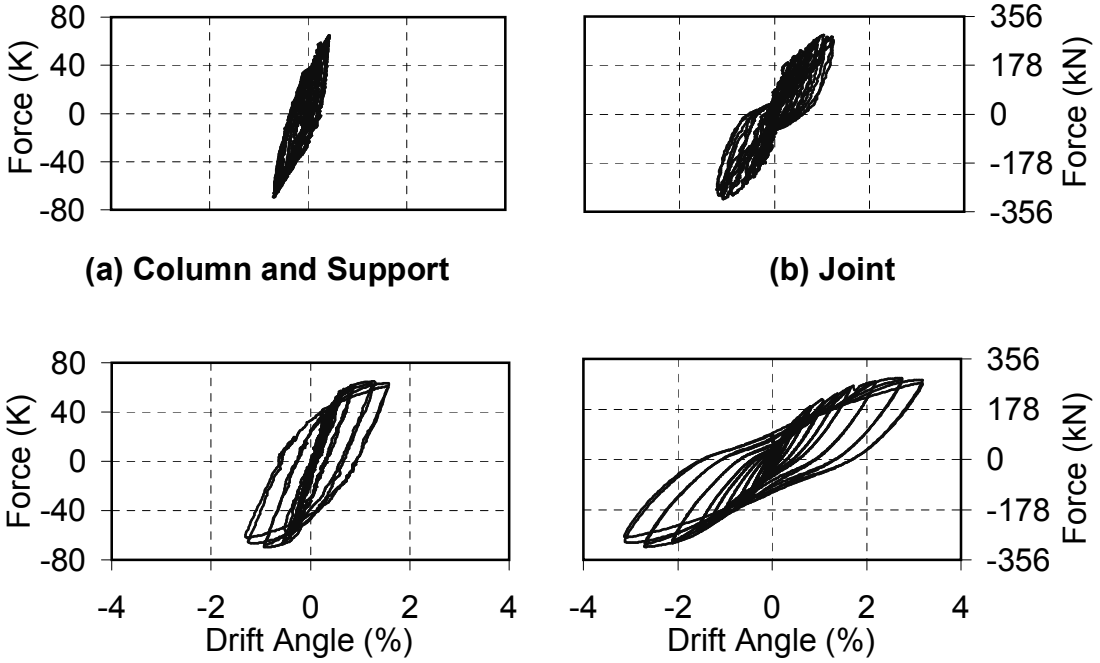

(a) Column and Support **(b) Joint**

(c) Beam **(d) Total**

FIG. 6.2 MAJOR COMPONENT RESPONSE (CP)

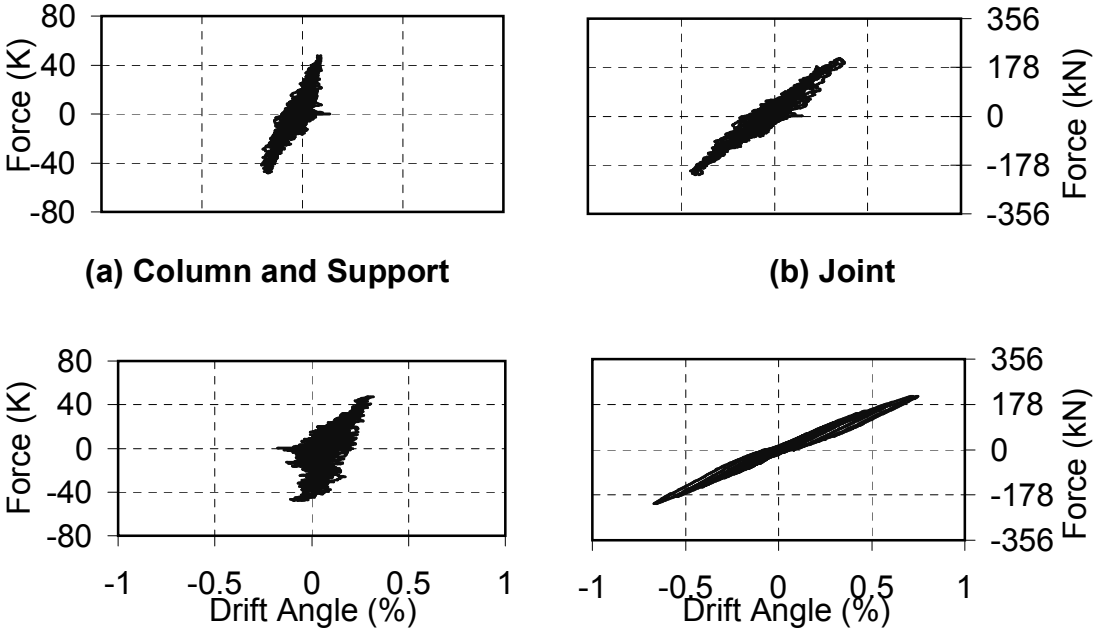

(a) Column and Support **(b) Joint**

(c) Beam **(d) Total**

FIG. 6.3 MINOR COMPONENT RESPONSE (CP)

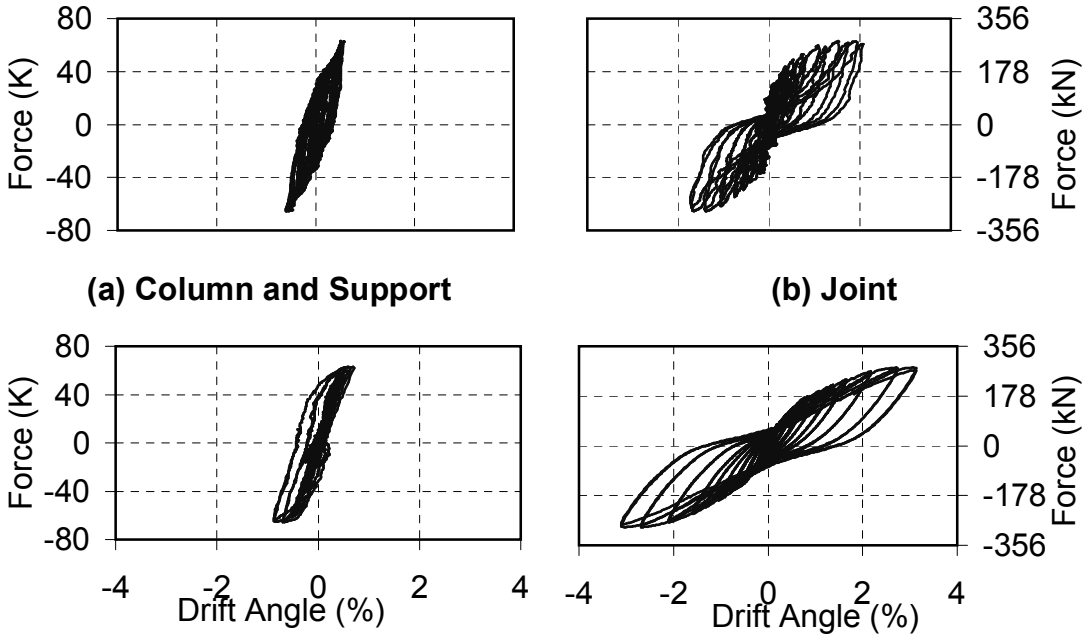

(a) Column and Support **(b) Joint**

(c) Beam **(d) Total**

FIG. 6.4 MAJOR COMPONENT RESPONSE (FBP)

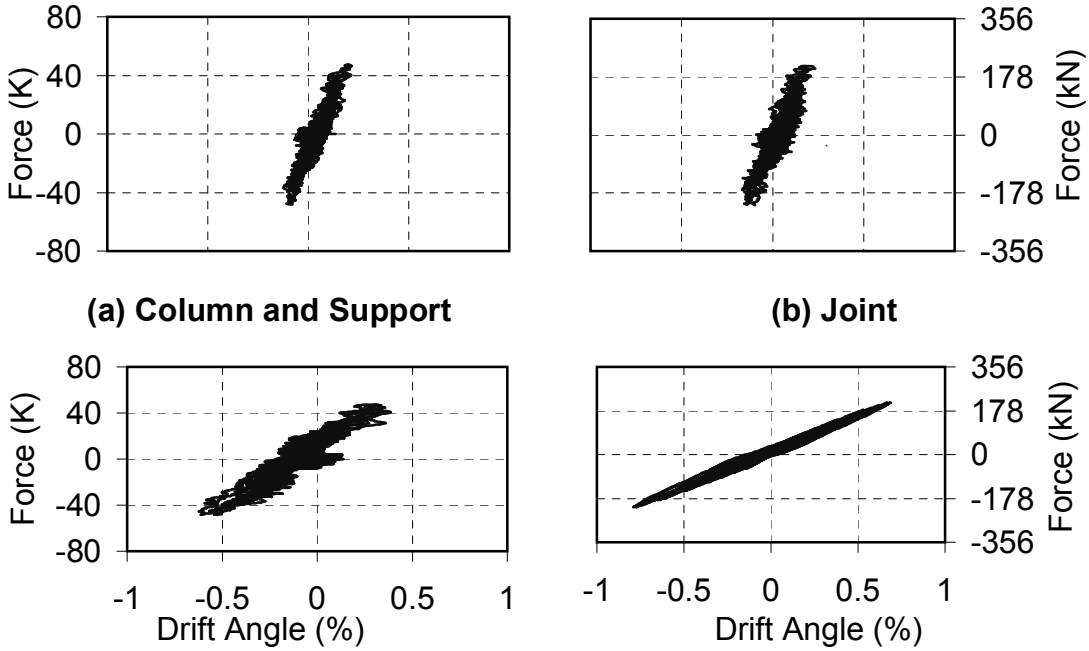

(a) Column and Support **(b) Joint**

(c) Beam **(d) Total**

FIG. 6.5 MINOR COMPONENT RESPONSE (FBP)

6.3 JOINT BEHAVIOR

The joint deformation component was further broken down into the failure components of vertical bearing, joint panel shear and elongation as shown in Fig. 6.6. Vertical bearing deformations were calculated using Eq. 6.6. The remaining deformations were considered to be shear deformations which were calculated by subtracting the bearing deformation from the total joint deformation (Eq. 6.7). The elongation deformation component is shown separately and calculated taking the difference of the clinometer rotations that were attached to the confinement plates or face bearing plates $\left(\theta_2 \text{ and } \theta_3 \text{ in radians}\right)$ (Eq. 6.8).

$$\delta_{\text{Bearing}} = \frac{\left(\delta_1 - \delta_2\right) - \left(\theta_2 + \theta_3 - \theta_5 - \theta_6\right) \text{L}_\text{d}}{\text{L}_\text{D}} 100 \tag{6.6}$$

$$\delta_{\text{Shear}} = \delta_{\text{Joint}} - \delta_{\text{Bearing}} \tag{6.7}$$

$$\theta_{\text{Elongation}} = \theta_2 - \theta_3 \tag{6.8}$$

where

δ_{Bearing} = joint deformation due to vertical bearing
δ_1, δ_2 = measured displacements $\left[\text{mm}\left(\text{in}\right)\right]$ defined in Fig. 4.7
L_D = horizonal distance between displacement transducer δ_1 and δ_2
L_d = horizonal distance between clinometers transducer θ_1 and θ_2 or θ_3 and θ_4
δ_{Shear} = joint deformation due to joint shear
$\theta_{\text{Elongation}}$ = joint deformation due to joint elongation

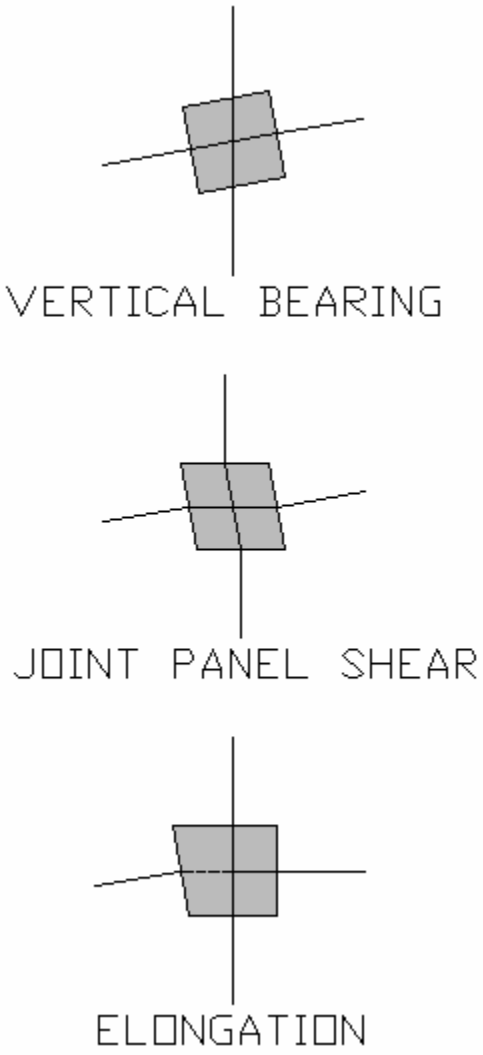

FIG. 6.6 JOINT DEFORMATION COMPONENTS (Bugeja et al. 1999)

In both specimens, the panel shear mechanism was the dominant deformation component, but joint shear deformation was much more prominent in the face bearing plate detailing (Fig. 6.7). This photograph was taken while the beam was loaded with a positive moment during a 6.7% story drift and shows the crack that was caused from shear deformation. The cover plate detail demonstrated slightly better performance compared to that of the face bearing plate detail due to confinement of the concrete joint

core. This was demonstrated by removing the confinement plate and inspecting the concrete underneath (Fig. 6.8). Figs. 6.9 and 6.10 separate the total joint deformations into vertical bearing and joint panel shear mechanisms. The joint elongation component is demonstrated in radians in Figs. 6.11 and 6.12.

FIG. 6.7 CRACK IN JOINT (FBP)

(a) Exposed Concrete in Joint

(b) Removed Confinement Plate

FIG. 6.8 INNER CONCRETE CORE (CP)

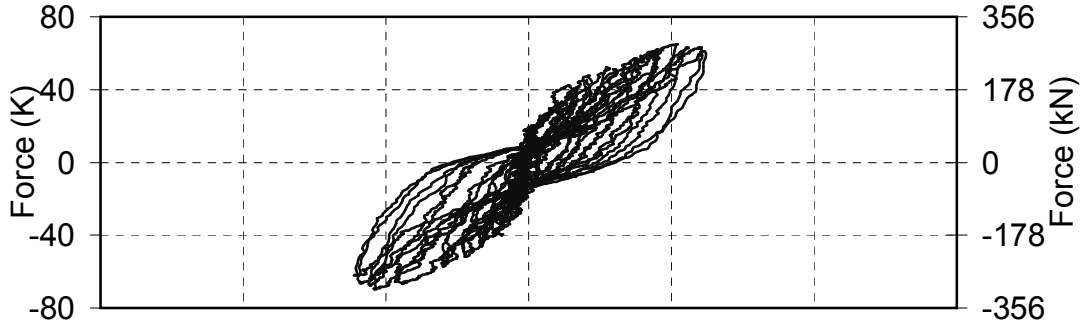

(a) Joint

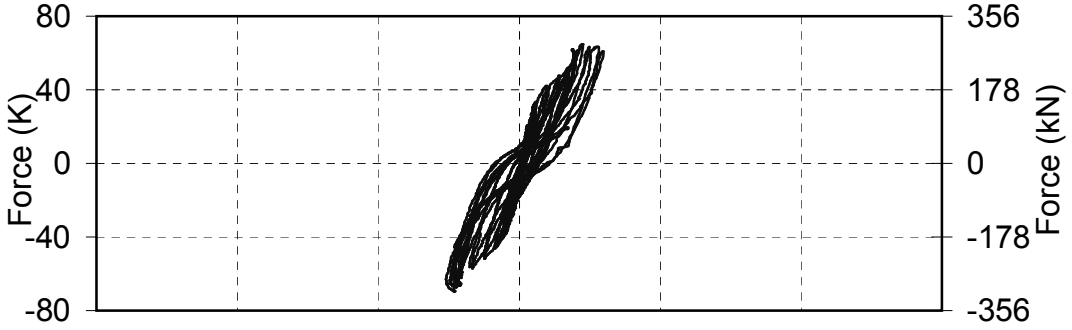

(b) Bearing

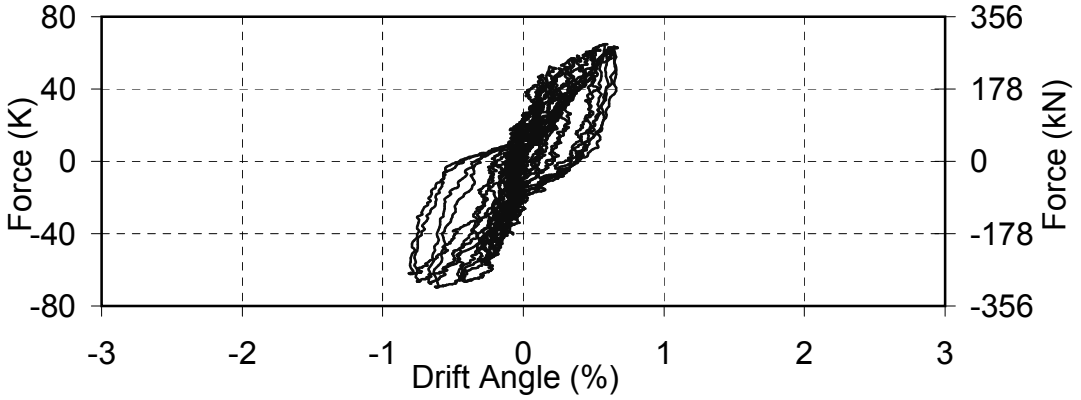

(c) Shear

FIG. 6.9 JOINT RESPONSE (CP)

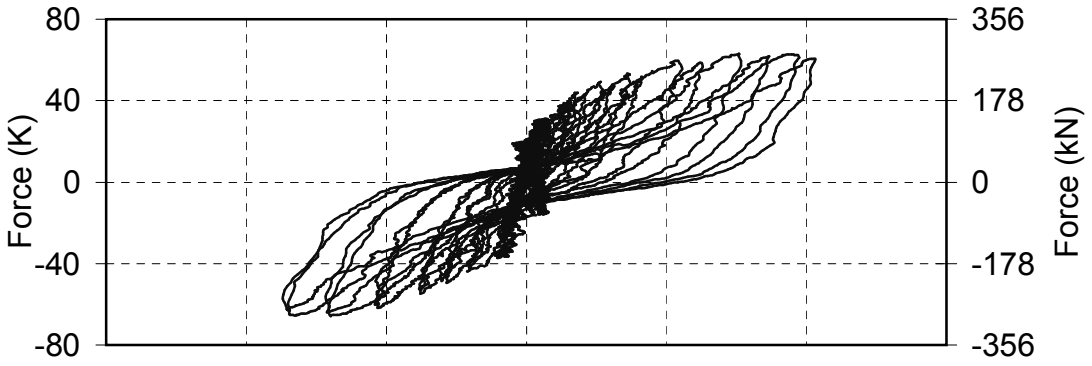

(a) Joint

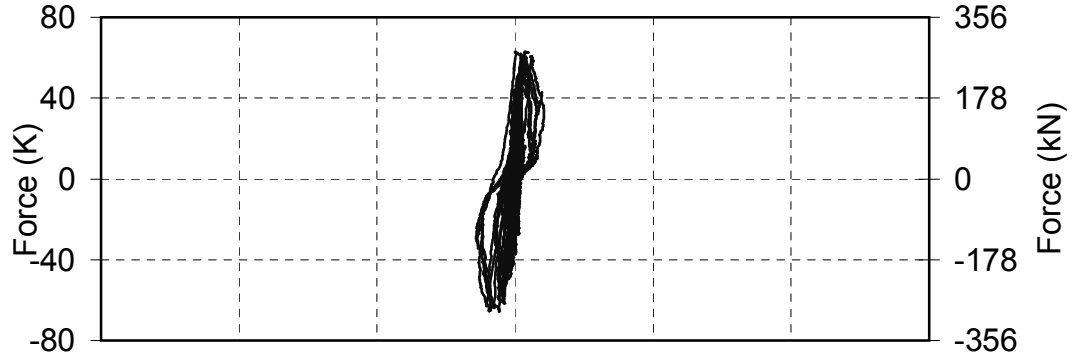

(b) Bearing

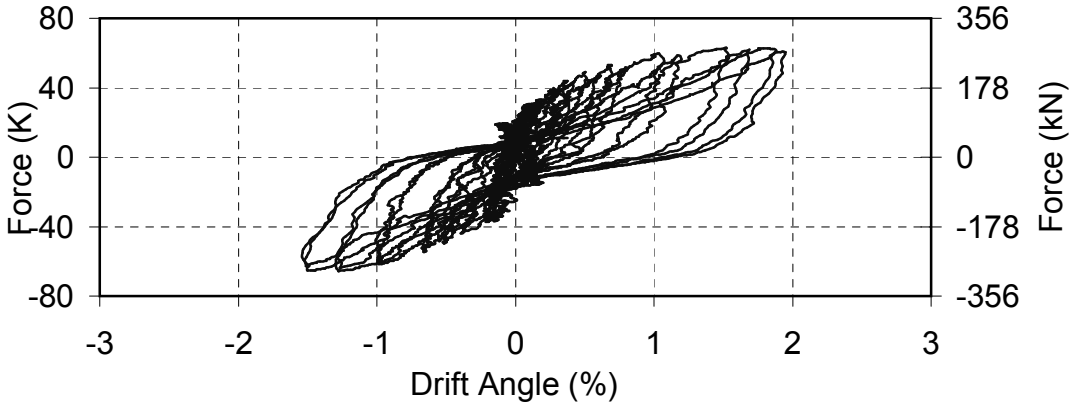

c) Shear

FIG. 6.10 JOINT RESPONSE (FBP)

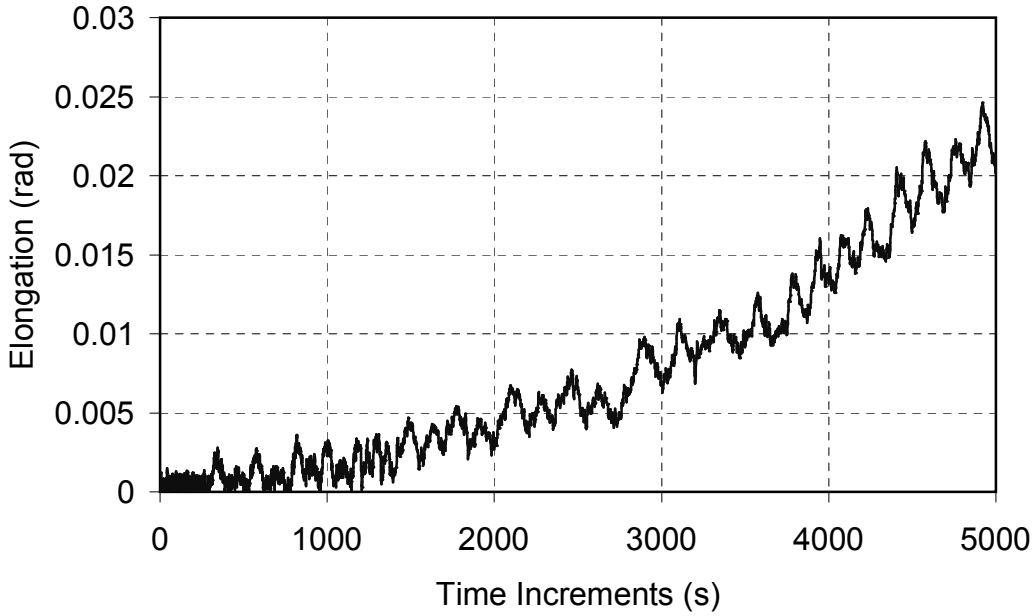

FIG. 6.11 JOINT ELONGATION (CP)

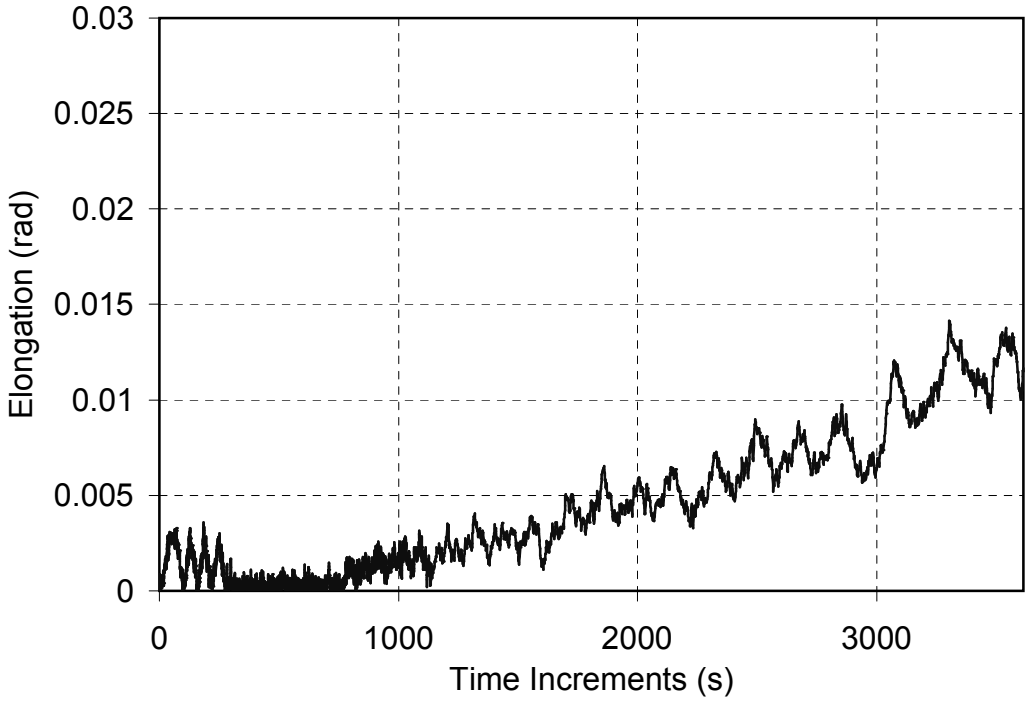

FIG. 6.12 JOINT ELONGATION (FBP)

The elongation of the confinement plate detail was approximately twice that of the face bearing plate detail most likely because the confinement plate increased the joint panel shear strength and engaged more of the concrete strut that forms in the joint.

6.4 COMPOSITE BEAM BEHAVIOR

The beam moment-rotation response is shown in Figs. 6.13 and 6.14. The ultimate moment capacities of the composite beam are based on AISC (2001), see Section 3.2. The moment that was resisted by the critical beam section was calculated by multiplying the applied actuator force by the length from the actuator to the column face (Eq. 6.9). The beam rotation was determined by subtracting the rotation measured by the interior clinometer attached to the web of the beam from the exterior clinometer attached to the web of the beam (Eq. 6.10).

$$\text{Moment} = \text{Force} * L_o \tag{6.9}$$

$$\theta_{\text{Beam}} = \theta_7 - \theta_1 \; or \; \theta_8 - \theta_4 \tag{6.10}$$

where

Force = load applied by the actuators
L_o = length of the composite beam from the face of the reinforced concrete column to the location of load application

Figs. 6.15 - 6.17 show the progression of the yielding and buckling of the web and bottom flange of the structural steel beam for both specimens.

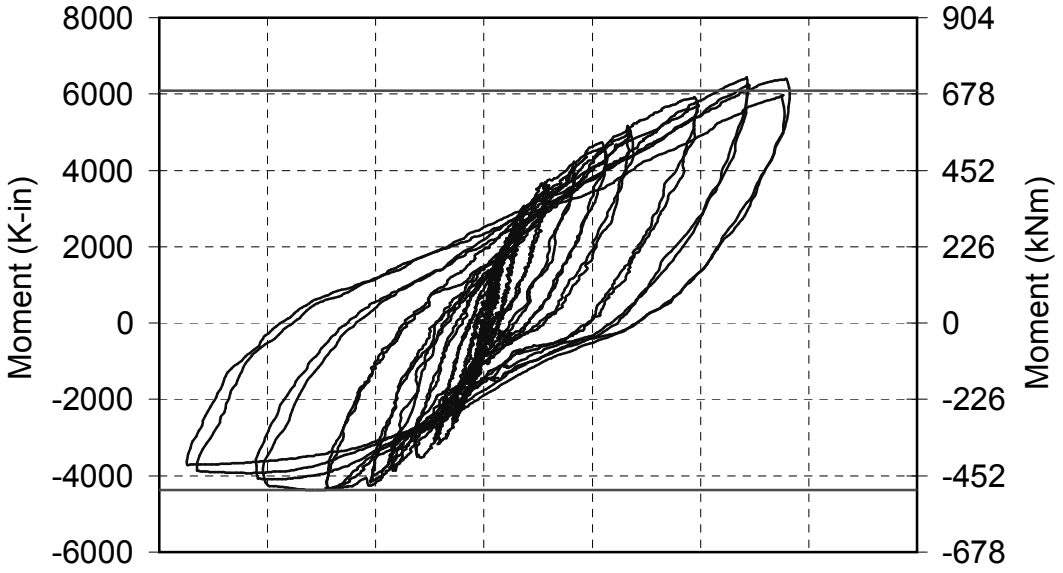

(a) BEAM LOADED BY 100A ACTUATOR

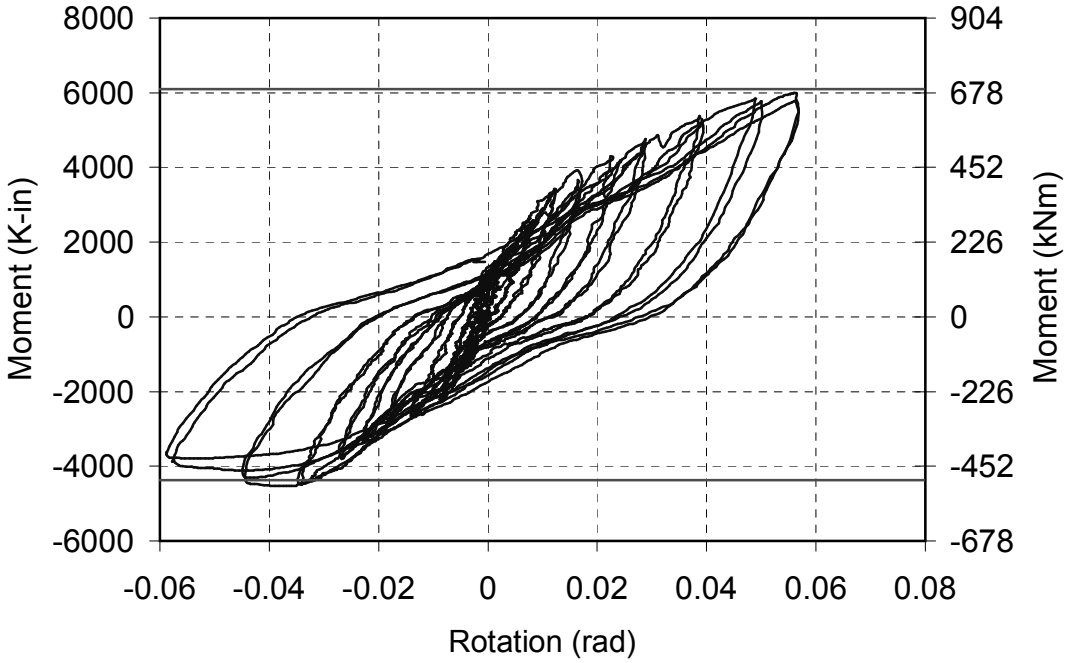

(b) BEAM LOADED BY 100B ACTUATOR
FIG. 6.13 BEAM MOMENT ROTATIONS (CP)

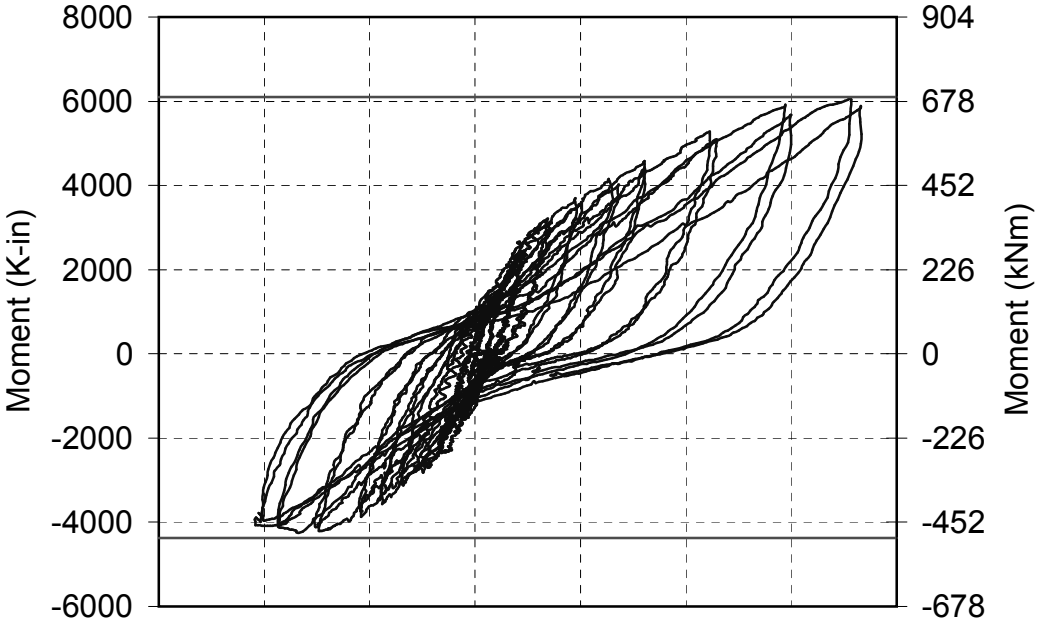

(a) BEAM LOADED BY 100A ACTUATOR

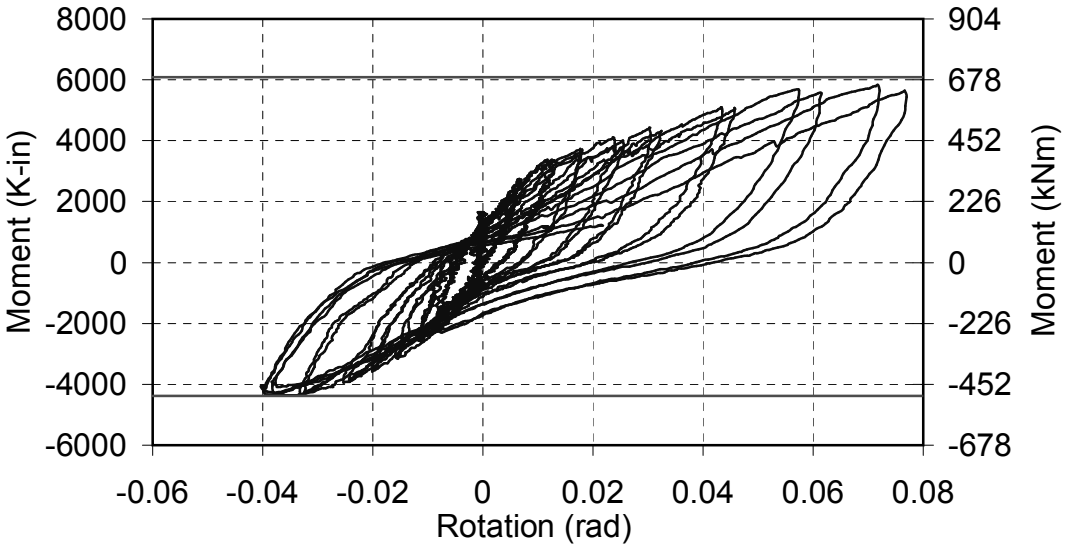

(b) BEAM LOADED BY 100B ACTUATOR
FIG. 6.14 BEAM MOMENT ROTATIONS (FBP)

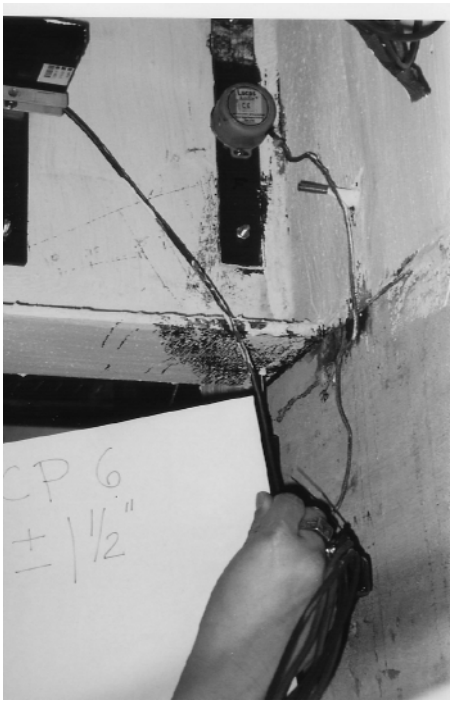

(a) ± 38 mm (1.5 in)

(b) ± 51 mm (2 in)

(c) ± 76 mm (30 in)

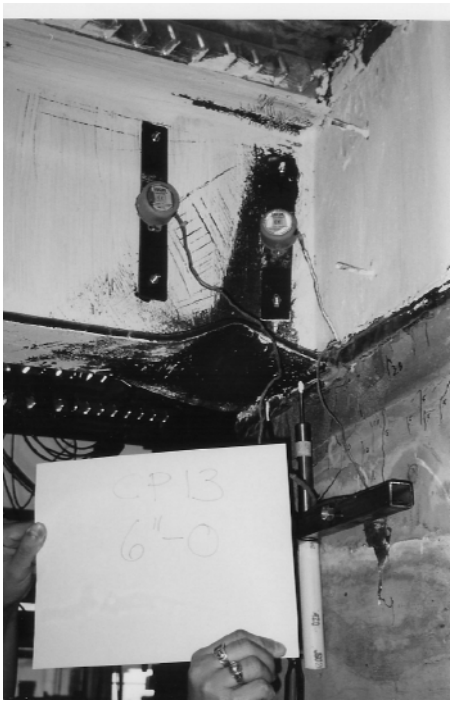

(d) 0 – 152 mm (6in)

FIG. 6.15 BEAM DEFORMATION DURING TESTING (CP)

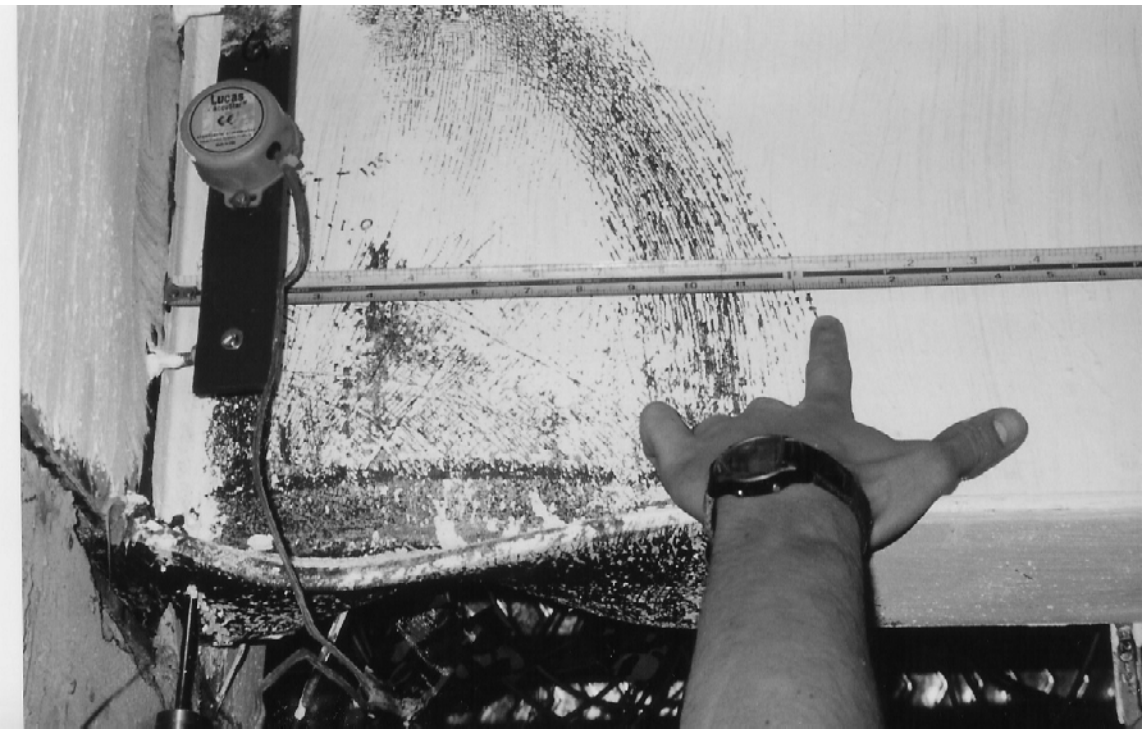

(e) Web Yielding
FIG. 6.15 CONTINUED

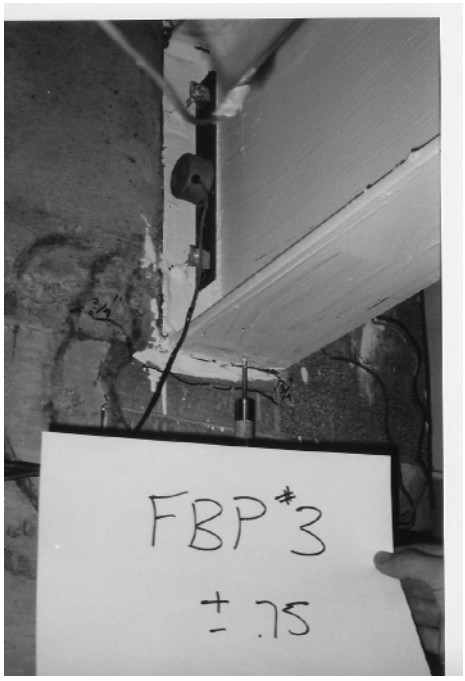

(a) ± 19 mm (0.75 in)

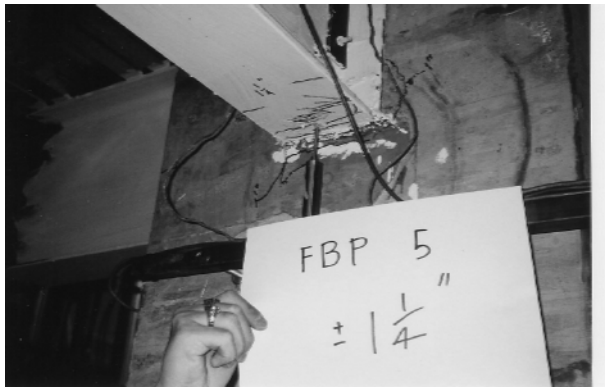

(b) ± 32 mm (1.25 in)

(c) ± 19 mm (0.75 in)

(d) ± 76 mm (3 in)

FIG. 6.16 BEAM DEFORMATION DURING TESTING (FBP)

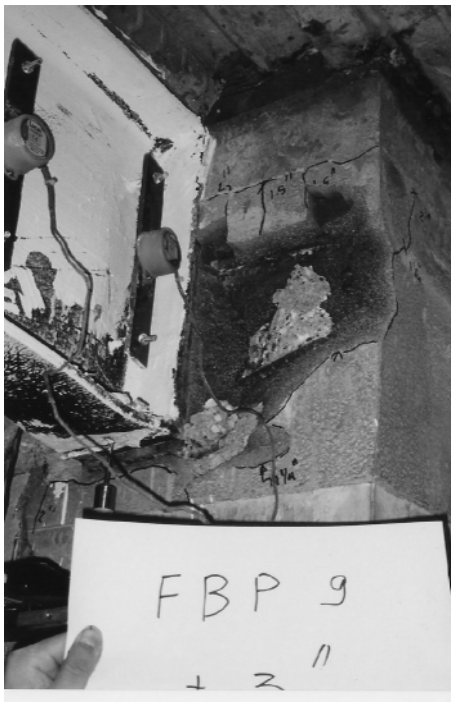

(e) ± 76 mm (3 in)

(f) ± 127 mm (5 in)

FIG. 6.16 CONTINUED

The beam moments and rotations for the confinement plate detail are shown in Fig. 6.15 and the results for the face bearing plate detail are shown in Fig. 6.16. The results for both actuators in the major loading direction are shown and for similar each respective specimen. The negative moment capacity of the beam was reached in both specimens when the 489 kN (110 K) actuators loading the specimen in the major direction reached a displacement of 63.5 mm (2 ½ in.) or a drift angle of 2.8% at which time it was noted during the experiment the bottom beam flanges were buckling. Comparatively, the negative rotations for the confinement plate detail were larger and the positive rotations for the face bearing plate detail were larger. However, both figures show the large deformation capability and hysteretic energy accumulation of properly designed composite beam-slab sections.

6.5 SLAB STEEL

Strain gages were placed on the slab reinforcement at both column faces to monitor the slab resistance of positive and negative moments simultaneously (Fig. 6.18). The strain gages were placed across half the width of the slab to determine the amount of slab participation. The strains in both the major and minor directions of both the positive and negative moment regions were recorded and shown in Figs. 6.19 – 6.26 at the maximum displacement of the corresponding actuators. Fig. 6.18 shows the four groupings of strain gages that were reported in Figs. 6.19 – 6.26 with arrows for the direction of the maximum displacement reported. The rebar strain gages that were labeled 13 – 28 recorded rebar strains in the minor loading direction and the gages that

were labeled 29 - 46 recorded rebar strains in the major loading direction. The data is reported in microstrains at a maximum displacement for each cycle vs. the location of the gage from the column face. A negative sign indicates tension and a positive sign indicates compression, where the steel reinforcing theoretically yields at 2000 microstrains. Once the strain exceeded 2000 microstrains for a particular gage, that gage was no longer reported.

The general similarity of data in Figs. 6.18 – 6.25 was the tendency for the reinforcing steel to remain in tension regardless of the compressive or tensile loading of the region in question. The data for the strain gages 13 – 28 in the minor loading direction and the strain gages located beyond 381 mm (15 in.) in the major loading direction were always in tension. This phenomenon was attributed to residual stresses in the reinforcing slab steel due to localized deformations in the concrete that immediately contact the slab reinforcement. Therefore, gages in regions with low compressive strain were not as effective when the RC concrete slab was in compression. Low compressive regions were the minor loading directions and the outer region of the effective slab width in the major loading direction. Only in the region nearest the column in the major loading direction were the slab strains large enough to yield the slab reinforcement in both compression and tension. In the major loading direction, 2.6 m (8.5 ft) of the available 3.4 m (11 ft) or 77.3% slab in the experimental cruciform recorded significant levels of slab reinforcement strain. This is close to the assumed effective flange width of

2.3 m (7.5 ft) that was used in first yield and plastic moment calculations of the composite beam-slab section.

Figs. 6.26 and 6.27 show the slab cracking in tension and crushing in compression at incremental deformations throughout testing.

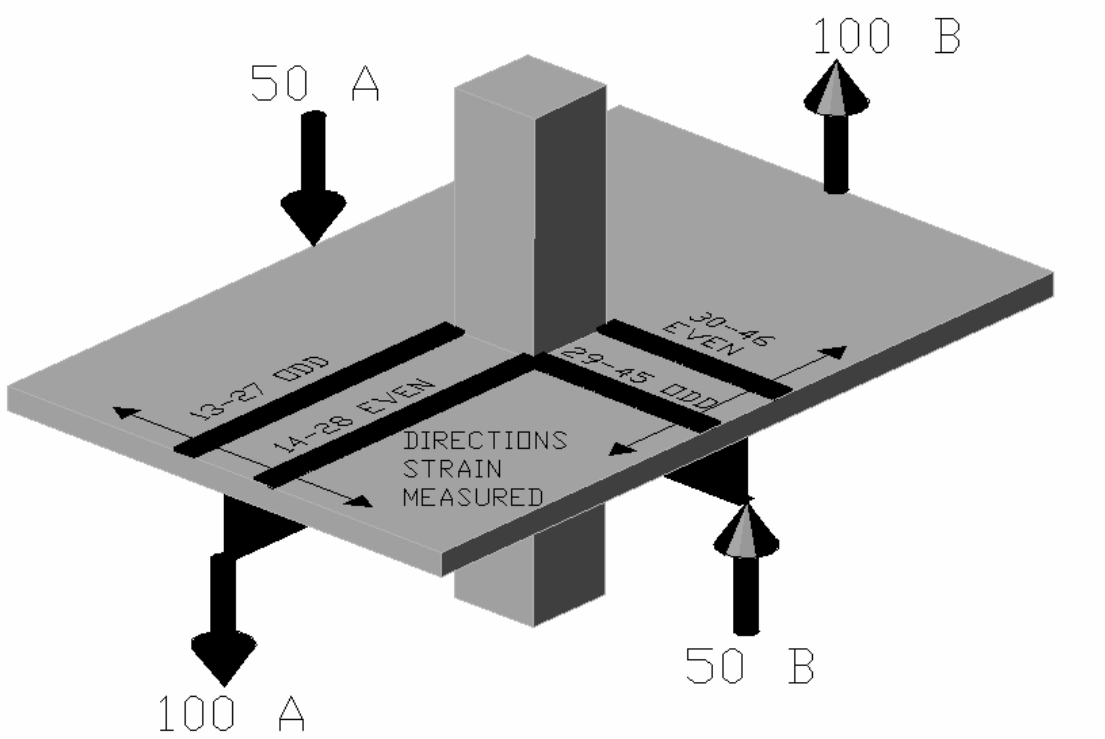

FIG. 6.17 REBAR STRAIN GAGES GLOBAL POSITION AND LOADING DIAGRAM

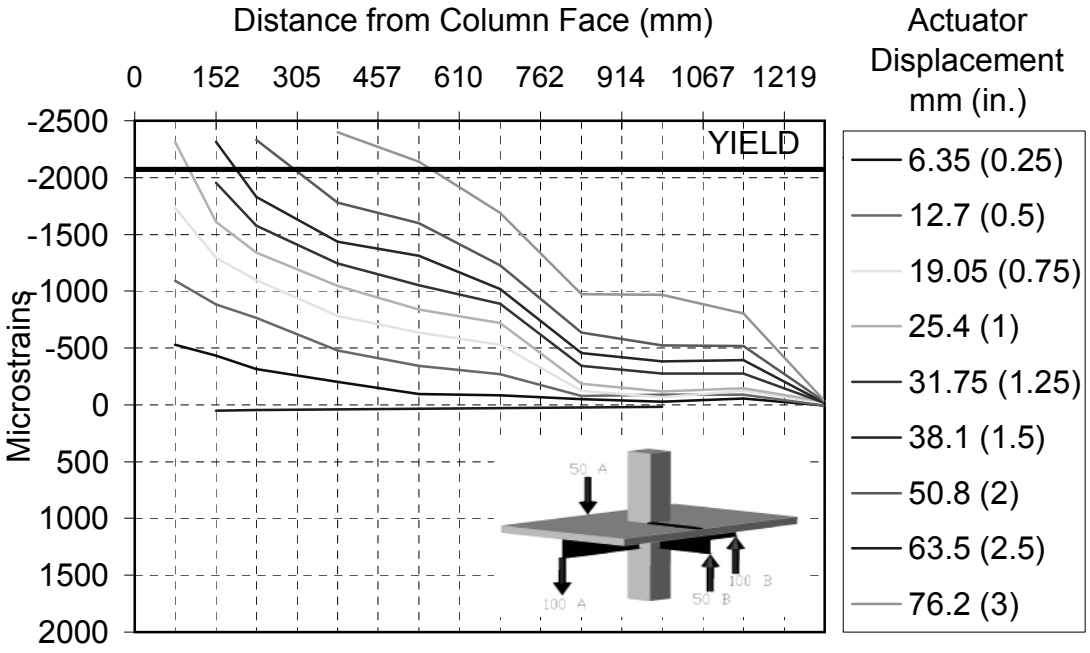

(a) 29 - 45 Odd, NegativeE Moment Region

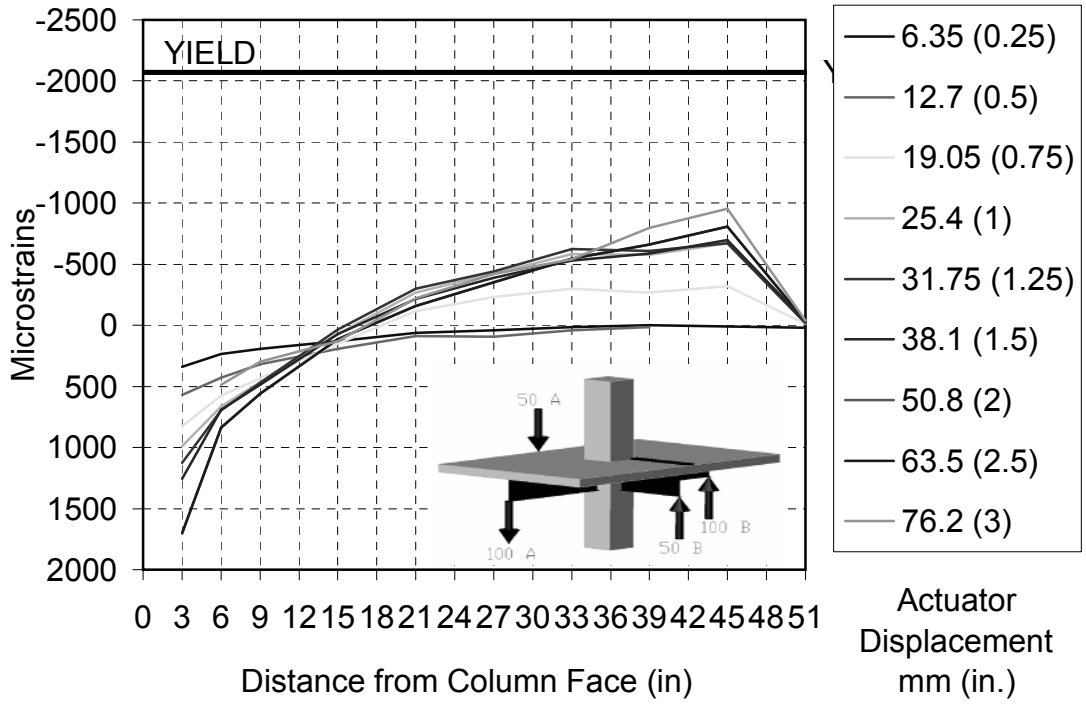

(b) 30 - 46 Even, Positive Moment Region

FIG. 6.18 REBAR STRAINS, MAJOR DIRECTION (CP)
ACTUATOR A100 MAX. NEGATIVE DISPLACEMENT

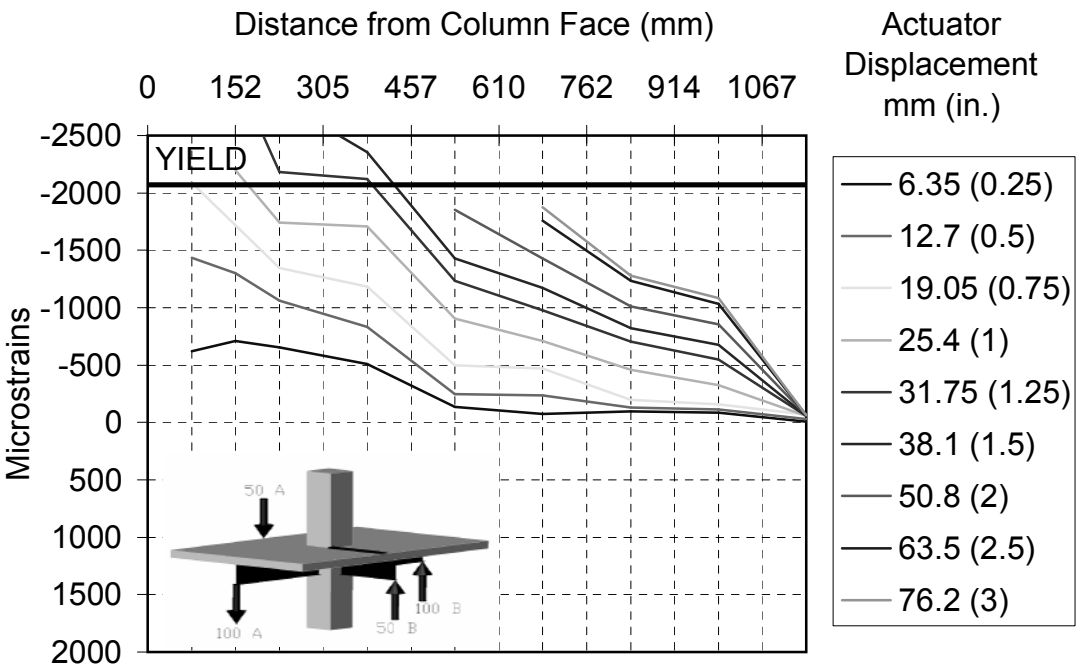

(a) 29 - 43 Odd, Negative Moment Region

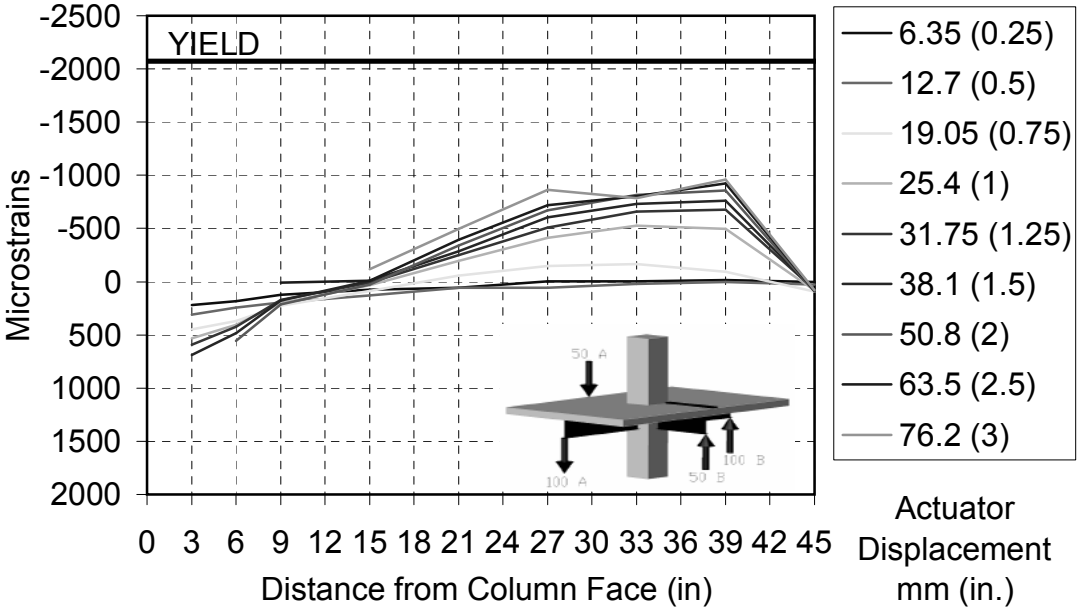

(b) 30 - 44 Even, Positive Moment Region

FIG. 6.19 REBAR STRAINS, MAJOR DIRECTION (FBP)
ACTUATOR 100A MAX. NEGATIVE DISPLACEMENT

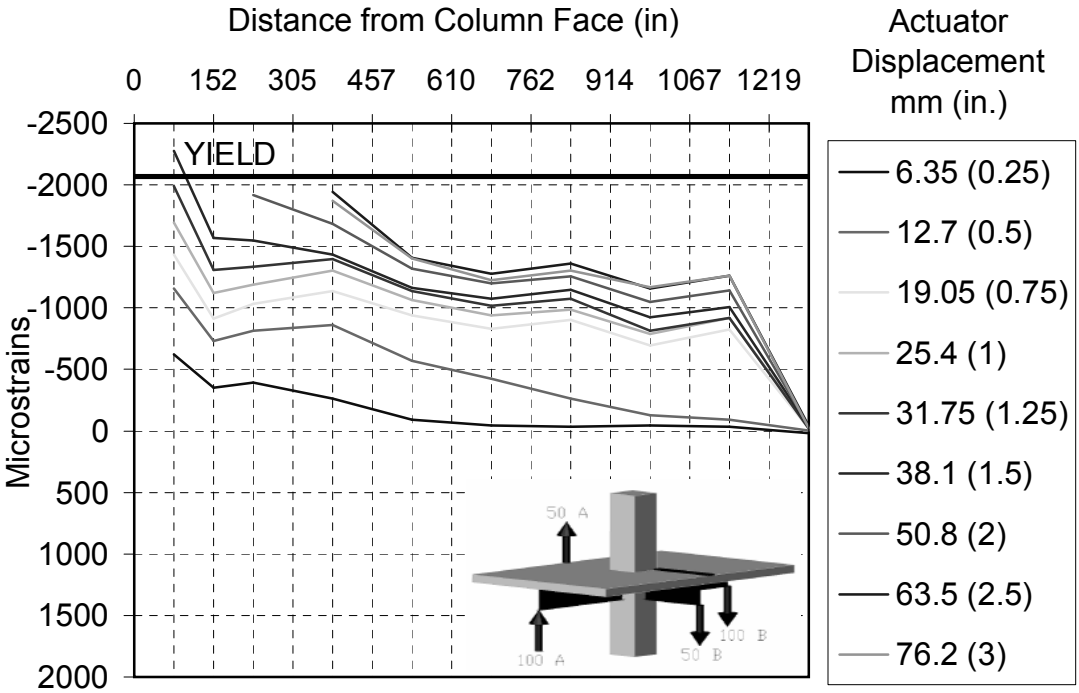

(a) 30 - 46 Even, Negative Moment Region

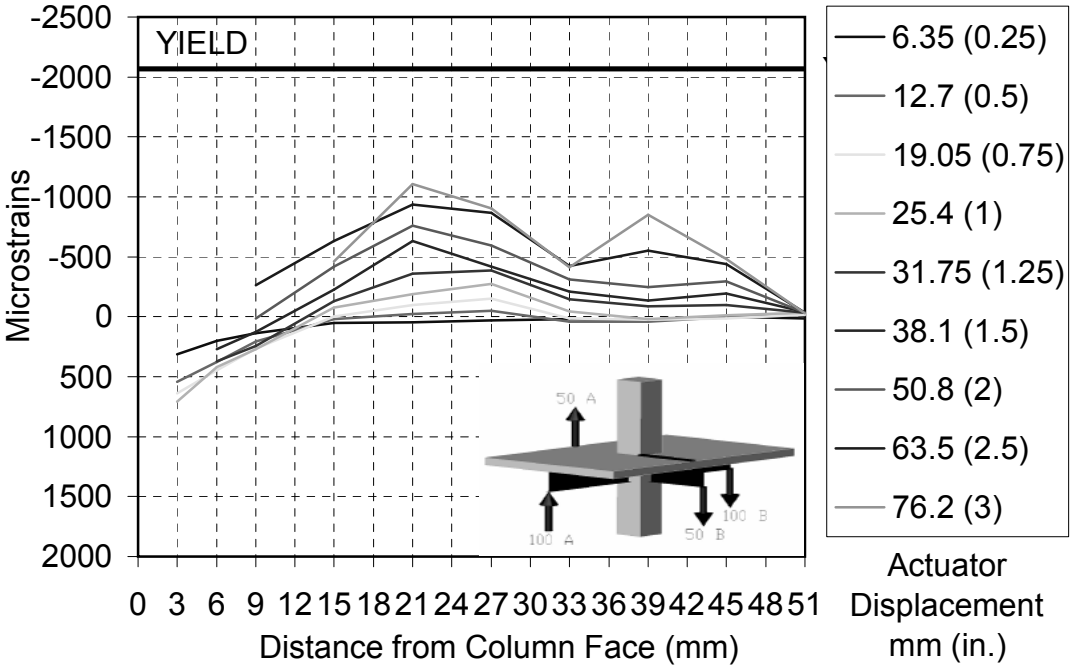

(b) 29 - 45 Odd, Positive Moment Region

FIG. 6.20 REBAR STRAINS, MAJOR DIRECTION (CP)
ACTUATOR A100 MAX. POSITIVE DISPLACEMENT

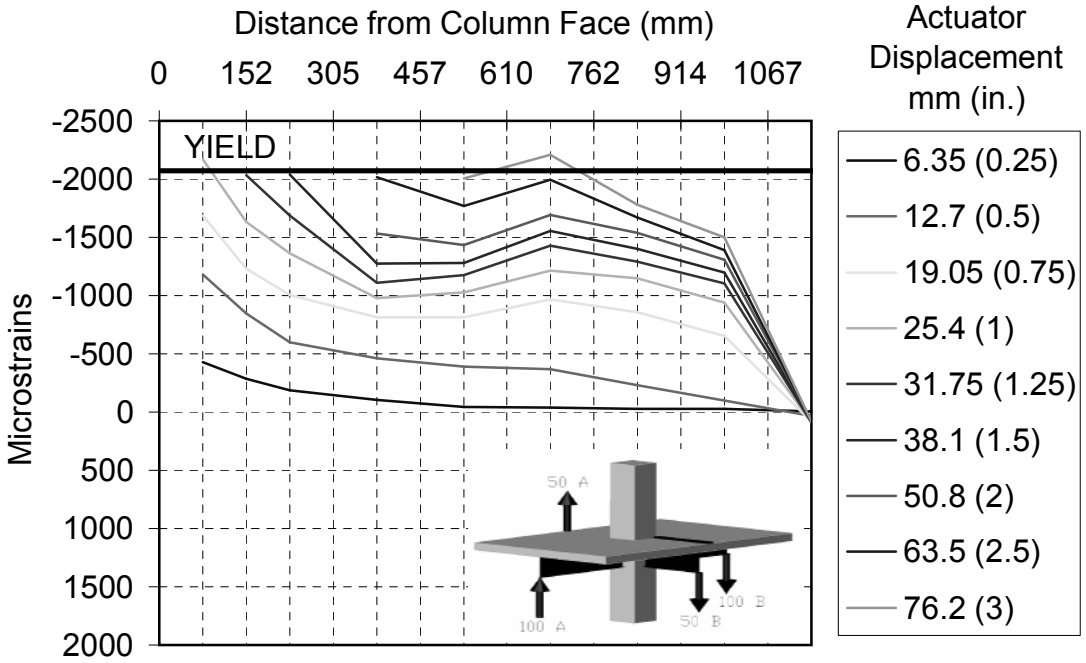

(a) 30 - 44 Even, Negative Moment Region

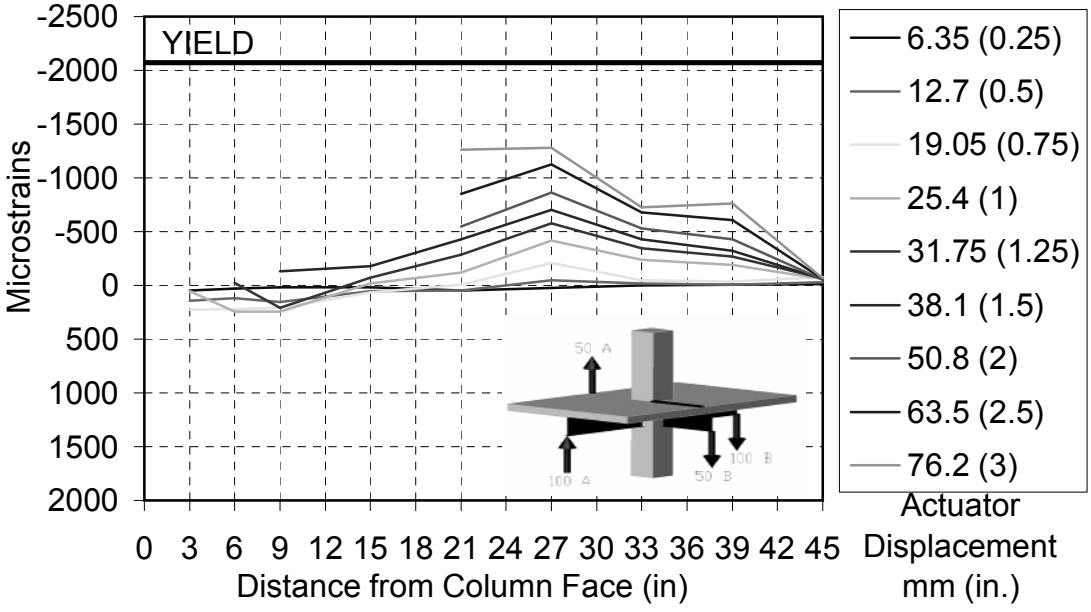

(b) 29 - 43 Odd, Positive Moment Region

FIG. 6.21 REBAR STRAINS, MAJOR DIRECTION (FBP)
ACTUATOR 100A MAX. POSITIVE DISPLACEMENT

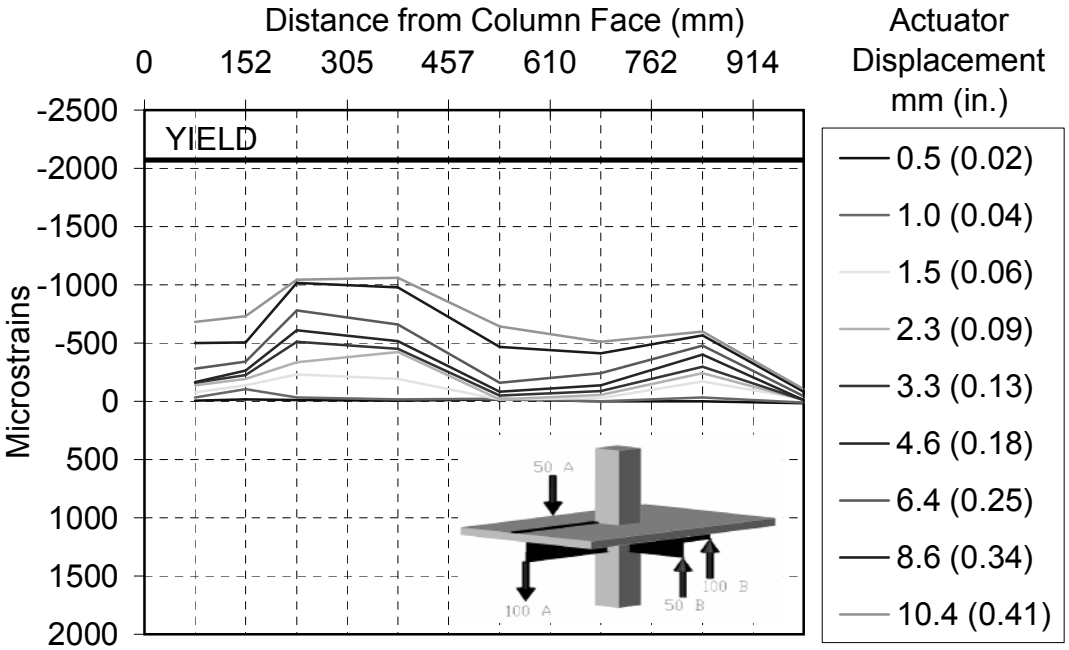

(a) 13 - 27 Odd, Negative Moment Region

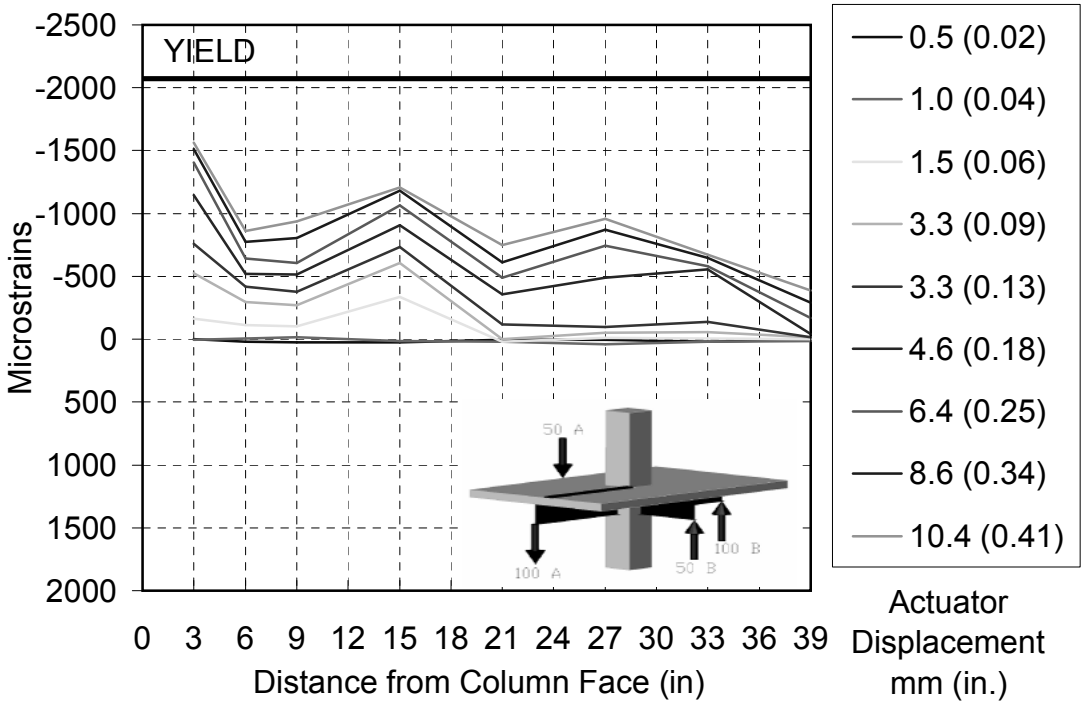

(b) 14 - 28 Even, Positive Moment Region

FIG. 6.22 REBAR STRAINS, MINOR DIRECTION (CP)
ACTUATOR A50 MAX. NEGATIVE DISPLACEMENT

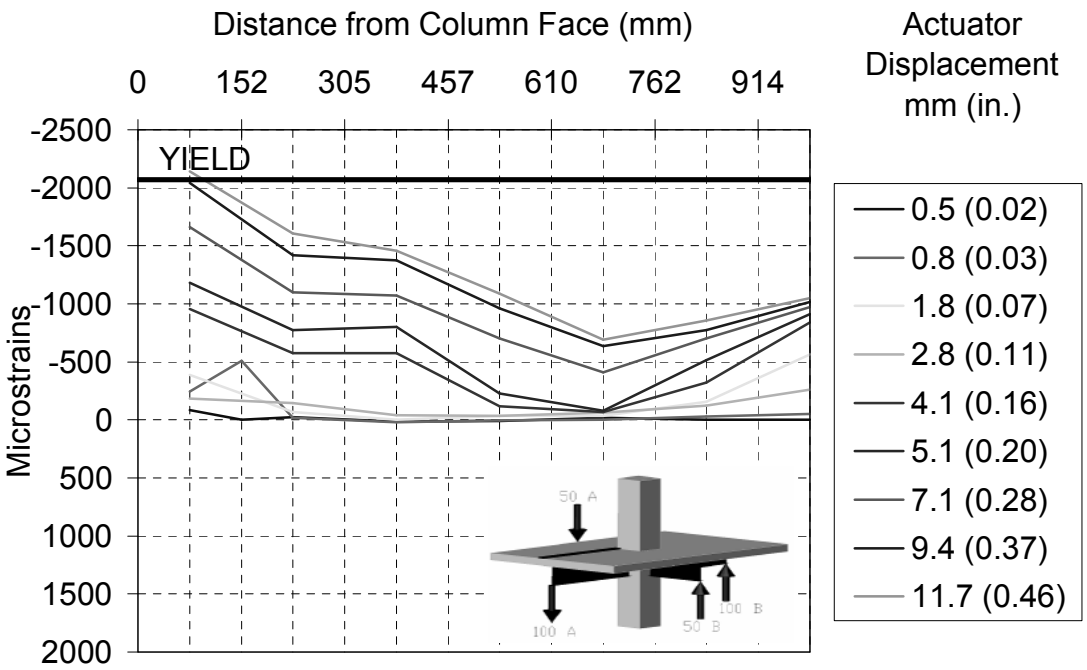

(a) 13 - 27 Odd, Negative Moment Region

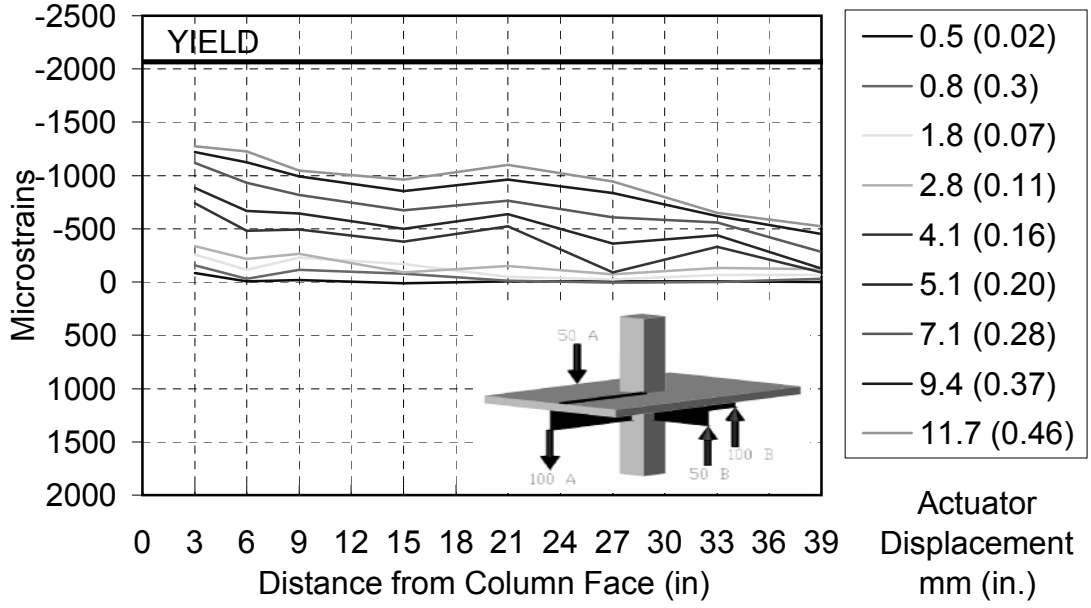

(b) 14 - 28 Even, Positive Moment Region

FIG. 6.23 REBAR STRAINS, MINOR DIRECTION (FBP)
ACTUATOR 50A MAX. NEGATIVE DISPLACEMENT

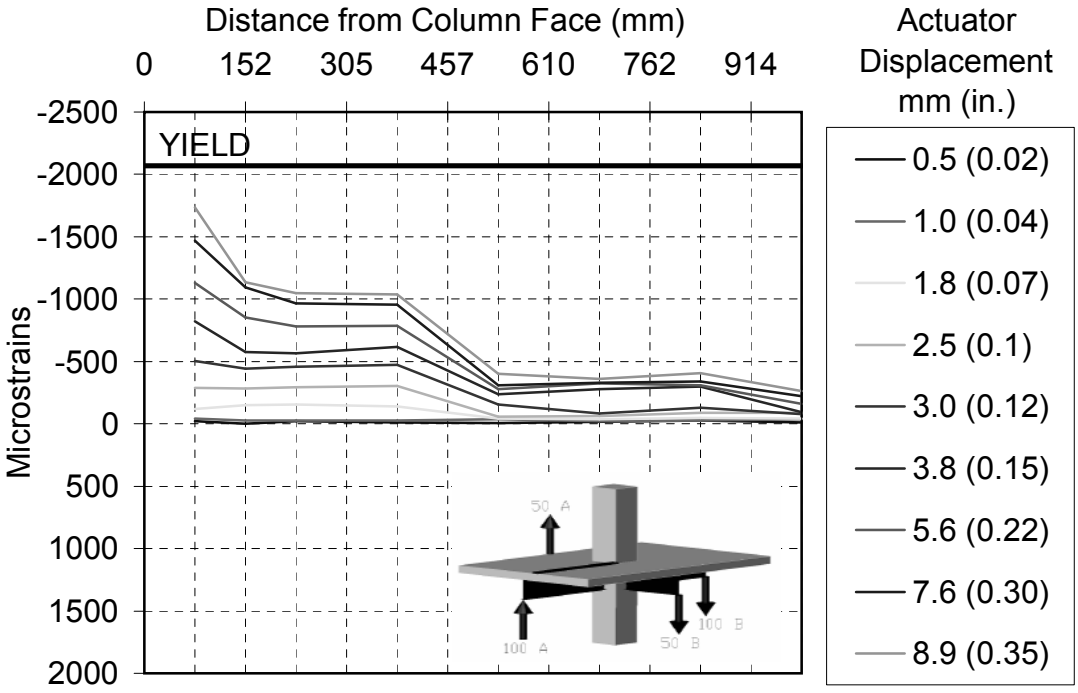

(a) 14 - 28 Even, Negative Moment Region

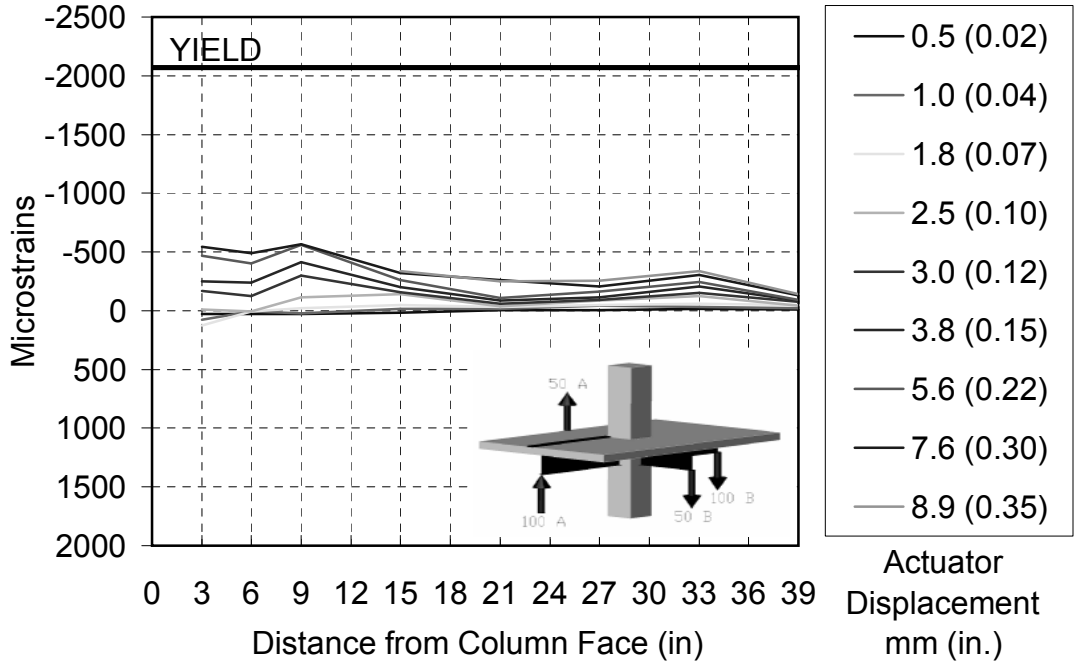

(b) 13 -27 Odd, Positive Moment Region

FIG. 6.24 REBAR STRAINS, MINOR DIRECTION (CP)
ACTUATOR A50 MAX. POSITIVE DISPLACEMENT

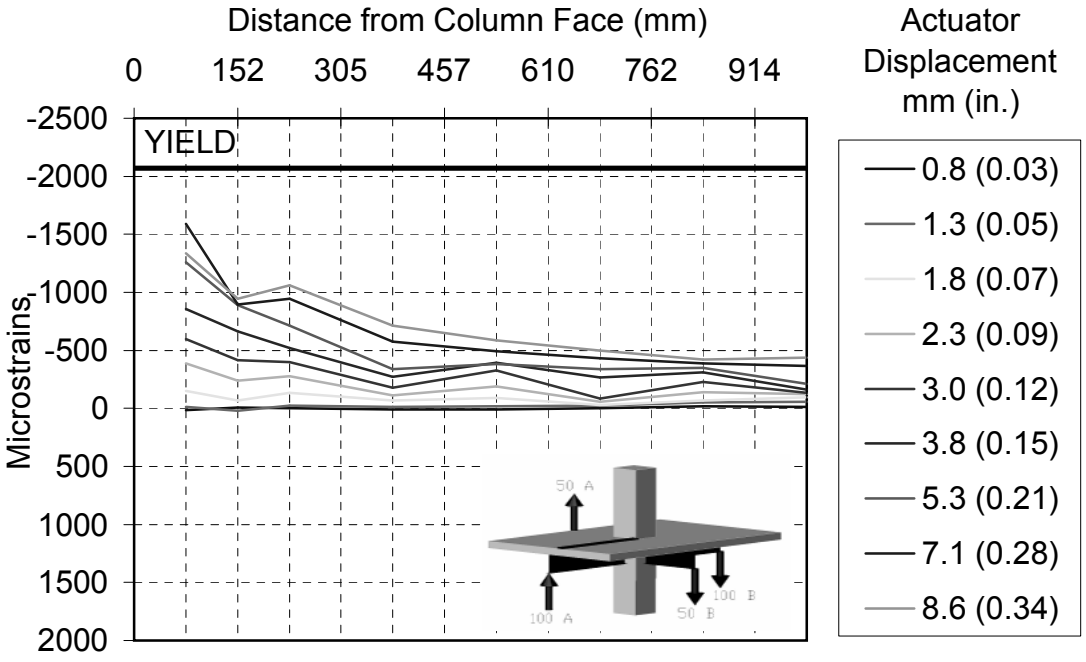

(a) 14 - 28 Even, Negative Moment Region

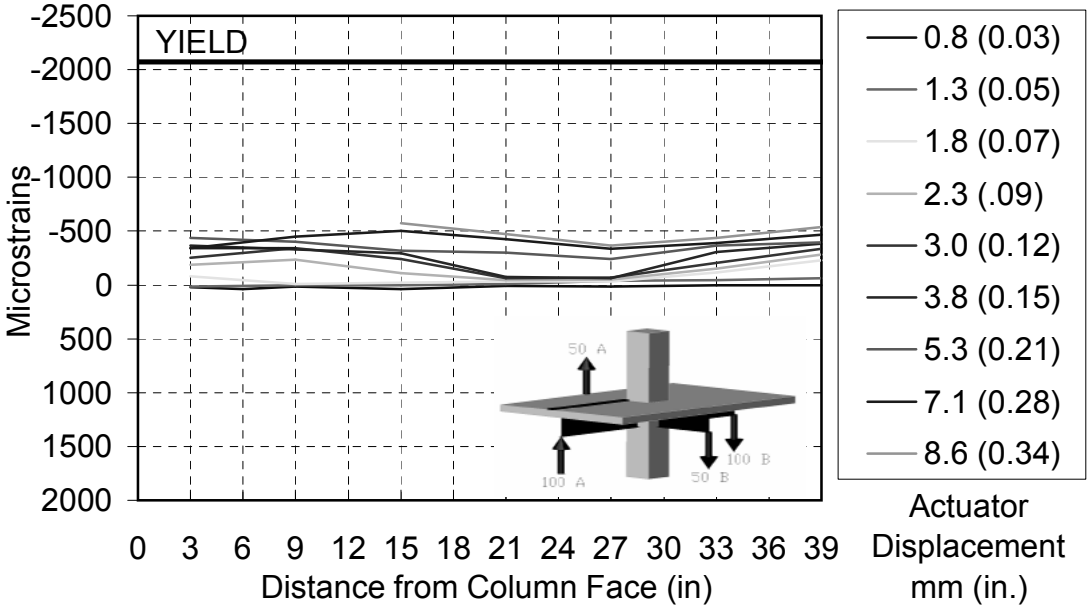

(b) 13 - 27 Odd, Positive Moment Region

FIG. 6.25 REBAR STRAIN, MINOR DIRECTION (FBP)
ACTUATOR 50A MAX. POSITIVE DISPLACEMENT

(a) ± 32 mm (1.25 in)

(b) ± 51 mm (2 in)

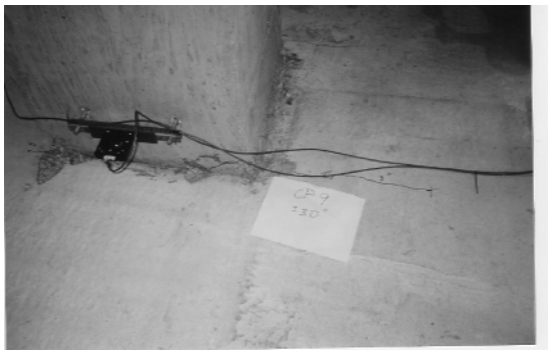

(c) ±76 mm (3 in)

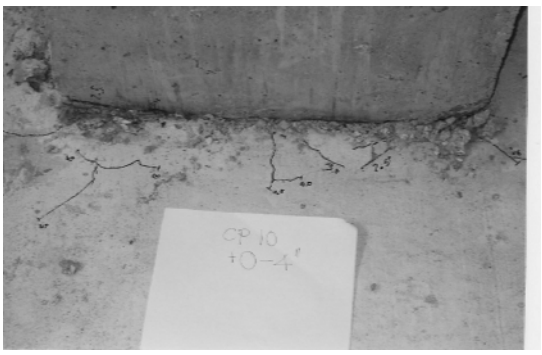

(d) 0 - 102 mm (4 in)

(e) 0 - 127 mm (5 in)

(f) 0 - 152 mm (6 in)

FIG. 6.26 SLAB BEHAVIOR OF COMPOSITE BEAM-SLAB (CP)

(e) 0 - 152 mm (6 in)

FIG. 6.26 CONTINUED

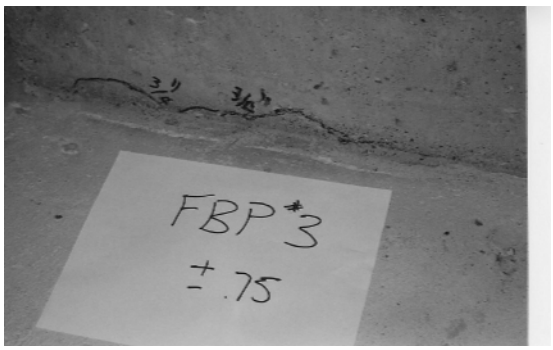

(a) ± 19 mm (0.75 in)

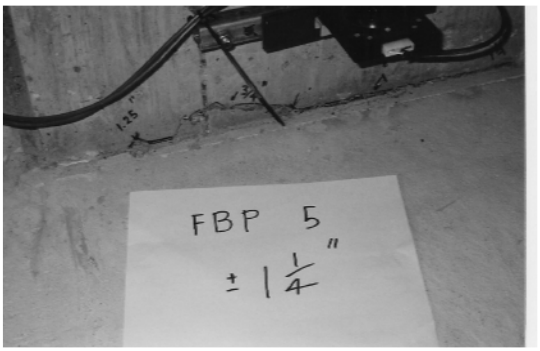

(b) ± 32 mm (1.25 in)

(c) ± 51 mm (2 in)

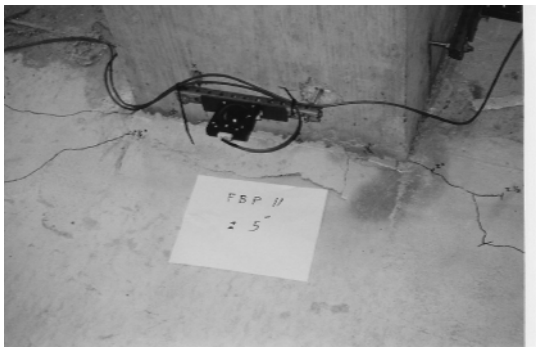

(d) ±76 mm (3 in)

FIG. 6.27 SLAB BEHAVIOR OF COMPOSITE BEAM-SLAB (FBP)

6.6 CONCRETE STRAIN GAGES IN JOINT

Four concrete strain gages were placed in the joint of each cruciform specimen. Two gages were placed in a quadrant and were oriented to measure the strain in the direction of the major loading direction. The concrete strain gages were placed at approximately 45 degrees from horizontal so that one was located in the vicinity of the inner strut, 25 mm (1 in.) from the web of the steel beam (within the steel beam flanges), and the other was in a probable location of the outer strut, 152 mm (6 in.) from the web of the steel beams, as shown in Fig. 4.10. Photographs of concrete strain gage placement in the joints of both specimens are shown in Fig. 4.11.

The average force applied in the major loading direction from the 489 kN (110 K) actuators are graphed vs. the microstrains recorded from the concrete strain gages (Fig. 6.28 and Fig. 6.29). Due to large deformations and/or cracking in the concrete, the gages became unreliable during the cyclic loading in which the actuators displaced ±31.1 mm (±1.25 in.). Therefore, the data beyond this point was not reported. The graphs show nonlinear strength degradation but there was not a correlation between the inner and outer gauges of the data between the two specimens. This could probably be attributed to the nonlinear properties of the cracked concrete and the unreliability of the concrete strain gages in this experiment.

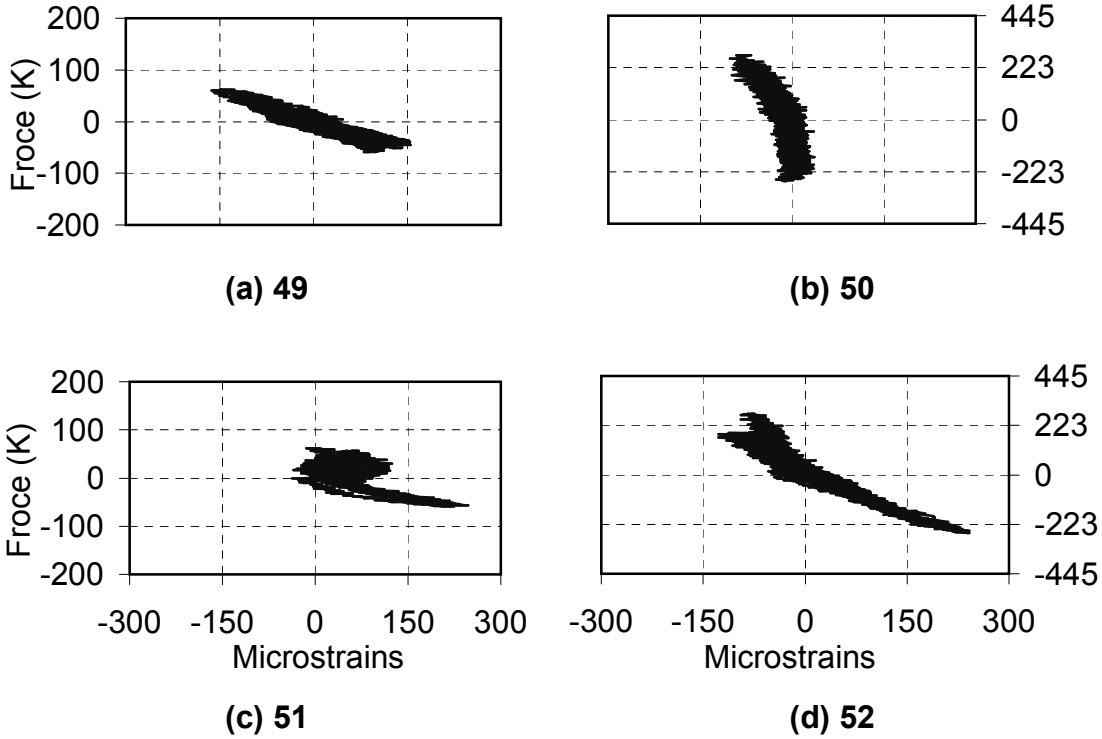

FIG. 6.28 CONCRETE GAGES (CP)

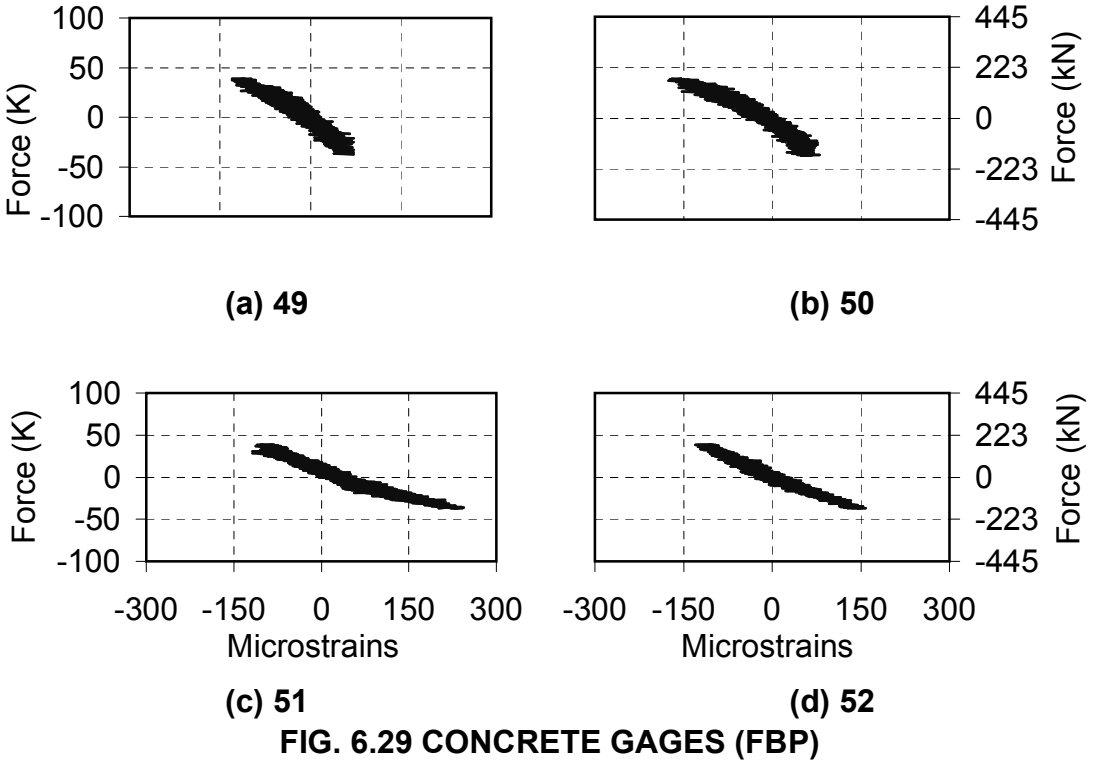

FIG. 6.29 CONCRETE GAGES (FBP)

6.7 BEAM WEB STRAINS IN JOINT

Rossette strain gages were placed on the web of the steel beams to detect the resistance to joint shear deformations. The rossette strain gages measured strains (Fig. 4.12) in the horizontal and vertical directions (ε_x and ε_y respectively) and the strain 45° from the horizontal and vertical directions (ε_{xy}). Using equations derived from Mohr's circle (Holman 1966), the maximum principle strain and the direction of the principle strain (θ) from the horizontal can be determined as follows:

$$\varepsilon_{\max}, \varepsilon_{\min} = \frac{\varepsilon_x + \varepsilon_y}{2} \pm \frac{1}{\sqrt{2}} \sqrt{\left(\varepsilon_x - \varepsilon_{xy}\right)^2 + \left(\varepsilon_{xy} - \varepsilon_y\right)^2} \tag{6.11}$$

$$\tan\left(2\theta\right) = \frac{2\varepsilon_{xy} - \varepsilon_x - \varepsilon_y}{\varepsilon_x - \varepsilon_y} \tag{6.12}$$

where

$\varepsilon_{\max}, \varepsilon_{\min}$ = maximum principle strains
$\varepsilon_x, \varepsilon_y$, and ε_{xy} = rossette srtains defined in Fig 4.12
θ = rotation (rad) of principle strain axis from ε_x

The strain data is reported in Figs. 6.30 and 6.31 in which the average force from the actuators was plotted vs. maximum principle strains. The graphs showed that the maximum principle strain remained in tension through out the test cycles and residual tension built as the tests progress. Data that appears to be compromised during testing

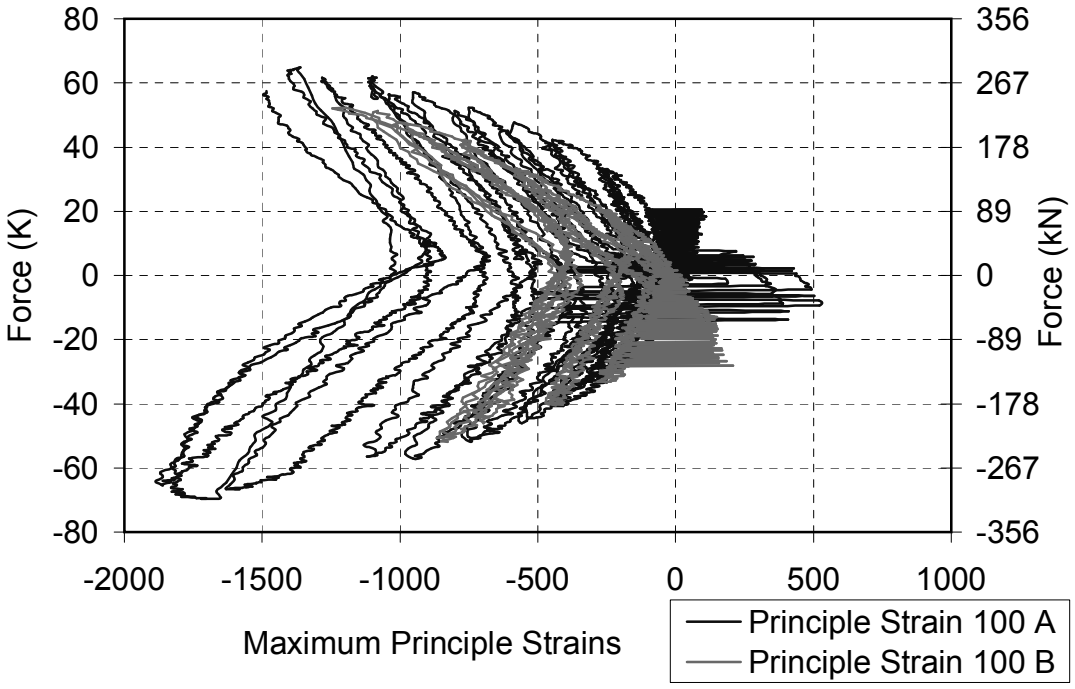

(a) Major Direction

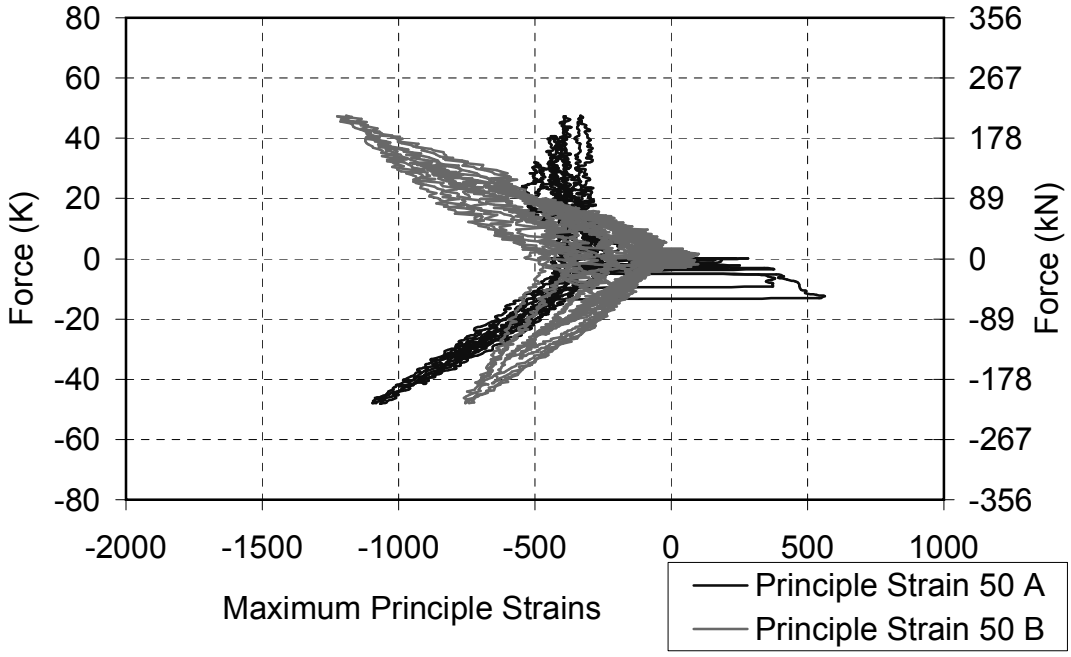

(b) Minor Direction

FIG. 6.30 JOINT WEB PRINCIPLE STRAINS (CP)

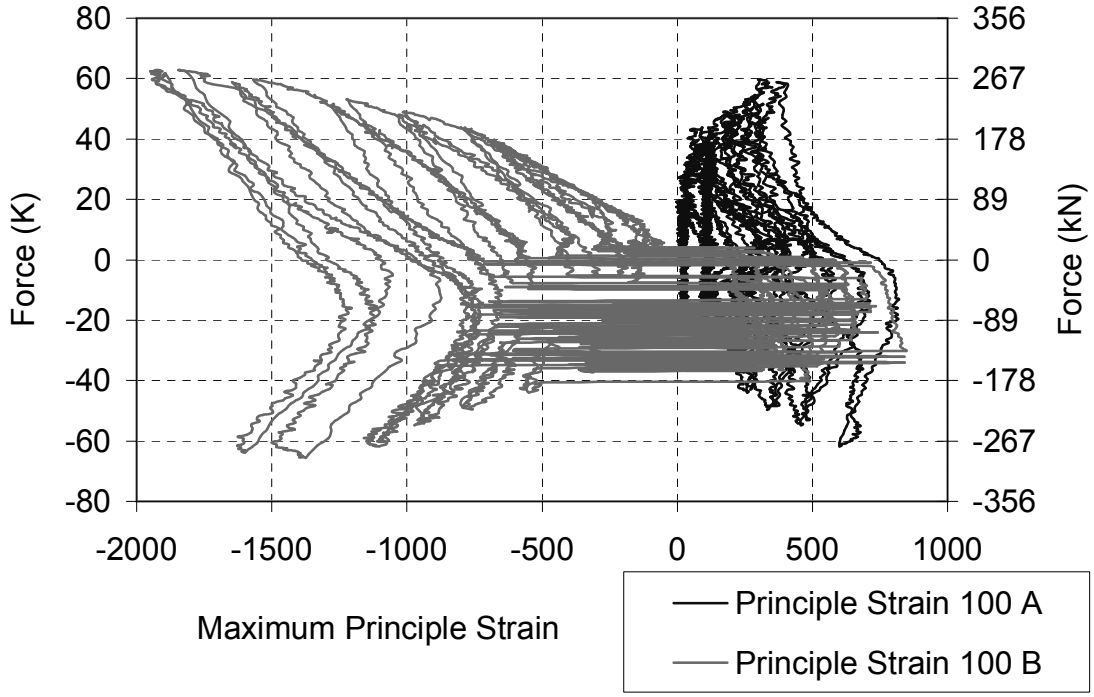

(a) Major Direction

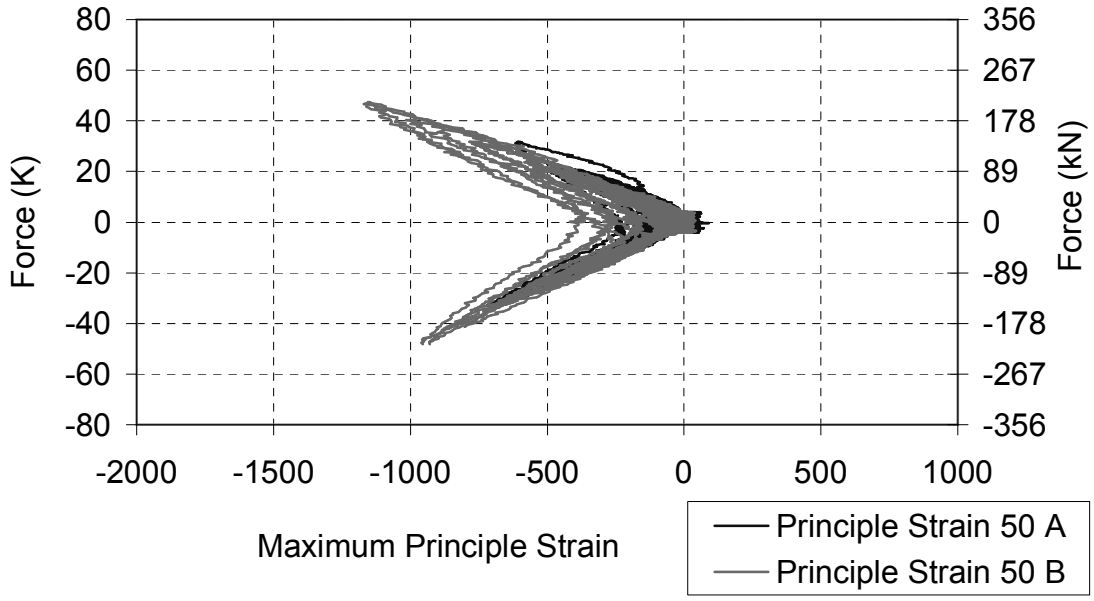

(b) Minor Direction

FIG. 6.31 JOINT WEB PRINCIPLE STRAINS (FBP)

was not reported. The maximum principle plane consistently was approximately 45° from horizontal strain axis for all the gages on both specimens.

6.8 LARGE DEFORMATION TEST RESULTS

The beam moment-rotations are reported from the test in which the 489 kN (110 K) actuators were displaced from 0.0 mm (0.0 in.) to 152.4 mm (6 in.) in Fig. 6.32 and Fig. 6.33. The beam moment-rotation figures compare the resisted moment of the composite beams and the rotations that the beams endured in radians. During this testing, the data from other parts of the specimen were believed to be unreliable and therefore were not reported. The moment-rotations were calculated with Eqs. (6.9) and (6.10), respectively. The confinement plate detail proved to be capable to endure very large plastic rotations without failing. The face bearing plate was pushed to the last set of cycles before joint failure occurred. A loud pop emanated from the joint region and a large crack was evident in the joint region caused by joint panel shear shown in Fig 6.34. The beam rotations of both specimens were able to undergo about 8% drift angle under negative moment. The similarity between the two specimens is because the bottom flange of the structural steel beam of both specimens buckled. The confinement plate detail (5.5% drift angle) remained stiffer under large positive deformations than the face bearing plate detail (15.6% drift angle). This is due to the joint shear panel failure mechanism that formed in the face bearing plate detail that was noted earlier in this section.

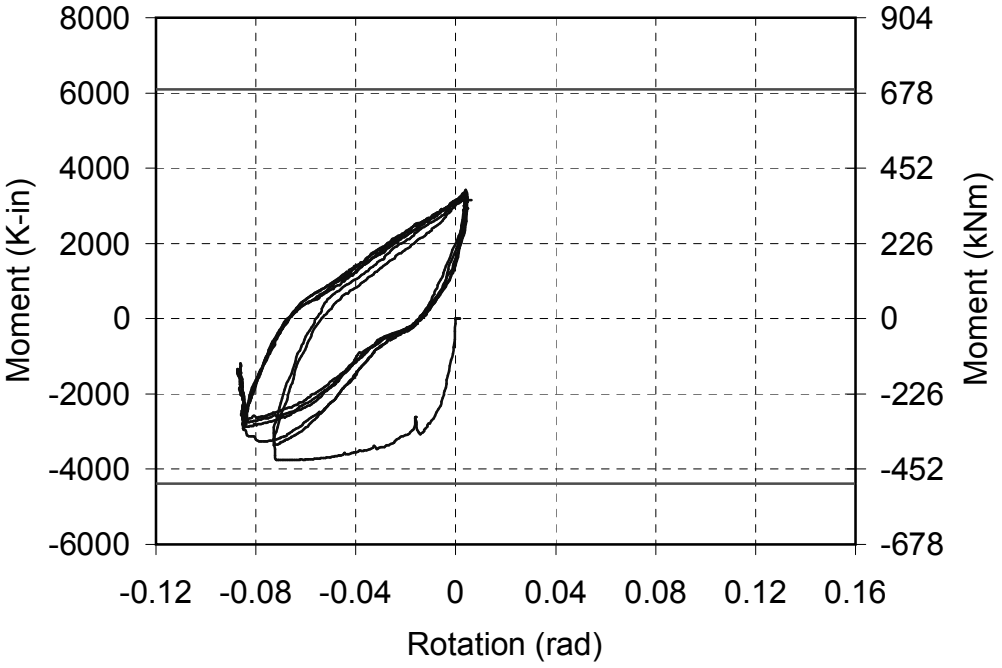

(a) BEAM LOADED BY 100A ACTUATOR

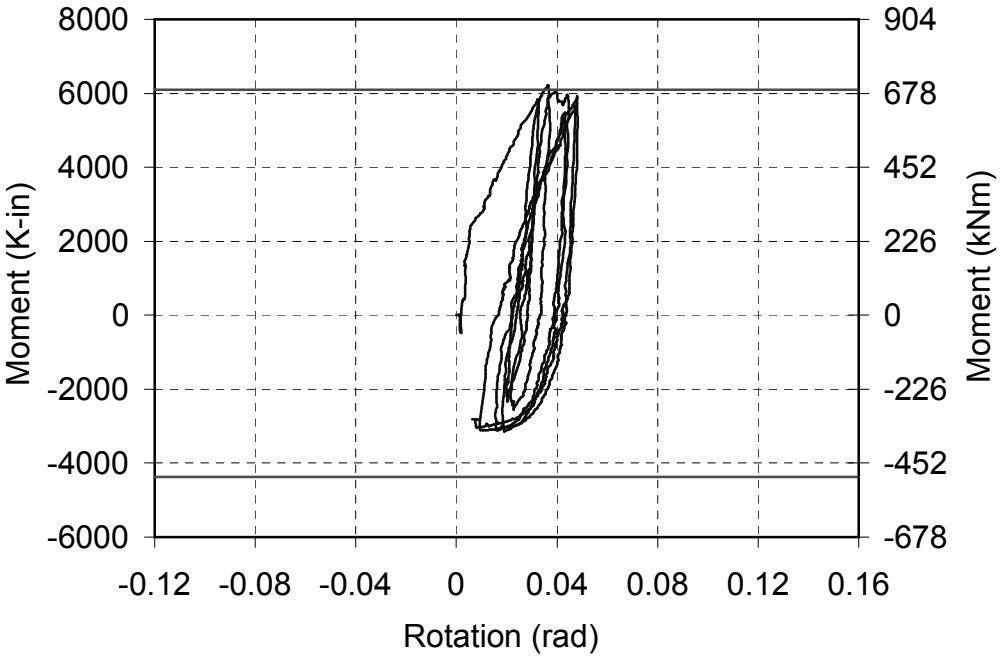

(b) BEAM LOADED BY 100B ACTUATOR

FIG. 6.32 LARGE DEFORMATION BEAM MOMENT ROTATIONS (CP)

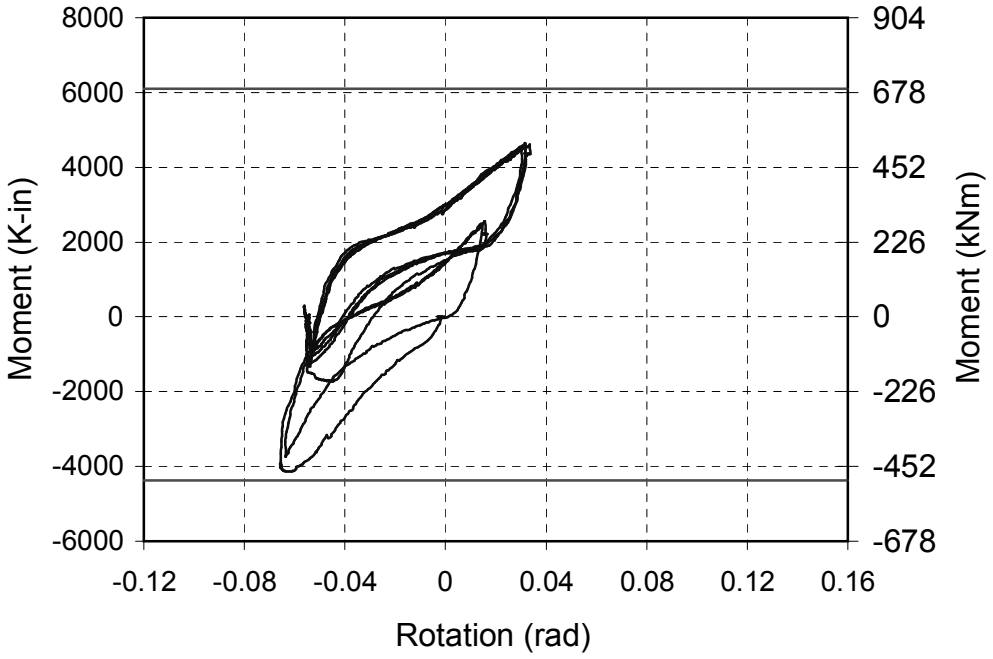

(a) BEAM LOADED BY 100A ACTUATOR

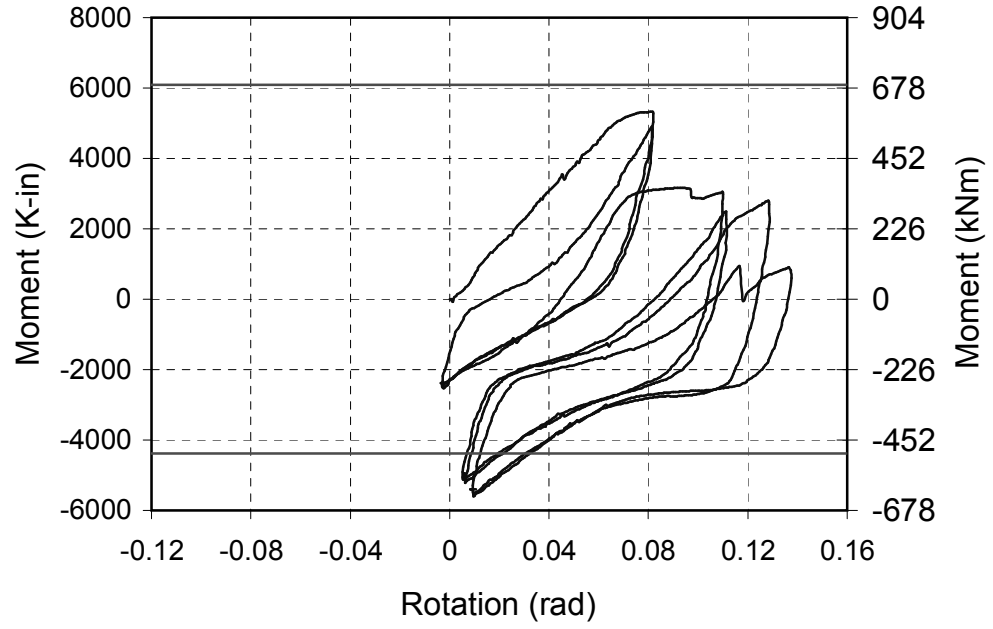

(b) BEAM LOADED BY 100B ACTUATOR

FIG. 6.33 LARGE DEFORMATION BEAM MOMENT ROTATIONS (FBP)

FIG. 6.34 JOINT PANEL SHEAR FAILURE (FBP)

CHAPTER VII

ANALYTICAL COMPARISON

In an attempt to analytically predict the behavior of the RCS specimen in this research, the ASCE (1994) guidelines and recommendations by the University of Michigan (2003) were used. The resistance calculations were made without using a strength reduction factor to directly compare the demands that were placed on the specimens during testing. In addition, nonlinear analysis was used to evaluate the overall system behavior of the specimens.

7.1 CALCULATION BASED ON ASCE (1994)

The ASCE guidelines under predicted the resistance capability of both of the specimens for joint panel shear. It should be noted that the 50 MPa (7.3 ksi) compressive strength of the concrete used in these experimental tests exceeded the recommended 40 MPa (6 ksi) concrete for which the ASCE equations were intended and may account for some of the discrepancy in the results.

There were some problems with ASCE joint strength calculations regarding the confinement plate detailing. ASCE does not specifically address strength calculations of a joint with confinement plate detailing. For this reason, the confinement plate detailing was treated as a face bearing plate, where the width of the cover plate was limited to 1.5 b_f. Thickness requirements for confinement plates were not addressed either. Even if

the required thickness were assumed to be applicable with the cover plate detailing, the required 30 mm (1.14 in.) thickness for a face bearing plate was shown to be excessively thick. These experimental tests showed that a 10 mm (0.375 in.) plate was sufficient for both of the specimens.

It should be noted that the calculations for the ASCE and Michigan joint panel shear utilize different units. To compare these two methods, the component resistances were converted to an average actuator force $\left(V_{ave}\right)$ that would theoretically induce a component failure. The component resistances were calculated without a strength reduction factor and with the test day compressive concrete strength. The joint resistances were then equated to the suggested demands and the average actuator forces were extracted from this equality. These results from the joint failure mechanisms are shown in Table 7.1 along with the induced average actuator force for the calculated plastic moment of the composite beam-slab section and ultimate moment of the RC column as determined from the interaction diagram. The maximum average forces applied during the experiments were reported in the "Max. Force Applied" column. With the exception of the ASCE panel shear prediction for the confinement plate specimen, the composite beam-slab section would be the controlling failure mechanism, which agrees with experimental observations.

7.2 UNIVERSITY OF MICHIGAN

The University of Michigan only addresses the joint panel shear failure mechanism which was also converted to an average actuator force that would induce a component failure which is shown in Table 7.1.

The resistance is categorized as design equations and model equations. The demand is the same for both methods of determining the composite joint strength. The design equations incorporate a strength reduction factor and are intended to be used in industry, where as the model equations are used to more accurately predict the behavior of the joint. The design equations are not equipped to incorporate the differences between the CP and the FBP detail, thus this is the reason that the calculated resistance was the same for both specimens. This may also be the reason that the resistance capacity of the confinement plate detailing was slightly understrength.

The only aspect that presented some difficulty with the application of the equations presented by Michigan was that the width of the outer compressive concrete strut (b_o) because of the steel column orientation. The orientation of the steel beam in the two specimens tested in this experimental program is orthogonal to that of the column orientation used to derive the equation for the outer concrete strut width shown in Fig. 2.6. A slight modification to the equation for the outer compressive strut width was made to account for these differences and is shown in Eq. (7.1).

$$b_o = \frac{\left(h_c + d_{scol}\right)}{3} + b_{scol} - b_f \rightarrow \frac{\left(h_c + \cancel{b_{scol}}^{0}\right)}{3} + d_{scol} - b_f \tag{7.1}$$

TABLE 7.1 AVERAGE ACTUATOR FORCE TO INDUCE COMPONENT FAILURE

								Vertical Bearing		Joint Panel Shear					
		Max. Force Applied		Beam Plastic Moment		Column with Axial load		ASCE		ASCE		Michigan Design		Michigan Model	
		K	kN	K	kN	K	kN	K	kN	K	kN	K	kN	K	kN
V_{ave}	CP	69.5	309	67.7	301	134	596	104	461	46.5	207	73.9	329	153	681
	FBP	64.9	289	67.7	301	134	596	94.8	421	76.9	342	73.9	329	98.4	438

7.3 ANALYTICAL COMPARISONS

To predict inelastic performance of the RCS test specimens, the program Inelastic Damage Analysis of Structural Systems (IDASS) (Kunnath 2002) was utilized. IDASS was used to run two-dimensional inelastic quasi-static analyses that included nonlinear geometric and material properties to model the cruciforms tested in the experimental program. The program is based on distributed flexibility models for the beams and columns and uses rigid links to model the joints. Trilinear moment-curvature backbone curves for members of the test specimen and the corresponding hysteretic parameters (degradation parameters) are required input for the program. Backbone curves are a derived from the cracking $\left(M_{cr}^{\pm}\right)$, and yielding $\left(M_{y}^{\pm}\right)$ moment capacities of the composite beam-slab sections and the corresponding curvatures $\left(\phi_{cr}^{\pm}, \phi_{y}^{\pm}\right)$ as shown in

Fig. 7.1. The degradation parameters take into account stiffness deterioration (α), strength deterioration (β), and slip/pinching behavior (γ), which is demonstrated in Fig. 7.2. The equations used to calculate the backbone curve parameters and hysteretic parameters for both the composite beams and columns are shown in Table 7.2 and Table 7.3 respectively. Rigid zones with lengths equivalent to the width of the column were placed at the beam-column joint to account for the stiffness provided by the joint region. The beam end cyclic displacements from the experiment were used input in to the model to determine the experimental response prediction as shown in Fig. 7.3.

TABLE 7.2 COMPOSITE BEAM PROPERTIES

	Plastic Beam		First Yield Beam		Column	
	Equations	Moment (K-in)	Equations	Moment (K-in)	Equations	Moment (K-in)
M_y^+	$M_{plastic}^+$	6017	M_{yield}^+	4249	M_{ult}^+	9200
M_{cr}^+	$0.5\ M_{plastic}^+$	3009	$0.5\ M_{yield}^+$	2125	$0.5\ M_{ult}^+$	4600
M_y^-	$M_{plastic}^-$	4380	M_{yield}^-	4115	M_{ult}^+	9200
M_{cr}^-	$0.5\ M_{plastic}^-$	2190	$0.5\ M_{yield}^-$	2058	$0.5\ M_{ult}^+$	4600
Φ_y^+		0.00903		0.00425		0.000162
Φ_y^-		0.00657		0.00617		0.000162
EI_o		1.00E+06		1.00E+06	$0.7\ EI_g$	5.96E+07
EI_y^+	$0.02\ EI_o^+$	2.00E+04	$0.05\ EI_o^+$	5.00E+04	$0.02\ EI_o^+$	1.79E+06
EI_{cr}^+	$0.5\ EI_o^+$	5.00E+05	$0.5\ EI_o^+$	1.00E+06	$0.35\ EI_o^+$	2.98E+07
EI_y^-	$0.02\ EI_o^-$	2.00E+04	$0.05\ EI_o^-$	5.00E+04	$0.03\ EI_o^-$	1.79E+06
EI_{cr}^-	$0.5\ EI_o^-$	5.00E+05	$0.5\ EI_o^-$	5.00E+05	$0.5\ EI_o^-$	2.98E+07

TABLE 7.3 HYSTERETIC PARAMETERS

α	10
β	0.0
γ	1.0

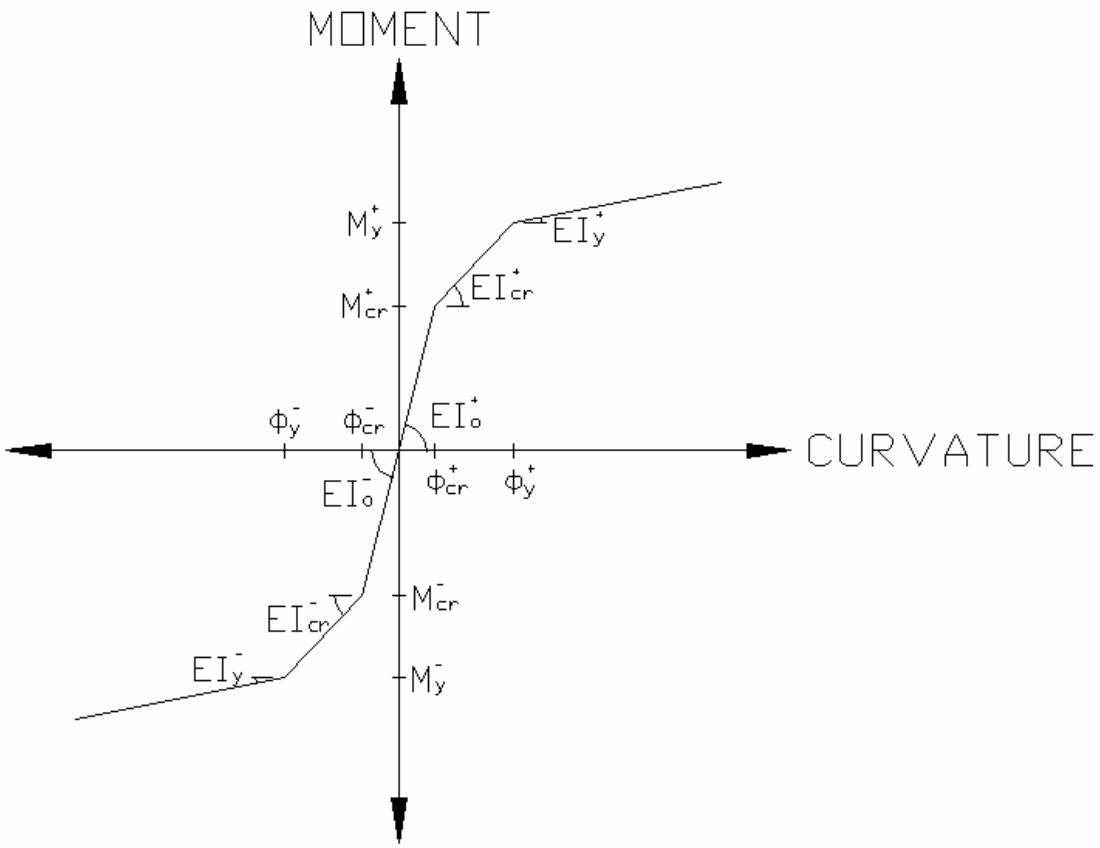

FIG. 7.1 TRI-LINEAR BACKBONE CURVE (Kunnath 2002)

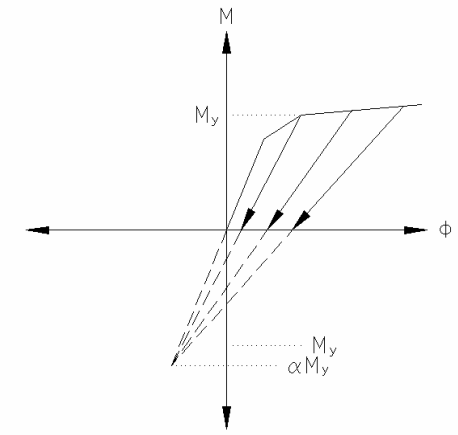

(a) Stiffness Degradation

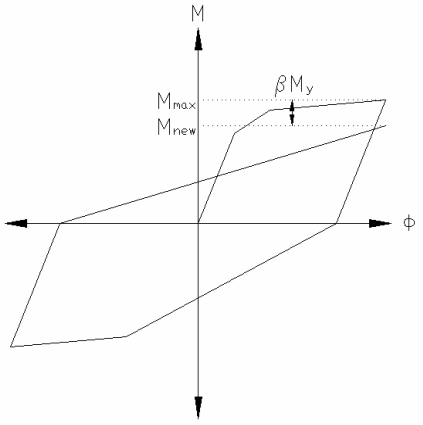

(b) Strength Deterioration

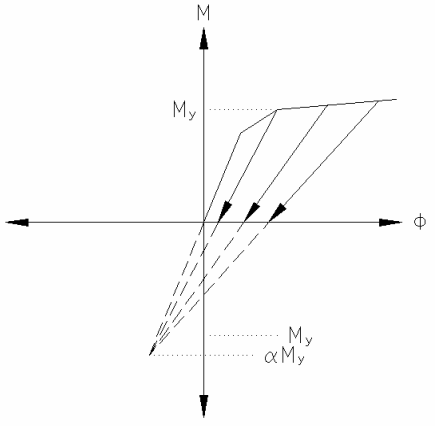

(c) Slip or Pinching

FIG. 7.2 HYSTERETIC PARAMETERS (Kunnath 2002)

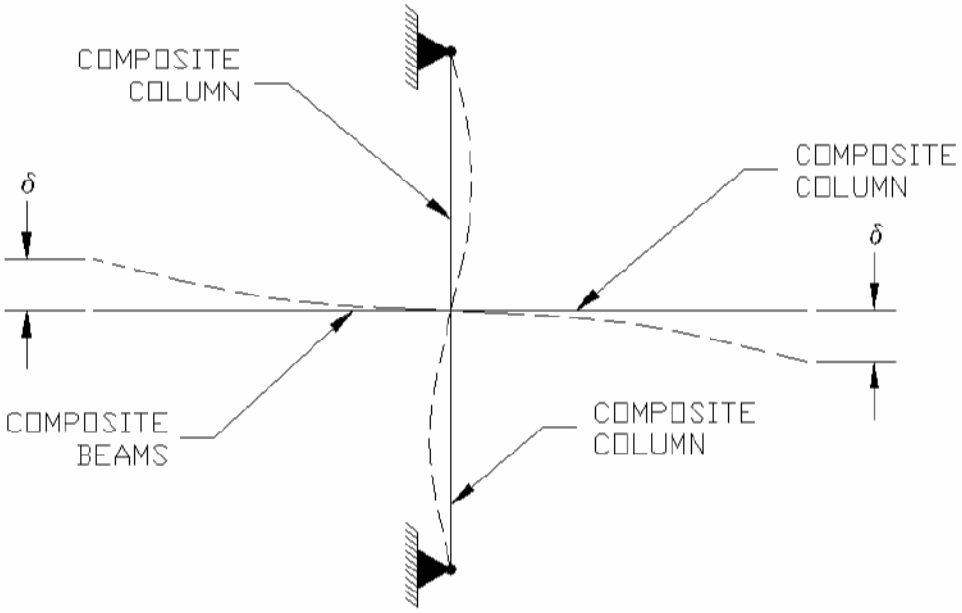

(a) Experimental Beam Loading

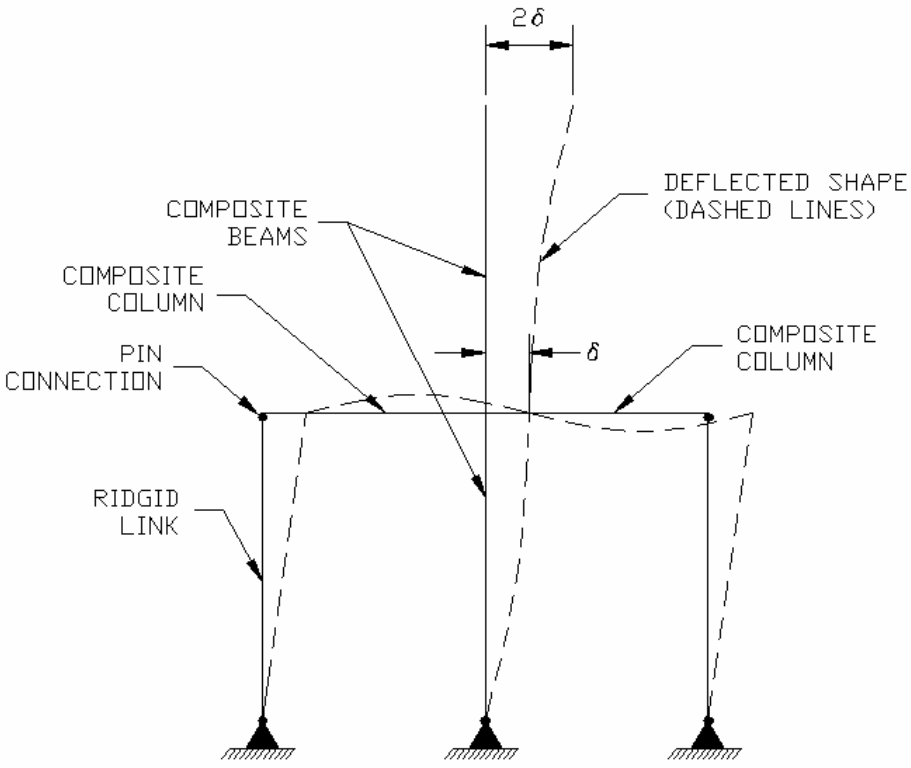

(b) Equivalent Analytical Column Loading

FIG. 7.3 EQUIVALENT IMPOSED DRIFT ANGLES

The analytical prediction of the cruciform specimens was made before testing began. The purpose of these numerical analyses was to ensure that the specimen resistance did not exceed the loading capacity of the test setup and make a prediction on the critical failure mechanism. To conservatively estimate the specimen resistance, the computed positive and negative plastic moment $\left(M^{\pm}_{plastic}\right)$ capacities of the specimens were used as the yield moments $\left(M^{\pm}_{y}\right)$ in IDASS. To account for overstrength and ensure that the loading capacity was not exceeded, a 2% post yield stiffness was used after yielding. The cracking moments $\left(M^{\pm}_{cr}\right)$ were then assumed to be half of $\left(M^{\pm}_{y}\right)$. The results from these predictions are compared with the experimental test results in Figs. 7.4 and 7.5 for both the confinement plate and face bearing plate specimens. This prediction is fairly accurately conveys the expected behavior of the experimental specimens and slightly overstates the yield strength and stiffness.

The second analysis was made after testing to accurately correlate the behavior observed during experimental testing. The correlated analysis used the computed positive and negative first yield moments $\left(M^{\pm}_{yield}\right)$ for the yield moments $\left(M^{\pm}_{y}\right)$ in IDASS. The first yield moments occur when the lower flange of the structural steel beam yields and the slab reinforcement yields, respectively for the positive and negative moment. A post yield stiffness of 5% was used in the correlated analysis. The cracking moments $\left(M^{\pm}_{cr}\right)$ were then assumed to be half of $\left(M^{\pm}_{y}\right)$. The results from these models

are compared with the experimental test results in Figs. 7.6 and 7.7 for both the confinement plate and face bearing plate specimens.

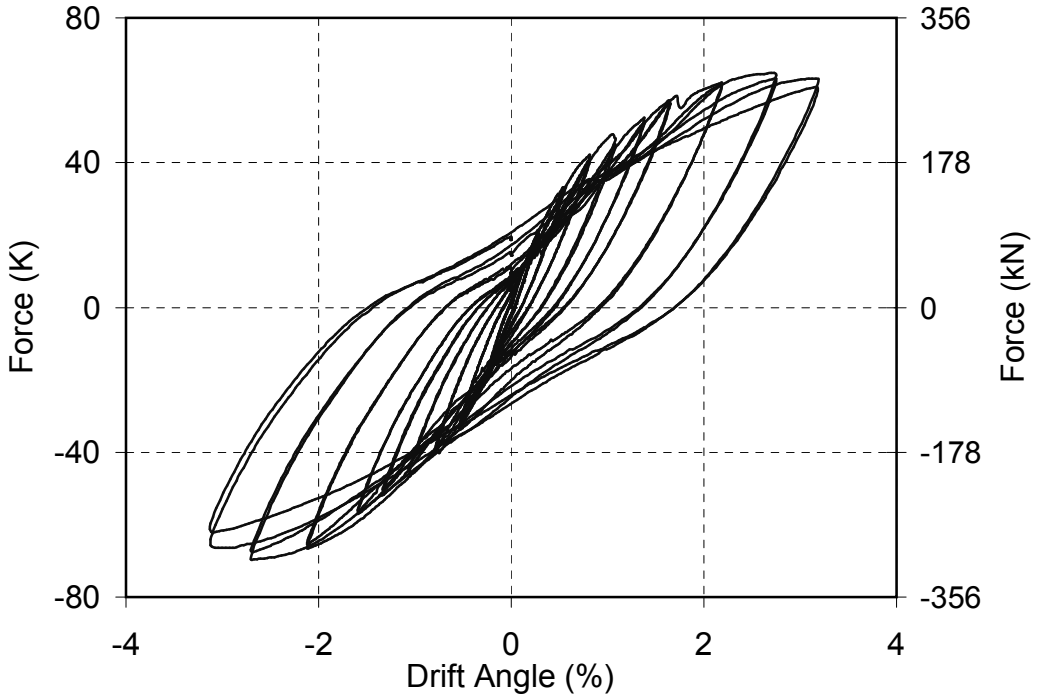

(a) Experimental

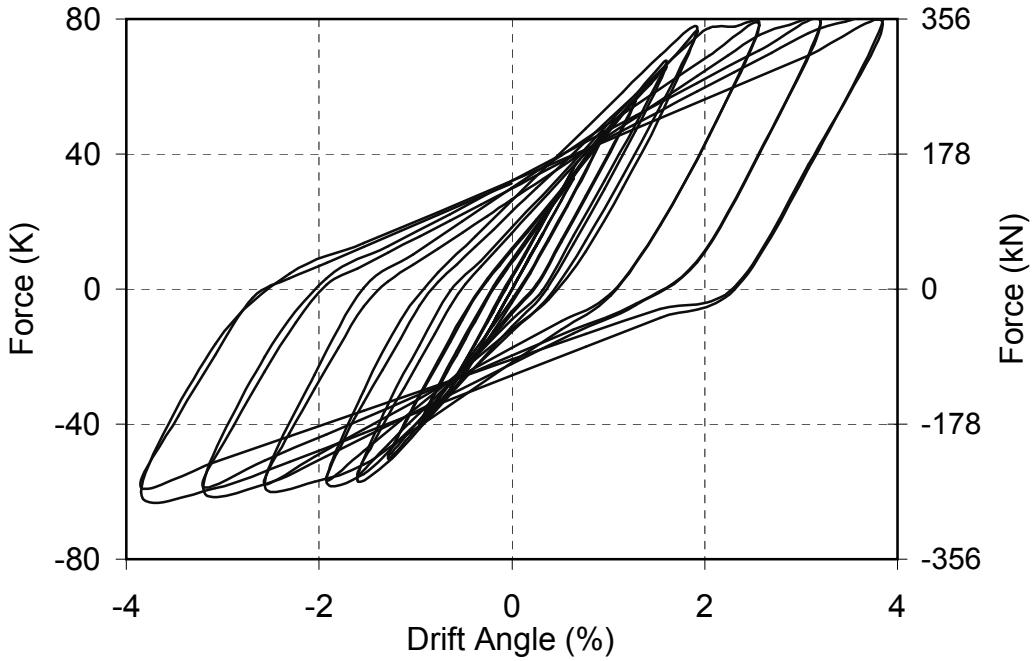

(b) Analytical Prediction

FIG. 7.4 PREDICTED TOTAL RESPONSE (CP)

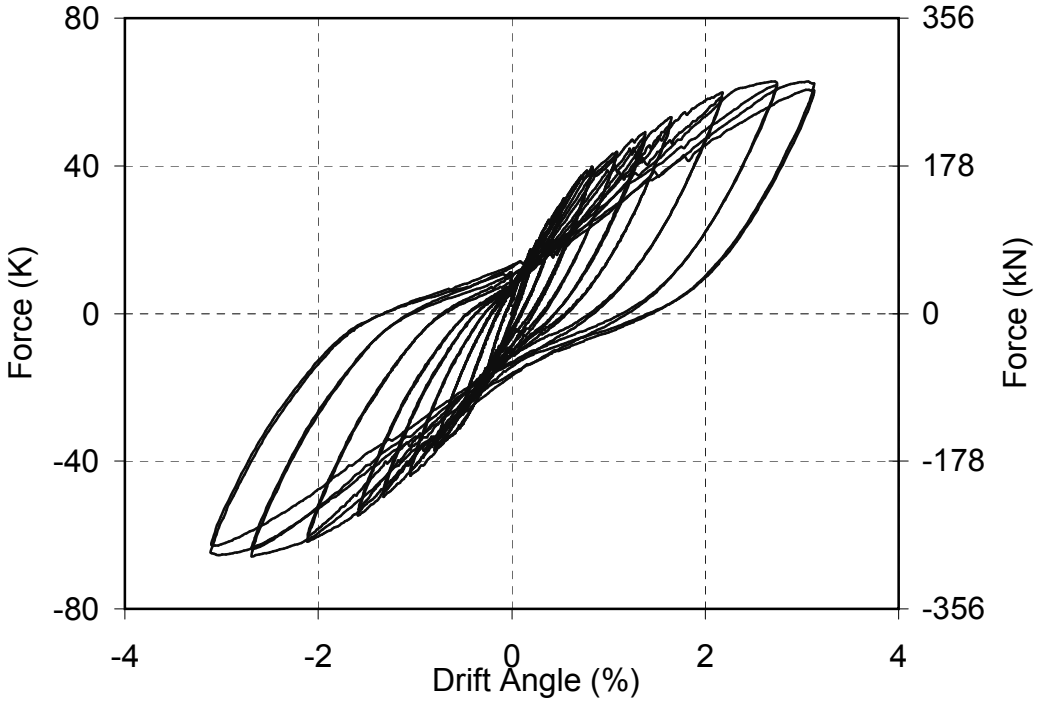

(a) Experimental

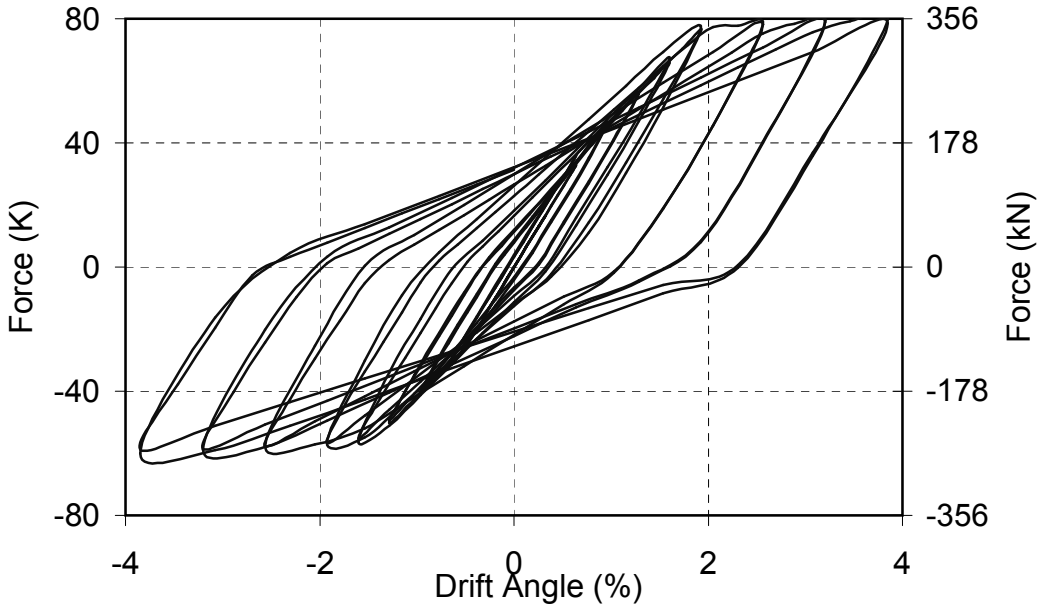

(b) Analytical Prediction

FIG. 7.5 PREDICTED TOTAL RESPONSE (FBP)

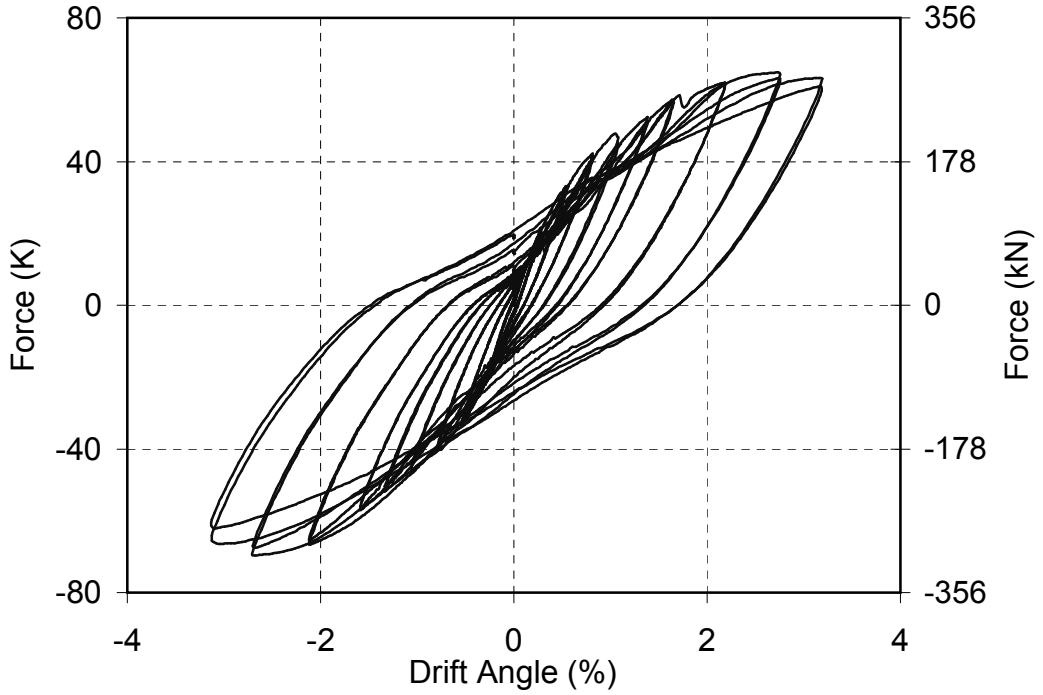

(a) Experimental

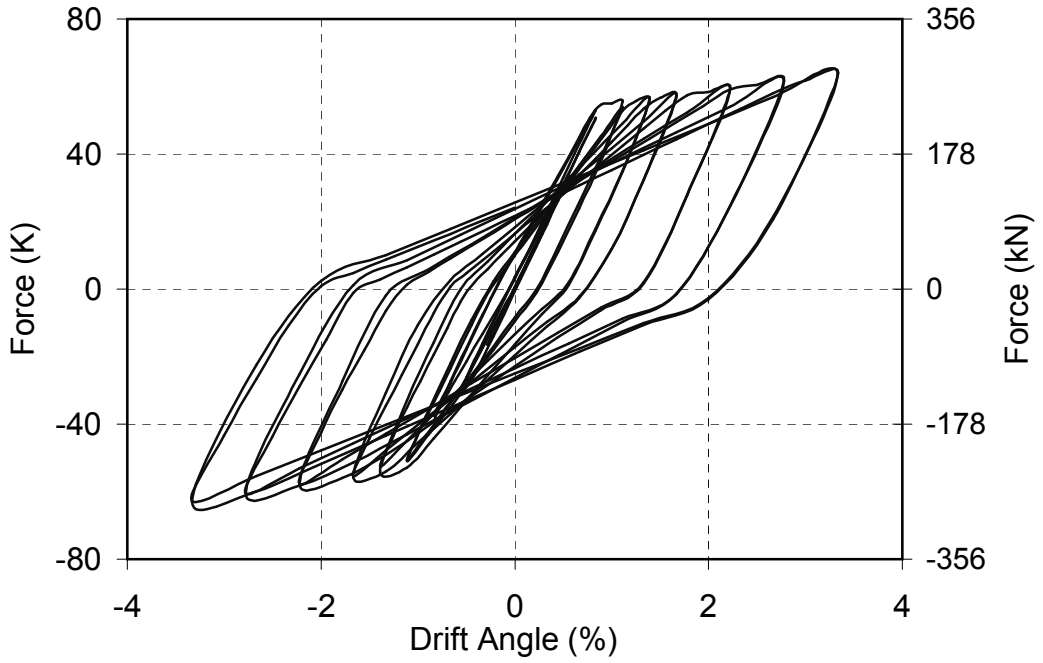

(b) Analytical Model

FIG. 7.6 CORRELATED TOTAL RESPONSE (CP)

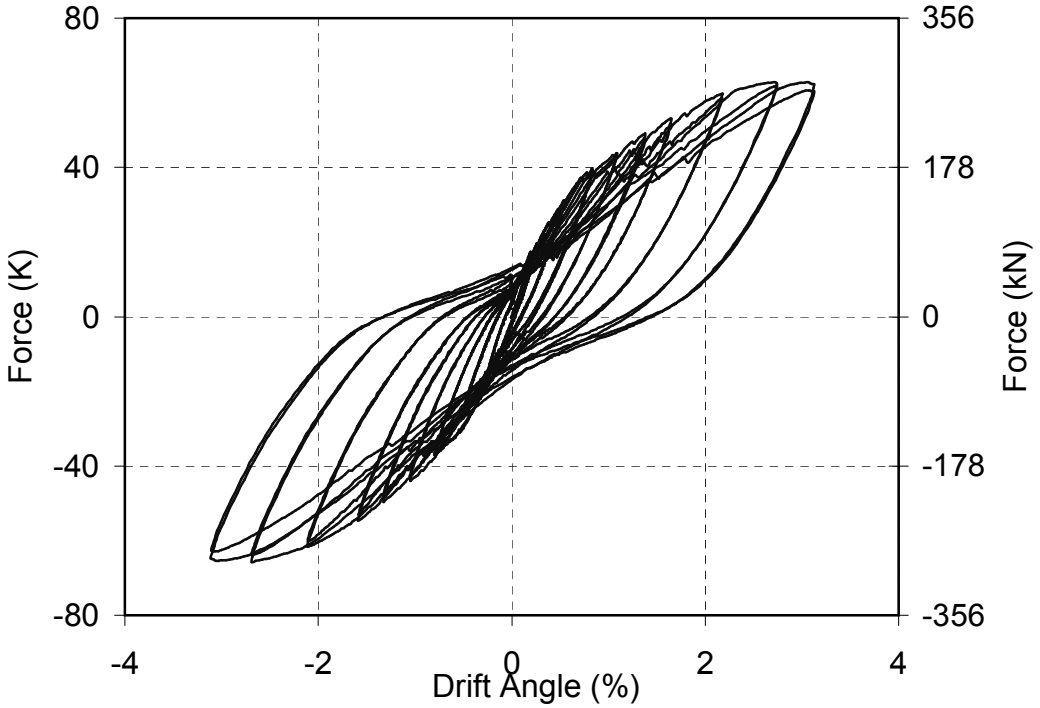

(a) Experimental

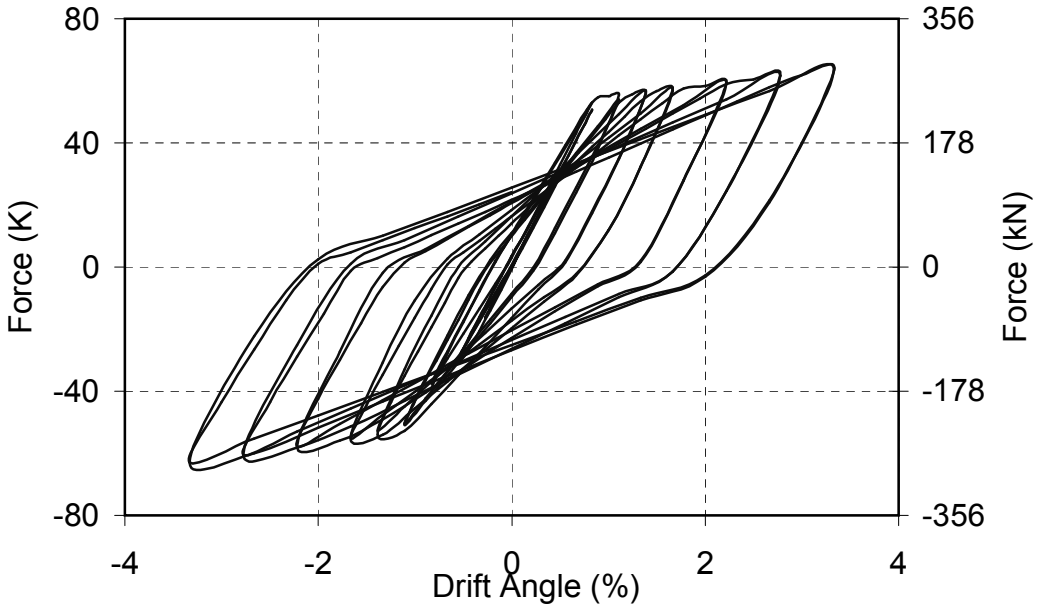

(b) Analytical Model

FIG. 7.7 CORRELATED TOTAL RESPONSE (FBP)

CHAPTER VIII

CONCLUSIONS

8.1 SUMMARY

The objective of this research program is to further evaluate the performance and constructability of reinforced concrete (RC) column-steel beam-slab systems (RCS) for use in low- to mid-rise space frame buildings located in regions of high wind loads and/or moderate seismicity. The experimental portion of this research program included the construction and testing of two full-scale cruciform specimens with identical overall dimensions but with different joint detailing. The two joint details evaluated were joint cover plates and face bearing plates with localized transverse ties. The construction process was recorded in detail and related to actual field construction practices. The specimens were tested experimentally to failure under bi-directional quasi-static reversed cyclic loading, while a constant axial force was applied to the column, to simulate the effects of lateral loading in a subassembly of a prototype building. To compliment the experimental work, nonlinear analyses were performed to evaluate the specimen strength and hysteretic degradation parameters for RCS systems. In addition, current recommendations in the literature on the design of RCS joints were used to estimate specimen joint strength and were compared with the experimental findings.

8.2 CONCLUSIONS

In terms of the structural performance of RCS moment frame systems, the following was concluded:

- The behavior of the specimens in the experimental program consisted of predictable strength and stiffness, and desirable hysteretic energy capability and ductility.

- The imposed bi-directional loading, 100% in the major loading direction and about 40% in the minor loading direction, did not cause any unexpected joint failure mechanisms as compared to only uni-lateral loading.

- Both specimens displayed desirable failure mechanisms by the composite beam-slab section yielding. However, the confinement plate detail better confined the inner concrete joint core which stiffened and strengthened the joint region, and ensured a more desirable failure mechanism in the composite beam-slab sections.

- Slab reinforcement within the effective flange width as defined by AISC-LRFD (2001) was shown to participate in bending in both test specimens. Slab steel in regions of low compressive strain remained in tension due to residual stresses that were created by the reversed cyclic loading.

- In terms of constructability, construction difficulties were encountered in the experimental program were related to the bolting and joint welding requirements for providing full moment resistance for the discontinuous beams of the test assembly and concrete placement in the joints. The tight tolerances required for the steel components in the joints made construction difficult. The alignment of the top and bottom seat angles with the steel column web and steel beam flanges could potentially be problem in field construction. The transverse beams with prefabricated cover plates that were intended to reduce the amount of field welding were found to create problems with bolt alignment to the shear tabs or large gaps between the cover plate and the continuous through-beam weld prevented proper field welding. A suggestion for practical application of these systems would be to require field welding in the joint regions. This should alleviate most of the alignment problems encountered in the experimental program. The other constructability problem was that the congestion in the joint region proved to be troublesome during concrete placement, though it was shown that concrete voids and honeycombing could be repaired and still perform well structurally.

- Analytically, the joint strength predictions and inelastic analysis accurately reflected the observed behavior of the test specimens. With the exception of the ASCE panel shear prediction for the confinement plate specimen, the composite beam-slab section was predicted to be the controlling failure mechanism, which agreed with experimental observations. However, large shear deformations and cracking in the joint region was observed in the face bearing plate detail specimen, which suggests that the

joint panel strength calculations may be unconservative for such joint detailing. The behavior of the specimens in the experimental program were adequately modeled using traditional strength limits derived for first cracking and first yield with a post-yielding stiffness of 5% of the initial section stiffness for the composite beam-slab section, traditional backbone curves for the RC columns and rigid joints.

8.3 RECOMMENDATIONS FOR FUTURE WORK

Future work in this area should emphasize improving the design guidelines for the face bearing plate requirements and also extend these guidelines to include the confinement plate detail as used in this work. Welding guidelines should be developed for the RCS joint details. As shown by the testing the confinement plate detail, welding the confinement plate to only the beam webs prevented failure of the confinement plate compared to previous tests that welded the confinement plate to both the beam web and flanges and the confinement plate tore at the corners.

To further improve the constructability, the top angle and bottom seat should be completely field welded. This would solve some of the alignment problems that where discussed in Section 5.3 with these joint components. During concrete placement, the joint region should be sufficiently vibrated and concrete with a high slump should be used so that voids will not form in the joint region.

REFFERENCES

ACI Committee 318 (2002). "Building code requirements for structural concrete (318-02) and commentary (318R-02)," ACI 318-02/318R-02, American Concrete Institute, Farmington Hills, Michigan.

AIJ (1994). "AIJ Design Guidelines for Composite RCS Joints," Architectural Institute of Japan, Japan.

AISC-LRFD (2001). "Manual of Steel Construction Load and Resistance Factor Design," American Institute of Steel Construction, 3rd ed. Chicago, Illinois.

ASCE Task Committee on Design Criteria for Composite Structures in Steel and Concrete. (1994). "Guidelines for design of joints between steel beams and reinforced concrete columns." Journal of Structural Engineering, ASCE, 120 (8) 2330-2357.

ASTM (1998). "Standard practice for making and curing concrete test specimens in the laboratory," C 192/C 192M-98, American Society for Testing and Materials, West Conshohocken, Pennsylvania.

ASTM (2001). "Standard test method for compressive strength of cylindrical concrete specimens," C39/C 39M-01, American Society for Testing and Materials, West Conshohocken, Pennsylvania.

Bracci, J.M., Moore,W.P., and Bugeja, M.N. (1999). "Seismic Design and Constructability of RCS Special Moment Frames," Journal of Structural Engineering. ASCE, 125 (4) 385-392.

Bracci, J.M., Powanusorn, S., and Steele, J.P. (2002). "Composite RCS Space Frame Systems: Constructability and Performance," Technical Paper, College Station, Texas.

Bugeja, M.N., Bracci, J.M., and Moore,W.P. (1999). "Seismic Behavior of Composite Moment Resisting Frame Systems," Technical Report CBDC-99-01, College Station, Texas.

Bugeja, M.N., Bracci, J.M., and Moore,W.P. (2000). "Seismic Behavior of Composite RCS Frame Systems," Journal of Structural Engineering, ASCE, 126 (4) 429-436.

Deierlein, C.G. (1988). "Design of moment connections for composite frames." Ph.D. Dissertation, The University of Texas , Austin, Texas.

Deierlein, C.G., Sheikh, T.M., Yura, J.A., and Jirsa, J.O. (1989). "Beam Column moment connections for composite frames:Part 2," Journal of Structural Engineering, ASCE, 115(11), 2877-2896.

Griffis, L.G. (1986). "Some Design Considerations for Composite-Frame Structures." AISC/Engineering Journal, Second Quarter, 59-64.

Holman, J.P. (1966). "Experimental Methods for Engineers." McGraw-Hill Inc., New York, 332-333.

Kanno, R. (1993). "Strength, deformation, and seismic restistance of joints between steel beams and reinforced concrete columns." Ph.D. Dissertation, Cornell University, Ithaca, New York.

Kunnath, S.K. (2002). "Inelastic Damage Analysis of Structural Systems Version 3.01," University of California at Davis, Davis, California.

Nishimura, Y., Mimami, K. and Wakabayashi, M. (1986). "Stress transfer mechanism of exterior connection consisting of steel beam and steel reinforced concrete (SR(C) column." Journal of Structural Engineering, 32 (B) 135-146 (in Japanese).

Noguchi, H. and Kim, K. (1997). "Analysis of Beam-Column Joints in Hybrid Structures," Proc. of ASCE Structures Congress XV, ASCE, 726-730.

Noguchi, H. and Kim, K. (1998). "Shear Strength of Beam-to-Column Connections in RCS System," Proc. of Structural Engineers World Congress, ASCE, Paper Ref. T177-3, 7.

Parra-Montesinos, G. and Wight, J.K. (2000). "Seismic Response of Exterior RC Column-TO-Steel Beam Connections," Journal of Structural Engineering, 126 (10) 1113-1121.

Parra-Montesinos, G. and Wight, J.K. (2001). "Modeling Shear Behavior of Hybrid RCS Beam-Column Connections," Journal of Structural Engineering, 127 (1) 3-11.

Parra-Montesinos, G., Liang, X., and Wight, J.K. (2003). "Towards Deformation-Based Design of RCS Beam-Column Connections," Engineering Structures, 25 (5) 681-690.

Sakaguchi, N., Tominaga, H., Murai, Y., Takase, Y., and Shuto, K. (1988) "Strength and ductility of steel beam-RC column joint." Proceedings of the 9th World Conference on Earthquake Engineering, Tokyo-Kyoto, 4, 713-718.

Sheikh, T.M. (1987). "Moment connections between steel beams and concrete columns." Ph.D. Dissertation, The University of Texas, Austin, Texas.

U.S.-Japan Planning Group (1992). “Recommendation for a U.S.-Japan cooperative research program. Phase 5: Composite and hybrid structures.” Technical Report No. UMCEE 92-29, University of Michigan, Ann Arbor, Michigan.

Wakabayashi, M., Minami, K., and Nishimura, Y. (1983). “Load carrying capacity of composite exterior joint with steel beam.” Transactions of the Japan Concrete Institute, 5, 339-346.

APPENDIX A

NOTATION

Symbols:

a = depth of Whitney equivilant stress distribution
A_b = area of steel beam
a_c = length of concrete bearing zone
A_o = arbitrary unit of area
A_r = area of rebar
a_{sh} = cross-sectional area of reinforcing bars in each layer of ties
A_{tie} = total cross-sectional transverse reinforcement area
b = RC column width measured perpendicular to steel beam
b_e = effective flange width of RC slab
b_f = width of steel beam flange
b_i = inner panel width, which is the larger of the FBP width and beam flange width
b_j = effective width of joint panel
b_m = maximum effective width of the joint region
b_o = outer panel width
b_p = effective face bearing plate width
b_p = width of face bearing plate
c = depth of compressive stress field
C = coefficient that is based on joint demensions
C_c = vertical bearing force
C_{cn} = nominal concrete bearing strength
C_{vrn} = nominal strength of vertical joint reinforcement in compression
d = depth of steel beam
d_f = center-to-center distance between the steel beam flanges
d_o = depth of outer compression field extension
d_y = depth from common location from which moments are summed
d_{top} = arbitrary depth measured from the top of the composite beam-slab cross section

d_w = depth of steel beam web

E_s = modulus of elasticity for steel $\left(199810 \text{ MPa} \left(2900 \text{ ksi}\right)\right)$

f = abitrary concrete stress (negative is defined as compressive)

f_c' = ultimate compressive concrete stress

F_{Left}, F_{Right} = left and right actuator force, respectively

Force = load applied by the actuators

F_{up} = specified tensile strength of the face bearing plate

f_y = yield strength of steel beam

F_y = arbitrary yield stress

$\left(F_y\right)_b$ = yield stress of the steel beam

F_{yp} = yield strength of the face bearing plate

$\left(F_y\right)_r$ = yield stress of steel reinforcement

F_{ysh} = yield strength of transverse reinforcing steel

F_{ysh} = yield strength of the transverse reinforcement

F_{ysp} = yield strength of steel web panel

h_c = depth of RC column measured parallel to the steel beam

h_{vr} = distance between vertical joint reinforcement

$\left(jh\right)$ = horizontal distance between bearing force resultant

K = coefficient

k_1 = joint loading due to location

k_2 = accounts for confinement conditions for the inner concrete strut

k_3 = effect of confinement on concrete

k_i = strength factor for inner strut

k_o = strength factor for outer compressive strut

k_w = stength factor of steel beam web $\left(0.9 \text{ interior joint or } 0.8 \text{ exterior joint}\right)$

L = distance from point of load to center of joint

L_d = horizonal distance between clinometers transducer θ_1 and θ_2 or θ_3 and θ_4

L_D = horizonal distance between displacement transducer δ_1 and δ_2

L_o = length of the composite beam from the face of the reinforced concrete column to the location of load application

M_{c1}, M_{c2} = moment demand on RC columns adjacent to joint at ends 1 and 2

$M_{cr}^{\pm}$ = positive and negative cracking moment capacity to define the trilinear yeild backbone curve for IDASS

$M^{-}_{plastic}$ = negative plastic moment capacity

$M^{+}_{plastic}$ = positive plastic moment capacity

$M^{\pm}_{yield}$ = positive and negative first yield moment capacity

$M^{\pm}_{y}$ = positive and negative yield moment capacity to define the trilinear yeild backbone curve for IDASS

s_h = spacing between transverse reinforcing steel

T = tensile force

t_f = flange thickness of the steel beam

t_p = thickness of face bearing plate

t_{sp} = thickness of steel web panel

t_w = thickness of steel beam web

V_b = shear demand on steel beam adjacent to joint

V_{b1}, V_{b2} = shear demand in steel beams adjacent to joint at ends 1 and 2

V'_c = nominal concrete strength in outer concrete compressive field

V_{cfn} = nominal shear resistance of outer concrete compression strut

V_{cs} = inner concrete compressive field force $\left(\leq V_{csn}\right)$

V_{csn} = nominal shear resistance of inner concrete compression strut

V_{ih} = design shear strength of inner concrete strut mechanism

$\left(V_j\right)_{\max}$ = maximum applied joint shear force demand under factored loading

V_{nih} = nominal shear strength of inner concrete strut mechanism

V_{njh} = combined joint shear resistance

V_{noh} = nominal shear strength of outer concrete strut mechanism

V_{oh} = design shear strength of outer concrete strut mechanism

V'_s = nominal transverse reinforcement strength in outer concrete compressive field

V_{sn} = nominal shear resistance of steel web panel

$\left(V_u\right)_{col}$ = maximum column shear force demand under factored loading

V_{wh} = shear strength of steel beam web

y = width of steel column

x = location of steel column

y_o = distance from neutral axis of steel beam to plastic neutral axis of composite beam-slab

α = stiffness degradation parameter

β = strength deterioration parameter

λ = slip or pinching parameter

$\delta = \delta_{\text{Support}} + \delta_{\text{Column}}, \delta_{\text{Joint}}, \delta_{\text{Beam}}$ *or* δ_{Total}

δ_1, δ_2 = measured displacements $\left[\text{mm}\left(\text{in}\right)\right]$

δ_{Beam} = deformation of composite beam

δ_{Bearing} = joint deformation due to vertical bearing

$\delta_{\text{Column}} + \delta_{\text{Support}}$ = deformation of RC concrete and supporting frame

δ_{Joint} = deformation of joint region

δ_{Shear} = joint deformation due to joint shear

δ_{Total} = total deformation of composite specimen

ε = abitrary strain (negative is defined as compressive)

$\varepsilon_{\max}, \varepsilon_{\min}$ = maximum principle strains

ε_o = strain which yeilds maximum compressive concrete stress

$\varepsilon_{top\,b}$ = strain at the top of the structural steel beam

ε_{ult} = ultimate compressive strain of concrete (0.003)

$\varepsilon_x, \varepsilon_y$, and ε_{xy} = rossette srtains

$\left(\varepsilon_y\right)_b$ = yield strain of the steel beam

ϕ = strength reduction factor for bearing failure (0.7)

ϕ = strength reduction factor for shear (0.7)

ϕ = strength reduction factor for shear failure (strength - 0.85, joint damage and drift - 0.7)

ν_{ibase} = non-demensional strength factor for the inner strut
$\left(1.07 \text{ interior joint or } 0.70 \text{ exterior joint}\right)$

ν_{obase} = non-demensional strength factor for the outer strut
$\left(0.53 \text{ interior joint or } 0.34 \text{ exterior joint}\right)$

θ = rotation (rad) of principle strain axis from ε_x

$\theta_1, \theta_2, \theta_3, \theta_4, \theta_5,$ *and* θ_6 = measured rotations (rad)

$\theta_{\text{Elongation}}$ = joint deformation due to joint elongation

$\Sigma\left(M_u\right)_{\text{beam}}$ = sum of the nominal moment capacities of composite beam-slab sections at both sides of the joint

VITA

John Phillip Steele received his Bachelors of Science from Texas A&M University in Civil Engineering in December of 2001. Upon completion of this thesis, a Masters of Science will be granted from the Civil Engineering Department of Texas A&M University. John Steele now permanently resides at 191 Lake View Circle in Montgomery, TX 77356.